CLEARINGHOUSE FOR FEDERAL SCIENTIFIC AND TECHNICAL INFORMATION CFSTI
DOCUMENT MANAGEMENT BRANCH 410.11

LIMITATIONS IN REPRODUCTION QUALITY

ACCESSION # AD 607916

☒ 1. WE REGRET THAT LEGIBILITY OF THIS DOCUMENT IS IN PART UNSATISFACTORY. REPRODUCTION HAS BEEN MADE FROM BEST AVAILABLE COPY.

☐ 2. A PORTION OF THE ORIGINAL DOCUMENT CONTAINS FINE DETAIL WHICH MAY MAKE READING OF PHOTOCOPY DIFFICULT.

☐ 3. THE ORIGINAL DOCUMENT CONTAINS COLOR, BUT DISTRIBUTION COPIES ARE AVAILABLE IN BLACK-AND-WHITE REPRODUCTION ONLY.

☐ 4. THE INITIAL DISTRIBUTION COPIES CONTAIN COLOR WHICH WILL BE SHOWN IN BLACK-AND-WHITE WHEN IT IS NECESSARY TO REPRINT.

☐ 5. LIMITED SUPPLY ON HAND: WHEN EXHAUSTED, DOCUMENT WILL BE AVAILABLE IN MICROFICHE ONLY.

☐ 6. LIMITED SUPPLY ON HAND: WHEN EXHAUSTED DOCUMENT WILL NOT BE AVAILABLE.

☐ 7. DOCUMENT IS AVAILABLE IN MICROFICHE ONLY.

☐ 8. DOCUMENT AVAILABLE ON LOAN FROM CFSTI (TT DOCUMENTS ONLY).

☐ 9.

PROCESSOR: GLee

TSL-107-10 64

DEPARTMENT OF THE ARMY, ORDNANCE CORPS
PITMAN-DUNN LABORATORY
FRANKFORD ARSENAL

Contract No. DA-19-020-ORD-5706(A)

with

Division of Sponsored Research, M.I.T.

Annual Report
June 1963

INVESTIGATION OF PARAMETERS INFLUENCING SOLIDIFICATION BEHAVIOR OF ALUMINUM ALLOYS

by

Casting and Solidification Section
Department of Metallurgy
H. D. Brody and M. C. Flemings (authors)
Massachusetts Institute of Technology
Cambridge, Massachusetts

DEPARTMENT OF THE ARMY, ORDNANCE CORPS

PITMAN-DUNN LABORATORY

FRANKFORD ARSENAL

Contract No. DA-19-020-ORD-5706(A)

with

Division of Sponsored Research, M.I.T.

ANNUAL REPORT

June 1963

INVESTIGATION OF PARAMETERS INFLUENCING SOLIDIFICATION BEHAVIOR OF ALUMINUM ALLOYS

by

Casting and Solidification Section

Department of Metallurgy

H. D. Brody and M. C. Flemings (authors)

MASSACHUSETTS INSTITUTE OF TECHNOLOGY

Cambridge, Massachusetts

Annual Report, June 1963

Contract DA-19-020-ORD-5706(A)

ABSTRACT

The analysis of the solidification curve for the traditional cases of equilibrium and normal non-equilibrium solidification has been extended to include computation for a binary alloy of any phase diagram. An additional case, taking into account diffusion within the solid phase, has been analyzed to give a solidification curve sensitive to the mode of solidification, in particular the size of the solidification element. Expressions have also been derived for each of the three solidification cases in order to compute the rate of solid formation, the interface and average compositions of each phase, the rate of change of the composition with the progress of the solidification, and the relation of the amount of non-equilibrium phase to the size of the solidification element. Numerical analysis was used to calculate the change of the concentration profile on a microscale within a dendrite, due to diffusion within the solid.

Apparatus and control equipment were designed and assembled for controlled ingot solidification. In addition to the extended solidification heats described below, the equipment permits (a) interrupted solidification, (b) isothermal solidification, (c) programmed solidification, (d) unidirectional solidification, (e) solidification under vibration, and (f) solidification with stirring.

Ingots of aluminum-4.5 per cent copper were solidified over periods ranging from twelve to one thousand hours. The results demonstrated that the increase in the size of the solidification element concomitant with a decrease in the rate of cooling for normal alloy solidification causes the rate of approach to equilibrium solidification to be slow; too slow for the extension of solidification times to be, in itself, a practical means of eliminating microheterogeneities in cast structures.

Comparison of the solidification curve derived from the thermal data of the slow cooled ingots to the solidification curve calculated for the case of limited solid diffusion indicated that the latter case does apply to alloy solidification. In addition, microsegregation measurements indicated that there was an increase of solute within the solid phase during dendritic growth and the results showed good agreement with the computations for the conditions of limited solid diffusion.

DISTRIBUTION LIST

Addressee	No. of Copies
HQ, U.S. Army Material Command ATTN: AMCRD-RC-M	1
AMCRD-DM	1
AMCRD-DW	1
Washington, D. C. 20315	
HQ, U.S. Army Material Command ATTN: AMSMU-LM	
U.S. Marine Corps Liaison Officer	1
Washington D. C. 20315	
Commanding General U.S. Army Missile Command ATTN: Tech. Info. Division	
Mr. G. Reinsmith	1
Rock Island Arsenal Rock Island, Ill. 61202	1
Commanding Officer U.S. Army Ballistics Res. Labs. Aberdeen Proving Ground Maryland 21005	1
Commanding Officer U.S. Army Materials Research Agency ATTN: PS & C Division Watertown Arsenal Watertown, Mass. 02172	1
Commanding Officer Picatinny Arsenal ATTN: Technical Group Dover, Jew Jersey 07801	1
Commanding Officer Watertown Arsenal ATTN: Library	
Mr. G. Darcy	1
Mr. J. P. Jones	1
Watertown, Mass. 02172	1
Commanding General U.S. Army Munitions Command ATTN: Tech. Info. Division Picatinny Arsenal Dover, New Jersey 07801	1

Addressee	No. of Copies
Commanding General U.S. Army Munitions Command ATTN: AMSMU-LC, CDC, Liaison Officer Picatinny Arsenal Dover, New Jersey 07801	1
Commanding General U.S. Army Test & Eval. Command ATTN: Tech. Info. Division Aberdeen Proving Ground Maryland 21005	2
Commanding Officer U.S. Army Tank Automotive Center ATTN: Research & Dev. Division Mr. V. Pagano Warren, Michigan 48090	1 1
Commanding Officer U.S. Army Research Ofc. - Durham Box CM, Duke Station ATTN: Dr. H. M. Davis Durham, North Carolina 27706	1
Commanding Officer Edgewood Arsenal ATTN: Director of Products Engrg. Edgewood Arsenal, Maryland 21010	1
Commanding Officer Rock Island Arsenal ATTN: Laboratory Rock Island, Illinois 61202	1
Commanding General U.S. Army Engrg. Res. & Dev. Labs. ATTN: Mr. W. Baer, SMOFB-SM Fort Belvoir, Virginia	1
Commanding Officer Springfield Armory ATTN: Mr. E. H. Abbe, SWESP-RERE Springfield, Mass.	1

Addressee	No. of Copies
Director U.S. Naval Research Lab. ATTN: Code 6340 Washington, D. C. 20025	1
Commandant U.S. Naval Weapons Lab. ATTN: Terminal Ballistics Lab Dahlgren, Virginia	1
Commandant U.S. Naval Weapons Lab. ATTN: Mr. Rossbacker, Code WC Dahlgren, Virginia	1
Chief, Bureau of Weapons Department of the Navy Washington, D. C. 20025	1
Commander U.S. Naval Engineering Experimental Station Annapolis, Maryland	1
Commander U.S. Naval Engineering Experimental Station ATTN: Materials Lab., WCTRL-2 Annapolis Maryland	1
HQ, Air Research & Development Command ATTN: RDRAA Andrews Air Force Base Washington, D. C. 20025	1
Dr. W. Rostoker IIT Research Institute Technology Center 10 W. 35th Street Chicago 16, Illinois	1
Professor J. Wallace Case Institute of Technology Cleveland, Ohio	1

Addressee	No. of Copies
Commanding Officer Watervliet Arsenal ATTN: Mr. L. Siawsky, SWEWV-RDR Watervliet, New York	1
Commander U.S. Naval Ordnance Lab. White Oak Silver Spring, Marland 20910	1
Commander Arnold Engrg. Dev. Center Air Research & Development Center Tullahoma, Tennessee	1
Defense Documentation Center Cameron Station Alexandria, Virginia 22314	20
Chief, Bureau of Ships Department of the Navy ATTN: Code 343 Washington 25, D. C.	1
Commanding General Aernautical Systems Div. ATTN: Tech. Info. Division Wright-Patterson Air Base Ohio 45433	1
Commanding General Aernautical Systems Div. ATTN: Aeronautical Resea ch Lab., WCRRL Wright-Patterson Air Base Ohio 45433	1
Mr. Robert H. Brown Aluminum Company of America Alcoa Research Lab. Post Office Box 772 New Kensington, Pennsylvania	1
Professor Merton C. Flemings Room 35 - 316 Massachusttts Institute of Technology Cambridge 39, Massachusetts	1

Addressee	No. of Copies
Mr. Carson L. Brooks Reynolds Metals Company 4th & Canal Streets Richmond, Virginia	1
Dr. Robert S. Busk Dow Chemical Company Midland, Michigan	1
Dr. Thomas A. Read University of Illinois Urbana, Illinois	1
Commanding Officer Harry Diamond Laboratories Attn: AMXDO-TIB Washington, D. C. 20438	1
Mr. J. B. Hess Department of Metallurgical Research Kaiser Aluminum & Chemical Corporation Spokane 69, Washington	1
Dr. C. M. Adams, Jr. Division of Sponsored Research Massachusetts Institute of Technology Cambridge, Massachusetts	1
Defense Materials Info. Center Battelle Memorial Institute 505 King Avenue Columbus 1, Ohio	1
Commanding Officer Frankford Arsenal ATTN: ORDBA-1321 Philadelphia 37, Pennsylvania	2
Commanding Officer Boston Procurement District ATTN: ORDEB-LD Army Base Boston 10, Massachusetts	1

Annual Report, June 28, 1964
Contract DA-19-020-ORD-5706(A)

TABLE OF CONTENTS

LIST OF ILLUSTRATIONS

I. INTRODUCTION

This report summarizes continuing research on solidification of aluminum alloys of the Casting and Solidification Section at Massachusetts Institute of Technology under Army Sponsorship (now Army Materials Research Agency) through Frankford Arsenal. In recent years work has concentrated on solidification structure, its control, its relation to casting characteristics, and its influence on mechanical properties.

Among other results of fundamental or practical value, techniques have been evolved from the research, which are now employed commercially, to produce "premium quality" castings; i.e., castings with strengths up to twice as high as those previously available, and with ductilities up to seven times greater.[1] These improvements in properties have been achieved in existing alloys, primarily by control of (1) microsegregation, and (2) microporosity.

It has also been evident that more complete control over microsegregation and microporosity (particularly the former) should permit development of new, wholly different and substantially stronger, casting alloys. As one example, castings with tensile strengths of 70,000 psi have been cast in our own laboratory; this compares with 50,000 psi as the maximum tensile strength in the current "premium quality" casting specification.[2] A research program is now underway in at least one laboratory to develop alloys which possess these high tensile properties and have adequate ductility for engineering applications.[3]

Development of wrought aluminum alloys has also been limited by microsegregation and microporosity in the original cast ingots. For example, only those alloys in which microsegregation can be held to a required minimum can be readily worked, or develop adequate mechanical properties in the wrought state. An example of the as yet untapped potential of wrought aluminum is that a recent study has shown that with sufficiently careful processing controls, tensile strengths in excess of 100,000 psi can be obtained in wrought products produced from cast ingots.[4]

To achieve mechanical properties in cast or wrought products significantly higher than those now available, a deeper fundamental understanding must be obtained of factors affecting such structural variables as microsegregation and microporosity. The time is particularly ripe for such study since (1) a variety of tools can now be employed to aid such a study that were not available only a decade ago, including the electron microprobe and high speed computers, and (2) a decade of experience has delineated important variables and shown the great improvement in properties of castings and wrought material that is possible.

This report summarizes a first year's effort in obtaining fundamental information as discussed above; it is concerned primarily with microsegregation. Detailed computer analyses of the solidification process are reported and comparisons are made with experiment. Preliminary suggestions are given as to how the principles developed may be applied to produce more

homogeneous castings or ingots. Work following that reported here is being directed along the dual paths of improving insight into the solidification process and of applying information developed, on a laboratory scale, to alter and improve cast structures.

II. ANALYSES AND COMPUTATIONS

Once the transport and equilibria that occur on the microscopic scale are specified or assumed, certain macroscopic properties of a solidifying system can be computed.[5-7] In this section the fraction solid, phase composition, heat content, and associated derivatives are computed for three limiting conditions: (1) equilibrium, (2) normal non-equilibrium, and (3) limited solid diffusion. The aluminum-rich portion of the aluminum-copper alloy system, a simple eutectic between the K, θ, and liquid phases (Figure 1), will be used as an example for computation. The analytical expressions derived, however, are general and can be applied to any binary alloy system whose phase diagram is accurately known.

Previously, laborious hand calculations were necessary to carry out this type of calculation for any but alloy systems whose phase diagrams were composed of straight lines. The availability of an IBM 7090 digital computer* for the evaluation of the expressions made feasible carrying through the calculations for any binary alloy system. The organization of the general programs for computing and recording the results of the analyses is included as Appendix B, and description of the expressions follows.

A. Fraction Solid

For a solidifying alloy of know phase diagram, the fraction solid at any temperature can be calculated by the appropriate application of mass

---

* This work was carried out in part at the Computation Center, Cambridge Massachusetts.

balances. An alloy system having m components and solidifying through a region of n solid phases and p liquid phases will have m-1 independent mass balances of the form

$$\sum_{j=1}^{r} \bar{C}_{S_{ij}} f_{S_j} + \sum_{k=1}^{p} \bar{C}_{L_{ik}} f_{L_k} = C_{O_i} \quad \ldots\ldots (1)$$

where* C_{O_i} = overall weight fraction of component i.

$\bar{C}_{S_{ij}}$, $\bar{C}_{L_{ik}}$ = the average weight fraction of component i in the j phase of the solid and the k phase of the liquid, respectively.

f_{S_j}, f_{L_k} = the weight fraction of the j phase of the solid and k phase of the liquid, respectively

Consider now a solidifying alloy of a specific binary system (such as that of Figure 1). At any point in the two phase region the mass balance for solute may be written in the form

$$\bar{C}_S f_S + \bar{C}_L f_L = C_O \quad \ldots\ldots (2)$$

where the subscripts i, j, k have been deleted, there being only one solid phase, one liquid phase, and one independent equation.

Differentiation of equation (2) gives the effect of an infinitesimal variation in the system

$$d(\bar{C}_S f_S) + d(\bar{C}_L f_L) = 0 \quad \ldots\ldots (3)$$

---

* The symbols used in this report are tabulated in Appendix A

which is expanded to

$$\bar{C}_S df_S + f_S d\bar{C}_S + \bar{C}_L df_L + f_L d\bar{C}_L = 0 \qquad (4)$$

As long as the system is closed

$$f_S + f_L = 1 \qquad (5)$$

$$df_S + df_L = 0 \qquad (6)$$

and equation (4) may now be rewritten

$$(\bar{C}_L - \bar{C}_S)\, df_S = f_S d\bar{C}_S + (1 - f_S)\, d\bar{C}_L \qquad (7)$$

The equality expressed by equation (7) is depicted for an infinitesimal amount of solidification, df_S, by Figure 2a. The condition before the transformation is represented by the line C_0 and the condition after transformation by the line C_1. Cross-hatched area B (represented by the left side of equation 7) must equal area A plus area C (represented by the right side of equation 7)

1 Equilibrium Solidification.

Equilibrium solidification refers to a liquid-solid transformation that occurs with complete transport within both liquid and solid phases and with compositions at the interface strictly as predicted by the phase diagram. The compositions of the solid and liquid will be uniformly those given by the intersection of the isothermal at that temperature (tie line) with the solidus and liquidus, respectively. Figure 2b depicts the change

produced by an amount of solidification df_S, and equation 7 modified for this special case is:

$$(C_L^* - C_S^*)\, df_S = f_S dC_S^* + (1 - f_S)\, dC_L^* \quad \ldots\ldots (8)$$

where C_L^*, C_S^* = weight fraction of liquid and solid present at interface

(a) Straight Phase Boundaries

One method of solution of equation (8) is to assume that both the solidus and liquidus are straight lines described by m_S and m_L where:

$$m_L = \frac{T_m - T_i}{C_{L_i}} \quad \ldots (9)$$

$$m_S = \frac{T_m - T_i}{C_{S_i}} \quad \ldots (10)$$

where T_m = melting point of solvent

T_i = temperature of invariant transformation

C_{S_i}, C_{L_i} = concentration of solvent in solid and liquid phases at invariant.

The ratio of the equilibrium solid concentration to the equilibrium liquid concentration within the two phase region is a constant termed the equilibrium "partition ratio".

$$k = \frac{C_S^*}{C_L^*} = \frac{m_L}{m_S} \quad \ldots\ldots (11)$$

and

$$dC_S^* = k dC_L^* \quad \ldots (12)$$

Now substituting expressions (11) and (12) into equation (8), separating variables, and imposing limits of integration yields

$$\int_0^{f_S} \frac{df_S}{1 + (k-1)f_S} = \frac{1}{(1-k)} \int_{C_0}^{C_L^*} \frac{dC_L^*}{C_L^*} \quad . \quad (13)$$

Integration leads either to the familiar lever rule

$$f_S = \frac{C_L^* - C_0}{C_L^* - C_S^*} \quad (14)$$

or the expression used for computations

$$f_S = \frac{T_L - T}{(T_m - T)(1-k)} \quad . \quad . \quad (15)$$

where T_L = liquidus temperature for alloy C_0

(b) Curved Phase Boundaries

Often the assumption of a straight liquidus and solidus leads to inaccurate results and/or loss of information. Such would be true, for example, for the aluminum-zinc system (Figure 3) or the aluminum-tin system (Figure 4).

If the phase boundaries are not straight, equation (15) no longer holds. Equation (14), however, is still valid and may be applied at every point in the path. Results of this computation for a series of aluminum-copper alloys of differing composition are plotted in Figure 5.

Although the results obtained from the curved line calculation often differ appreciably from the results obtained from a straight line approximation (equation 15), equilibrium solidification is rarely approached and the significance of the differences will be discussed in relation to the non-equilibrium calculations (page 11 and Figure 7)

2. Normal Non-Equilibrium Solidification.

Normal non-equilibrium solidification refers to the condition of (1) complete mass transport within the liquid phase (e.g., diffusion coefficient is infinite, $D_L = \infty$), (2) no mass transport within the solid phase ($D_S = 0$), and (3) equilibrium maintained at the interface. The solidification assumptions are depicted by Figure 2c. There being no mass transport within the solid phase, equation (7) is simplified by the deletion of the term $f_S dC_S$ and the mass balance is written in the form

$$(C_L^* - C_S^*)\, df_S = (1 - f_S)\, dC_L^* \quad \ldots\ldots \quad (16)$$

(a) Straight Phase Boundaries

Assuming the liquidus and solidus to be straight lines, substituting expressions (11) and (12) into equation (16) and integrating leads to the result

$$f_S = 1 - \left(\frac{C_0}{C_L^*} \right)^{1/(1-k)} \quad \ldots\ldots \quad (17)$$

or the expression used for computation

$$f_S = 1 - \left(\frac{T_m - T_L}{T_m - T} \right)^{1/(1-k)} \quad \ldots\ldots \quad (18)$$

(b) Curved Phase Boundaries

When the phase boundaries are not sufficiently straight over their entire length ot justify the use of equations (17) and (18), the phase boundaries are treated as a series of straight line segments that follow the actual phase boundary within the experimental accuracy. Then, for a temperature, T, within the interval, $T_J - T_{J-1}$, that the phase boundaries are considered straight, define

$$m_{S_J} = \frac{T_J - T_{J-1}}{C_{S_J} - C_{S_{J-1}}} = \frac{T_J - T}{C_{S_J} - C_S^*} \qquad (19)$$

$$m_{L_J} = \frac{T_J - T_{J-1}}{C_{L_J} - C_{L_{J-1}}} = \frac{T_J - T}{C_{L_J} - C_L^*} \qquad \ldots \quad (20)$$

where C_{L_J} and C_{S_J} are weight fraction of solute at intersections of isothermal at T_J (tie line) with the liquidus and solidus, respectively, $C_{L_{J-1}}$ and $C_{S_{J-1}}$ represent similar quantities at T_{J-1}. Expressions (19) and (20) combine to yield

$$C_L^* - C_S^* = C_L^* - \frac{m_{L_J}}{m_{S_J}} C_L^* - C_{S_J} + \frac{m_{L_J}}{m_{S_J}} C_{L_J} \qquad (21)$$

Let

$$A_J = 1 - \frac{m_{L_J}}{m_{S_J}} \qquad \ldots \quad (22)$$

$$B_J = \frac{m_{L_J}}{m_{S_J}} C_{L_1} - C_{S_1} \qquad (23)$$

and replace $(C_L^* - C_S^*)$ in equation (16) by $A_J C_L^* + B_J$

$$\int_{f'_S}^{f_S} \frac{df_S}{1 - f_S} = \int_{C'_L}^{C_L^*} \frac{dC_L^*}{A_J C_L^* + B_J} \quad \ldots (24)$$

Integrating* equation (24) over a short range T' to T within the interval T_{J-1} to T_J using as lower limits of integration that a fraction solid f_S' exists at temperature T' and liquid composition C_L'.

$$f_S = 1 - (1 - f_S') \left\{ \frac{A_J C_L' + B_J}{A_J C_L^* + B_J} \right\}^{1/A_J} \quad \ldots (25)$$

To calculate the value of f_S at any temperature T within the interval T_{J-1} to T_J, equation (25) must be successively evaluated within each of the intervals from the liquidus T_L to the temperature T_{J-1} and then in the interval from T_{J-1} to T.

The results of this calculation for a series of aluminum-copper alloys are plotted in Figure 6.

In Figure 7 results obtained for several systems by using the expression for curved phase boundaries (equation 25) are compared to results obtained using the straight line assumption (equation 18). The aluminum-iron system, Figure 7b, has been included as an example because the phase diagram is composed of straight lines within the experimental accuracy of the determination, hence results calculated from both expressions coincide

---

* When the solidus and liquidus are parallel, $A_J = 0$. Integration then gives instead of equation (25), $f_S = 1 - (1 - f_S') \exp (C_L' - C_L^*/B_J)$. A similar exception exists in other integrations for curved phase boundaries that follow.

The main deviation for the aluminum-copper system, Figure 7a, is that the curved boundary calculation predicts a higher liquidus and thus the curve is displaced to higher temperatures. The predicted amounts of non-equilibrium second phase are only slightly different.

The straight line approximation is not even qualitatively applicable to the aluminum-tin system, Figure 7c.

The straight line approximation is valid for aluminum-zinc alloys in which zinc content is low, Figure 7d, in spite of irregularities in the phase diagram, Figure 3. This is due to the fact the irregularities occur at higher zinc contents and the low zinc alloys are mostly solid before entering those regions.

3. Limited Diffusion in the Solid.

Limited diffusion in the solid refers to the assumptions (1) complete mass transport in the liquid, (2) mass transport in the solid solely by volume diffusion, and (3) equilibrium maintained at the interface These solidification conditions are depicted in Figure 2d For this calculation an additional assumption specifying the growth morphology is taken The growth form is considered to be plates separated by a distance d. The plates start to grow at the liquidus temperature and complete their growth when solidification is complete at a time θ_f later (See Figure 8 for growth model)

An increase in the solute content due to solid diffusion must be the result of a flux that enters the solid at the liquid-solid interface. Thus the solute increase behind the interface $f_S d\bar{C}_S$ is set equal to the flux at the interface.

$$f_S d\bar{C}_S = - J_i \frac{2}{\rho d} \, d\theta = \frac{2D_S}{d} \left(\frac{dC_S}{dX} \right)_i d\theta \qquad (26)$$

where J_i = flux at interface in solid phase (gr/cm^3)

ρ = density of alloy (gr/cm^3)

D = diffusion coefficient (cm^2/sec)

$\left(\frac{dC_S}{dX} \right)_i$ = concentration gradient at interface (weight fraction/cm)

θ = time from initiation of solidification (seconds)

To simplify equation (26) the amount of diffusion is assumed relatively small, i.e.,

$$\left(\frac{dC_S}{dX} \right)_{X=X_i} = \frac{dC_S^*}{dX_i} \qquad \ldots\ldots\ldots\ldots (27)$$

(a) Parabolic Growth

First, let the rate of advance of the interface be parabolic in time

$$X_i = \lambda \sqrt{\theta} \qquad (28)$$

where X_i = position of interface

λ = growth rate constant

and

$$\frac{d\theta}{dX_i} = \frac{2X_i}{(\lambda)^2} = \frac{f_S d}{(\lambda)^2} \quad \ldots\ldots\ldots \quad (29)$$

For the case of limited solid diffusion and plate-like growth form, equation (7) becomes

$$(C_L^* - C_S^*)\, df_S = \alpha f_S dC_S^* + (1 - f_S)\, dC_L^* \quad \ldots \quad (30)$$

where $\alpha = 2D_S/\lambda^2$ $\ldots\ldots\ldots\ldots\ldots\ldots\ldots$ (31)

and equation (30) may only be applied for $\alpha < 1$ due to the assumption (27).

Straight Phase Boundaries, Constant Diffusion Coefficient: Once again the partition ratio is assumed to be constant and, in addition, the diffusion coefficient is assumed constant over the solidification interval. Separating variables, now

$$\frac{df_S}{\alpha k f_S - f_S + 1} = \frac{1}{(1 - k)} \frac{dC_L^*}{C_L^*} \quad (32)$$

and integrating

$$f_S = \frac{1 - \left(\frac{C_0}{C_L^*}\right)^{(1-\alpha k)/(1-k)}}{1 - \alpha k} \quad (33)$$

or

$$f_S = \frac{1 - \left(\frac{T_m - T_L}{T_m - T}\right)^{(1-\alpha k)/(1-k)}}{1 - \alpha k} \quad (34)$$

Curved Phase Boundaries, Constant Diffusion Coefficient: Equation (30) can be evaluated for a system with curved phase boundaries by dividing the liquidus and solidus into a series of straight line segments (as done previously for the normal non-equilibrium case). Using definitions (21), (22), and (23) and the relation

$$dC_S^* = (1 - A_J)\, dC_L^* \quad \ldots\ldots\ldots \quad (35)$$

equation (30) can be rewritten

$$(A_J C_L^* + B_J)\, df_S = (1 - A_J)\alpha f_S dC_L^* + (1 - f_S)\, dC_L^* \quad \ldots\ldots \quad (36)$$

Separating variables and integrating

$$\frac{1 - \delta f_S}{1 - \delta f_{S'}} = \left\{ \frac{A_J C_{L_{J'}} + B_J}{A_J C_L^* + B_J} \right\}^{/A_J} \quad \ldots\ldots\ldots \quad (37)$$

where $\delta = (1 - [1 - A_J]\alpha)$ . . . . . (38)

and

$$f_S = \frac{1}{\delta} \left\{ 1 - \left[(1 - \delta f_{S'}) \left(\frac{A_J C_{L'} + B_J}{A_J C_L^* + B_J} \right)^{/A_J} \right] \right\} \quad \ldots \quad (39)$$

Straight Phase Boundaries, Temperature-Dependent Diffusion Coefficient:

The diffusion coefficient of solute may vary by more than an order of magnitude over the temperature range of solidification of an alloy. The aluminum-4.5 per cent copper alloy, for example, has a solute diffusion coefficient of 1.62×10^{-9} cm^2/sec at the liquidus and at the eutectic of

1.99×10^{-10}. A closer approximation is made by allowing the diffusion coefficient to be an exponentially varying function of temperature of the form

$$D = D_0 \exp(-Q/RT_K) \quad \ldots\ldots\ldots\ldots (40)$$

where D_0 = empirical constant

Q = heat of activation, empirical

R = gas content

T_K = absolute temperature

Now α becomes a function of temperature of the form

$$\alpha(T) = \frac{2D_0}{(\lambda)^2} \exp(-Q/RT_K) \quad \ldots\ldots\ldots\ldots (41)$$

and equation (32) is integrated over short temperature ranges between the liquidus temperature and the temperature of consideration At each interval the proper value of $\alpha(T)$ is substituted

$$f_S = \left(\frac{1}{1-\alpha(T)k}\right)\left\{1 - \left[1 - (1-\alpha(T)k f_S\right]\left(\frac{T_M - T'}{T_M - T}\right)^{1-\alpha(T)k/1-k}\right\}, \quad (42)$$

Curved Phase Boundaries, Temperature-Dependent Diffusion Coefficients:

For this computation the dependence of D_S on temperature is inserted into the analysis by relating α to the liquid composition. The absolute temperature at some position within the interval between T_{J-1} and T_J is given by:

$$T_K = T_J - m_{L_J}(C_{L_J} - C_L^*) + 273.0 \quad (43)$$

and $\alpha(T)$ is defined as in equation (40) Now setting

$$\beta(T) = 1 - (1 - A_J)\alpha(T) \qquad (44)$$

Use for each successive interation:

$$f_S = \frac{1}{\beta(T)} \left\{ 1 - \left[(1 - \beta(T) f_S') \left(\frac{A_J C_L' + B_J}{A_J C_L^* + B_J} \right)^{\beta(T)/A_J} \right] \right\} \qquad (45)$$

Transformation at the Eutectic Temperature: The analysis of solidification for the limited solid diffusion case has carried the alloy to the point of eutectic transformation. This case differs from the previous two cases in that the phase redistribution resulting from the eutectic transformation and the cooling to room temperature must be taken into account. In the equilibrium case the phase distribution is simply obtained from the phase diagram. An aluminum-4.5 per cent copper alloy (Figure 1) is totally primary solid solution, K, after solidification and the θ phase only appears as the alloy crosses below the solvus line. In the normal non-equilibrium case there can be no mass transport within the solid phase and thus no diffusion controlled solid state change can occur. An aluminum-4.5 per cent copper alloy that has 90 % primary solid and 9 1% liquid phase just above the eutectic temperature will form just 9.1% eutectic This requirement is relieved for the case of limited solid diffusion An analysis of the formation of the primary phase at the eutectic temperature is presented below An analysis of solid diffusion below the eutectic temperature will be presented in Section D (page 38)

Considering the eutectic to be a pseudophase and evaluating the materials balance, equation (1), for three phase equilibrium of a binary alloy

$$\bar{C}_S f_S + \bar{C}_E f_E + \bar{C}_L f_L = C_0 \quad . \quad . \quad . \quad (46)$$

where $\bar{C}_S$, f_S refer to the primary solid

$\bar{C}_E$, f_E refer to the eutectic solid

$\bar{C}_L$, f_L refer to the eutectic liquid

for an infinitesimal change

$$d(\bar{C}_S f_S) + d(\bar{C}_E f_E) + d(\bar{C}_L f_L) = 0 \quad . \quad . \quad . \quad (47)$$

Expanding equation (47) but taking into account

$$d\bar{C}_E = 0; \qquad d\bar{C}_L = 0, \qquad \bar{C}_L = \bar{C}_E = C_L^* \quad . \quad (48)$$

$$df_E = -df_S - df_L \quad . \quad (49)$$

it simplifies to

$$(C_S^* - C_E^*)\, df_S + f_S d\bar{C}_S = 0 \quad . \quad (49)$$

The second term of equation (50) is evaluated by referring to equation (26)

$$f_S d\bar{C}_S = \frac{2D_S(T_E)}{d} \left(\frac{dC_S}{df_S} \right)_{T_E} \left(\frac{df_S}{dX} \right)_{T_E} d\theta \quad (51)$$

Again, the assumption is taken that the solid diffusion does not change significantly the concentration profile at the interface, equation (27), and

$$f_S d\bar{C}_S = \frac{4D_S(T_E)}{d^2} \frac{C_S^* (1-k)}{1 - (1-\alpha k) f_S'(T_E)} \quad \ldots\ldots (52)$$

where $f_S'(T_E)$ refers to the solid fraction just above the eutectic temperature. Rewritting equation (50) and setting limits

$$\int_{f'_S(T_E)}^{f_S(T_E)} (C_S^* - C_E^*) df_S + \int_{\theta_E = f'_S(T_E)^2 (d^2/4\lambda^2)}^{\theta_f = (d^2/4\lambda^2)} \frac{4D_S(T_E) C_S^* (1-k)}{d^2 \left[1 - (1-k) f'_S(T_E)\right]} d\theta = 0$$

$\ldots\ldots (53)$

and integrating

$$f_S(T_E) = f'_S(T_E) + \frac{\alpha k}{2} \frac{1 - f'_S(T_E)^2}{1 - (1 - \alpha k) f'_S(T_E)} \quad \ldots (54)$$

for curved phase boundaries the analogous expression is

$$f_S(T_E) = f'_S(T_E) + \frac{\alpha(1 - A_1)}{2} \frac{1 - f'_S(T_E)^2}{1 - \delta f'_S(T_E)} \quad \ldots (55)$$

Evaluation for an Aluminum-4.5 Copper Alloy: The analysis for limited solid diffusion was applied to an aluminum-4.5 per cent copper alloy using the published phase diagram (Figure 1), the following constants in the expression for the diffusion coefficient

$$D_o = 8.4 \times 10^{-2} \text{ cm}^2\text{sec}^{-1}$$

$$Q = 32{,}600 \text{ calories mole}^{-1}$$

and a parabolic growth rate constant

$$\lambda = 6 \times 10^{-5} \text{ cm sec}^{-1/2}$$

The fraction solid at each temperature, i.e., the solidification curve, for the limited solid diffusion condition is compared to those for the equilibrium and normal - nonequilibrium limiting cases in Figure 9*. The calculated curve, based on equation (45), falls between the limiting curves for the equilibrium and normal non-equilibrium case, the position of the curve shifts in the direction from non-equilibrium to equilibrium as the value of λ decreases.

For parabolic growth of dendritically freezing alloys λ is equal to one half the dendrite spacing divided by the square root of solidification time; i.e., from equation (28) and Figure 8:

$$\lambda = 1/2 \; d/\sqrt{\theta_f} = 1/2 \; \gamma^{\lambda} \qquad . \qquad . \qquad (56)$$

where θ_f = total solidification time

γ^{λ} = empirical ratio of dendrite spacing to square root of solidification time

In dendritic solidification of ingot cast from most alloys, γ^{λ} is found to be nearly constant over a considerable range of freezing [8,9] From

---

* Note: Figure 9 includes some experimental data described in Section IV

aluminum-copper alloys the values of δ^{λ} ($=2\lambda$) observed are such that some solid diffusion is to be expected during normal solidification.

(b) Linear Growth

Now consider the advance of the interface to be linear in time

$$X_1 = u\,\theta \qquad \ldots\ldots\ldots \quad (57)$$

and

$$\frac{dX_1}{d\theta} = u \qquad \ldots\ldots\ldots \quad (58)$$

For the case of limited solid diffusion, plate-like dendrites, and linear growth, equation (7) becomes

$$(C_L^* - C_S^*)\, df_S = \alpha_L\, dC_S^* + (1 - f_S)\, dC_L^* \qquad \ldots \quad (59)$$

where $\alpha_L = 2D/ud$

The result of integration for the conditions of straight line phase boundaries and constant diffusion coefficient is

$$f_S = (1 + \alpha_L k)\left(1 - \left(\frac{C_0}{C_L}\right)^{1/1-k}\right) \qquad \ldots \quad (61)$$

The analysis has also been applied to the conditions of curved phase boundaries and/or temperature dependent diffusion coefficient in a fashion analogous to that described above for parabolic growth.

To evaluate the result at the eutectic temperature of diffusion in the primary solid the expression for $f_S d\bar{C}_S$ (equation 51) is evaluated for linear growth rate

$$f_S d\bar{C}_S = \frac{4D_S(T_E)}{d^2} \quad \frac{(1 - k)\, C_S^*(T_E)}{1 + \alpha_L k - f_S} \qquad (62)$$

Upon substitution for this term in the materials balance for the eutectic temperature (equation 50) and integrating

$$f_S(T_E) = f'_S(T_E) + \alpha_L k \frac{1 - f'_S(T_E)}{1 + \alpha_L k - f'_S(T_E)} \qquad (63)$$

Similarly for curved phase boundaries:

$$f_S(T_E) = f'_S(T_E) + \alpha_L (1 - A_J) \frac{1 - f'_S(T_E)}{1 + \alpha_L (1 - A_J) - f'_S(T_E)} \qquad (64)$$

The quantitative results of this analysis for linear growth rate and limited solid diffusion are presented in the next section.

If the growth form is again considered to be dendrites grown from the melt, the growth rate constant u is half dendrite spacing divided by the solidification time; i.e., from equation (57) and Figure 8.

$$u = \frac{1}{2} \frac{d}{\theta_f} \qquad (65)$$

and

$$ud = \frac{1}{2} \frac{d^2}{\theta_f} = \frac{1}{2} \gamma'^2 \qquad (66)$$

where γ' still is, as previously defined, the empirical ratio of dendrite spacing to the square root of solidification time. The relation of the solidification curve, and thus the microsegregation, to the behavior of

receives closer attention in the next section (page 29)

B. Properties of the Solidification Curve

1. Comparison of Several Aluminum Systems.

The solidification curve (temperature versus fraction solid) is important in the prediction of many casting properties and the interpretation of certain solidification stuctures. As examples, the solidification curve aids in understanding relative tendency for alloys to hot tear,[10] relative shrinkage characterisitics of different alloys,[11] and it may affect dendrite morphology as well.

The solidification curves for a series of compositions in each of nine binary aluminum alloy systems were computed. The results for the case of normal non-equilibrium are presented in Figure 10. The ordinate values in these plots are not degrees as previously but rather a dimensionless temperature scale defined by

$$T_R = \frac{T - T_E}{T_L - T_E} \qquad . \quad . \quad . \quad (67)$$

where T_R will be referred to as the reduced temperature.

For an alloy that transformed uniformly over its solidification range, the curve would be a straight line of slope minus one (-1)

Note the degree of similarity that exists from system to system in Figure 10. One difference between the curves is the amount of solid that forms in an initial temperature interval (e g., the first five per cent temperature decrease) Comparing equivalent alloy contents of the systems

aluminum-zinc, aluminum-mangnesium, and aluminum-copper indicates that the amount of solid to form in the same drop of reduced temperature increases in the order stated. These differences may be expected to influence not only solute redistribution but perhaps also dendrite morphology in the different systems.

2. Rate of Solid Formation.

Through their description of the solidification curve, the first derivative of the fraction solid with temperature, df_S/dT, and with concentration, df_S/dC_L, are valuable quantities for (1) analyzing solidification phenomena and (2) insertion in solidification calculations (e.g , the calculation of rate of shinkage of heat realease that follows). These derivatives, obtainable by rearrangement of the differential mass balances (equations 8, 16, 30, and 59), are summarized in the tabulation that follows

The reciprical of the slope at the liquidus of the solidification curve, $(df_S/dT_R)_{T_R=1}$, are plotted for several solute contents of the aluminum-magnesium, aluminum-copper, and aluminum-zinc systems in Figure 11 The temperature rate of solid formation decreases sharply with fraction solid (see inset Figure 11) Note that the rate of solid formation of the aluminum-zinc system is about five fold higher than the two former systems

TABLE I: Rate of Solid Formation

Case	First Derivative	Straight Line Assumption		Curved Line Assumption	
Equilibrium	df_S/dC_L	$\frac{(1-f_S) + kf_S}{C_L\ (1 - k)}$	(68)	$\frac{(1-f_S) + (1-A_J)f_S}{A_JC_L + B_J}$	(70)
	df_S/dT	$-\frac{(1-f_S) + kf_S}{(1-k)\ (T_m-T)}$	(71)	$\left(\frac{df_S}{dC_L}\right)_J \frac{1}{m_{L_J}}$	(72)
Normal Non-Equilibrium	df_S/dC_L	$\frac{1 - f_S}{C_L\ (1 - k)}$	(73)	$\frac{1 - f_S}{A_JC_L + B}$	(74)
	df_S/dT	$-\frac{1 - f_S}{T_m - T}\ \frac{1}{1-k}$	(75)	$\left(\frac{df_S}{dC_L}\right)_J \frac{1}{m_{L_J}}$	(76)
Limited Solid Diffusion	df_S/dC_L	$\frac{1-f_S + \alpha kf_S}{(1 - k)\ C_L}$	(77)	$\frac{1-f_S + (1-A)\alpha f_S}{A_JC_L^* + B_J}$	(78)
	df_S/dT	$-\frac{1-f_S + \alpha kf_S}{(1-k)\ (T_m-T)}$	(79)	$\left(\frac{df_S}{dC_L}\right)_J \frac{1}{m_{L_J}}$	(80)
Limited Solid Diffusion (linear growth)	df_S/dC_L	$\frac{1 + \alpha_L K - f_S}{(1 - k)C_L}$	(81)	$\frac{1 + (1-A_J)\alpha_L f_S}{A_JC_L^* + B_J}$	(82)
	df_S/dT	$-\frac{1 - f_S + \alpha_L K}{(1 - k)\ (T_m - T)}$	(83)	$\left(\frac{df_S}{dC_L}\right)_J \frac{1}{m_{L_J}}$	(84)

3. Composition of the Solid.

(a) Composition Within the Primary Dendrite

The amount of segregation (coring) which results in each of the three idealized solidification cases discussed in Section IIA is of interest. The minimum segregation will be experienced for the equilibrium case; the maximum segregation for the normal non-equilibrium case, and an intermediate amount of segregation for the limited solid diffusion case. As an extension of the previous analyses the composition at the interface and the average composition of the primary dendrite are calculated as follows.

Interface Composition as Function of Temperature: The composition present at the interface must, for each solidification case, be just that given by the phase boundary at that temperature. For straight phase boundaries interface equilibrium is established between the following compositions in each case.

$$C_L^* = \frac{T_m - T}{m_L} \quad \ldots \quad (85)$$

$$C_S^* = k \frac{T_m - T}{m_L} = k C_L^* \quad \ldots \quad (86)$$

and also

$$\frac{dC_L^*}{dT} = -\frac{1}{m_L} \quad \ldots \quad (87)$$

$$\frac{dC_S^*}{dT} = -\frac{k}{m_L} \quad \ldots \quad (88)$$

For curved phase boundaries the interface compositions take the form:

$$C_L^* = C_{L_J} - \frac{T_J - T}{m_{L_J}} \quad \ldots\ldots\ldots \quad (89)$$

$$C_S^* = (1 - A_J)\, C_L^* - B_J \quad \ldots\ldots\ldots \quad (90)$$

and

$$\frac{dC_L^*}{dT} = \frac{1}{m_{L_J}} \quad \ldots\ldots\ldots\ldots\ldots \quad (91)$$

$$\frac{dC_S^*}{dT} = \frac{1 - A_J}{m_{L_J}} \quad \ldots\ldots\ldots\ldots\ldots \quad (92)$$

Interface Composition as a Function of Fraction Solid: It is of interest to express C_S^* as a function of fraction solid, as this relates closely to the concentration profile within a dendrite. The relations, using straight phase boundary assumptions, are as follows:

Equilibrium:
$$C_S^* = kC_o \left[1 - (1-k)\, f_S\right]^{-1} \quad \ldots\ldots\ldots \quad (93)$$

$$\frac{dC_S^*}{df_S} = \frac{(1 - k)}{kC_o}\, C_S^{*2} \quad \ldots\ldots\ldots\ldots \quad (94)$$

Normal Non-Equilibrium:
$$C_S^* = kC_o\, (1 - f_S)^{k-1} \quad \ldots\ldots\ldots \quad (95)$$

$$\frac{dC_S^*}{df_S} = \frac{C_S^*\, (1 - k)}{(1 - f_S)} \quad \ldots\ldots\ldots\ldots \quad (96)$$

Limited Solid Diffusion (parabolic growth):
$$C_S^* = kC_o\, (1 - \left[1 - \alpha k\right] f_S)^{(k-1)/(1-\alpha k)} \quad \ldots\ldots\ldots \quad (97)$$

$$\frac{dC_S^*}{df_S} = \frac{C_S^* (1 - k)}{1 - (1-\alpha k) f_S} \quad \ldots \quad (98)$$

Limited Solid Diffusion:
(linear growth)

$$C_S^* = kC_o \frac{1 + \alpha_L k - f_S}{1 + \alpha_L k} \quad \ldots \quad (99)$$

$$\frac{dC_S^*}{df_S} = \frac{C_S^* (1 - k)}{1 + \alpha_L k - f_S} \quad \ldots \quad (100)$$

Average Composition of the Solid: For equilibrium the composition within the solid is uniformly the same as that at the interface; that is, the average composition is equal to the interface composition. For the normal non-equilibrium case, the solid composition does not change after the interface passes. For the limited solid diffusion case the solute content within the solid changes continuously and approaches the interface composition For each of the three cases, the average composition of the solid at any point during the solidification is given by the relation:

$$\bar{C}_S = \frac{C_o}{f_S} - \frac{(1 - f_S)}{f_S} C_L^* \quad \ldots \quad (101)$$

and

$$\frac{d\bar{C}_S}{dT} = \frac{1}{f_S} (C_L^* - \bar{C}_S) \frac{df_S}{dT} - \frac{(1 - f_S)}{f_S} \frac{dC_L^*}{dT} \quad (102)$$

where the derivatives relating to the appropriate conditions are substituted on the right side of equation (102) The average composition as a function of the fraction solidified is plotted for a case of limited solid diffusion and the limiting cases for an aluminum-4 5% copper alloy in Figure 12.

From the solidification curve for the limited solid diffusion conditions it is only possible to calculate the interface composition and the average composition. The computation of the actual segregation pattern at each interval of solidification is computed by a numerical analysis technique described in Section D (page 35)

(b) Amount of Second Phase

The solidification curves for several compositions of the systems aluminum-copper, aluminum-magnesium, and aluminum-zinc were computed using the limited solid diffusion conditions and several values of $\lambda^2 (=d^2/\theta_f)$ for both parabolic and linear growth. The fraction eutectic formed during solidification as a function of λ^2 is plotted for several compositions of aluminum-copper having parabolic growth, Figure 13, and linear growth, Figure 14.

For the aluminum-copper alloys up to the maximum solid solubility limit at 5.65 per cent copper a change of λ $(=2\Lambda)$ from 5×10^{-5} cm/sec$^{1/2}$ to 1.0×10^{-3} is sufficient to shift the behavior from essentially equilibrium to normal non-equilibrium. These results, which are summarized by Figures 13 and 14, are supported by numerical analysis calculations described later (section D).

The results, as plotted in Figures 13 and 14, show the sensitivity of the segregation behavior of several aluminum-copper alloys to the value of (the ratio of the growth element size, e g., the dendrite spacing, to the square root of the solidification time) Figure 15, which delineates

the value of λ to produce a given amount of non-equilibrium eutectic, is derived by a transformation of Figure 13 A horizontal line drawn on Figure 13, as shown at one per cent retained eutectic, intersects the curve for each composition at the value of λ^2 just necessary to form a given amount of eutectic, e.g., one per cent. The intersections of several horizontal lines are plotted in Figure 15. Thus, the area below the curve marked 0.5 is the locus of points for which one half per cent or less eutectic will be formed: similarly, for the curves marked 2.5, 5.0, 10 0.

The results for the aluminum magnesium alloys up to the maximum solid solubility limit at 14.9 per cent magnesium indicate a shift in λ from 1×10^{-3} cm/sec$^{1/2}$ to 2×10^{-4} is sufficient to shift behavior from the non-equilibrium type to essentially equilibrium. For aluminum-zinc alloys up to 10 per cent zinc a shift from $\lambda = 2 \times 10^{-3}$ cm/sec$^{1/2}$ to $\lambda = 2 \times 10^{-4}$ cm/sec$^{1/2}$ is sufficient to cause t ge in solidification behavior.

C. Heat Content of a Solidifying Alloy

The determination of the solidification curve for an alloy makes possible calculation of a variety of solidification parameters, the actual measurement of which is often extremely difficult. The computation of two such groups of porperties has been included in the FORTRAN program for macroscopic properties described in Appendix B. These are:

1. The specific volume of the phases and the amount and rate of shrinkage.

2. The heat content of the phases and the rate of the heat release. Only the latter computation is discussed in this year's report.

The total heat released during the liquid to solid transformation of a binary alloy of components A and B depends only on the initial and final states of the alloy. The heat released at any temperature during the transformation, however, is intimately dependent on the solidification path. This dependence on the path is significant when the composition changes of the solid and liquid phases during solidification are considerable

General: The heat content of a binary alloy at any temperature in a two-phase region is expressed by the following relations:

$$H_T = f_S H_S + f_L H_L \quad \ldots\ldots\ldots\ldots \quad (103)$$

where

$$H_S = \bar{C}_S H'_S + (1 - \bar{C}_S) H''_S + H_S^M (T, \bar{C}_S) \quad \ldots \quad (104)$$

$$H_L = C_L^* H'_L + (1 - C_L^*) H''_L + H_L^M (T, C_L^*) \quad \ldots\ldots \quad (105)$$

Having used the following expressions for the solute

$$H'_S = \int_{T_B}^{T} C'_{P_S} \, dT \quad \ldots\ldots\ldots\ldots \quad (106)$$

$$H'_L = \int_{T_B}^{T'_M} C'_{P_S} \, dt + H^{F'} + \int_{T'_M}^{T} C'_{P_L} \, dT \quad \ldots \quad (107)$$

Analogous expressions were used for the solvent parameters, H''_S, H''_L where single primes refer to solute and double primes refer to solvent and

H_T = total heat content of alloy relative to a base temperature, T_B (calories/gram alloy)

H_S, H_L = heat content of solid and liquid phases (calories/gram phase)

T'_M, T''_M = melting point of pure component (°C)

C'_{P_S}, C'_{P_L} = heat capacity of pure solute in the solid and liquid states, respectively (calories/gram°C)

$H^{F'}$ = heat of fusion of pure solute (calories/gram)

$H_S^M(T,\bar{C}_S)$, $H_L^M(T,C_L^*)$ = heat of mixing of solid and liquid phases at temperature T and average compositions $\bar{C}_S$ and C_L^*, respectively (calories/gram)

The assumption has been made that the properties of a phase are accurately represented by its average composition. This is essentially use of the Kopp-Neumann rule of heat capacities.

Equally general as the previous expressions are the following derivates that are the rate of heat release of the phases and the aggregate,

$$\frac{dH_T}{dT} = f_S \frac{dH_S}{dT} + (1 - f_S) \frac{dH_L}{dT} + (H_S - H_L) \frac{df_S}{dT} \quad . \quad (108)$$

where

$$\frac{dH_S}{dT} = \bar{C}_S C'_{P_S} + (1-\bar{C}_S)C''_{P_S} + (H'_S+H''_S) \frac{d\bar{C}_S}{dT} + \frac{\partial H_S^M}{\partial T}\Big)_{\bar{C}_S} + \frac{\partial H_S^M}{\partial \bar{C}_S}\Big)_T \frac{d\bar{C}_S}{dT}$$

. (109)

$$\frac{dH_L}{dT} = C^*_L C'_{P_L} + (1-C^*_L)C''_{P_L} + (H'_L+H''_L)\frac{dC^*_L}{dT} + \left(\frac{\partial H^M_L}{\partial T}\right)_{C^*_L} + \left(\frac{\partial H^M_L}{\partial C^*_L}\right)_T \frac{dC^*_L}{dT} \quad . \quad . \quad (110)$$

The rate of heat release with increase of solid fraction (dH_T/df_S, dH_L/df_S, dH_S/df_S) is simply obtained by multiplying the appropriate derivative above by dT/df_S (see Table I).

For a dendritically freezing alloy the liquid is considered to be homogeneous on the microscale and thus the terms that depend on the solidification path are f_S, $\bar{C}_S$, $d\bar{C}_S/dT$. dT/df_S. The method of evaluation of these parameters has been discussed previously.

The analysis has been applied to the particular case of an aluminum-4 5 per cent copper alloy. The method of evaluating each of the thermal parameters using data from K. K. Kelley[12] and from O Kubashaewski and J. A. Catterall[13] is summarized in Appendix C.

The heat content is plotted as a function of temperature in Figure 16 and as a function of the solid fraction in Figure 17 The heat content curves of Figure 16 are shaped similarly to the solidification curves for the same alloy (Figure 9) The curves for the non-equilibrium case differ, in detail, in the following manner.

1. The curves are extended in the direction of the abscissa During solidification of an alloy, the sensible heats of the solid and liquid phases must be removed, in addition to the heat of fusion of the solidifying fraction

2. The ratio of heat released during the eutectic hold to heat released during the solidification interval is not equal to the weight fraction eutectic formed During the eutectic transformation, which is isothermal, no sensible heat is removed from the solid or liquid phases. Only heat of fusion is released In addition, the θ phase, which is one of the eutectic constituents, has an appreciably negative heat of formation, approximately twice the number of calories per gram as the negative heat of mixing of the eutectic liquid

3. There is an inflection in the heat content curve near 70 per cent solid. The composition of each phase and of the transforming fraction increases continuously during solidification. The heat capacity of each phase, the heat of mixing of the liquid, and the heat of fusion of the solidifying fraction are each dependent on the composition Reference to Figure 17 indicates that the heat that need be removed for each fraction solidified increases as solidification proceeds and the solute content increases in each phase.

If the heat released for each fraction solidified were constant, then a heat content curve could be transformed to a solidification curve using the construction of Stonebrook and Sicha.[14] The slope of the curve in Figure 17 equals the amount of heat that need be extracted to form a gram of solid at a particular stage of solidification. It is clear that the slope, dH_T/df_S, is not a constant throughout the solidification interval of an aluminum-4.5 per cent copper alloy, rather, dH_T/df_S, continually increases as solidification progresses. However, for some calculations (e.g., qualitative application of

the Stonebrooke and Sicha calculation) a value of dH_T/df_S averaged over the solidification interval would not be tto crude an approximation

D. Diffusion Within the Dendrite

1. Analysis.

The computation of the limit solid diffusion case (Part A-3, page 12) delineates the conditions necessary for significant solid diffusion during solidification. Enhancement of this diffusion reduces the severity of microsegregation and is, therefore of great engineering interest. Previous calculations, however, do not fully describe microsegregation in that they do not describe the distribution of solute within the dendrite. A more complete description is obtained by the application of numerical analysis techniques to the diffusion equation.

The model used in the numerical analysis computation is analogous to the model of Section A-3 and is depicted by Figure 8. The pertinent conditions and assumptions are described below.

1. The growth forms (or dendrites) are considered to be plates separated at their centers by the final dendrite spacing, d. The plates start to grow smoothly at the liquidus temperature and each plane face advances a distance d/2 within the solidification time θ_f.

2 End and corner effects are neglected

3 The solute transport within the solid phase is solely by volume diffusion. The diffusion coefficient is an exponential function of temperature described by equation (40).

4. Density differences due to solidification shrinkage are neglected.

5. Temperature is uniform throughout the dendrite plate at any given time, θ Although a casting may be solidifying under a steep thermal gradient, the temperature difference between any two dendrite plates will always be small.

6. The rate of advance of the interface is taken to be a continuous function of time.

parabolic $$X_i = \lambda \sqrt{\theta} \quad \ldots\ldots (111)$$

or

linear $$X_i = u\ \theta \quad \ldots\ldots (112)$$

7. (a) In the first analysis, diffusion behind the interface is considered not to alter the rate of growth. For this assumption, the interface composition at each position of the moving solid-liquid interface is given by the normal non-equilibrium expression for interface composition, equation (95), which becomes for the coordinates of this model

$$C^*_S = KC_o\ (1 - 2X_i/d)^{k-1} \quad \ldots\ldots (113)$$

(b) A second, more accurate analysis, but one that requires more computer time, assumes the envelope of interface composition is given by the limited solid diffusion expressions for the interface composition, equation (97) for the parabolic growth, equation (99) for the linear growth. Results were obtained using both analyses.

Solid Diffusion Within the Solidification Range: Diffusion within the solid phase for the above described model was studied using Fick's second law:

$$\frac{dC}{d\theta} = D \frac{\partial^2 C}{\partial X^2} \qquad \ldots\ldots\ldots (114)$$

with the initial and boundary conditions implied by the model:

when, $T = T_L$, then $\theta = 0$, $X_i = 0$, and $C_i = kC_o$ . . . (115)

at $X = 0, \partial C/\partial X = 0$

$X = X_i$, $C_S = C^*_S$ . . . . . (116)

(where C^*_S is given either by the normal non-equilibrium or the limited solid diffusion expression as stated in assumptions 7 above).

Using the method of finite differences equation (114) is transformed to

$$A\Delta X \frac{C_{J,k} - C_{J,k-1}}{\Delta\theta} = DA\left[\frac{C_{J+1,k-1} - C_{J,k-1}}{\Delta X} - \frac{C_{J,k-1} - C_{J-1,k-1}}{\Delta X}\right] \qquad \ldots (117)$$

where the subscript J refers to steps in the X direction and k refers to steps in time. Solving equation (117) for $C_{J,k}$:

$$C_{J,k} = \frac{C_{J+1,k-1} + (M - 2)\, C_{J,k-1} + C_{J-1,k-1}}{M} \quad . . \quad (118)$$

where $$M = \frac{\Delta X^2}{D \Delta \theta} \quad . . . . . (119)$$

Equation (118) is evaluated iteratively over J and k and the boundary conditions are simulated by the sequence of the steps taken by the computer solution.

Solid Diffusion During the Eutectic Transformation: Again, as the liquid remaining at the eutectic temperature is transforming, diffusion occurs within the primary solid. This diffusion is calculated by evaluating equation (118) at all the J positions within the primary solid solution for successive iterations, each $\Delta \theta$ in duration, from the time of reaching the eutactic temperature to time θ_f when freezing is complete

Diffusion in the Solid Solution Region: As the alloy cools from the eutectic to room temperature, a certain amount of homogenization can occur. If this homogenization is significant, then one would expect to see less second phase and more level concentration gradients at room temperature than were present immediately after solidification Once the time-temperature path for the alloy is determined, the above analysis can be extended to calculating the amount of solid state homogenization. Just as for the solidification range, two classes of cooling curves are considered.

The condition of linear advance of the liquid solid interface, equation (112), for the model requires a constant rate of heat removal, q, that is

$$q = \text{constant} = C_1 \quad . . . . . (120)$$

Such a heat flow condition would be largely true for (1) an ingot cast so that interface resistance to heat flow is the limiting factor, (2) an ingot cooled by the "differential thermocouple technique" described later in this report, and (3) for "unidirectionally" solidified ingots, solidified under steep thermal gradients, for distances not to close to the chill and temperatures not far from T_E.

If the heat released in solidification were the same for each fraction solidified and equal to H' (calories/gram), then

$$\frac{dX_1}{d\theta} = \frac{q}{\rho H'A} = \frac{C_1}{\rho H'A} \quad \ldots\ldots (121)$$

Now, in the solid region,

$$q = -\rho C_{p_S} A \frac{d}{2} \frac{dT}{d\theta} \quad \ldots\ldots\ldots (122)$$

where C_{p_S} = heat capacity of solid (calories)

Substituting (122) into (121) and rearranging

$$\frac{dT}{d\theta} = \frac{2H'u}{C_{p_S} d} \quad \ldots\ldots\ldots\ldots (123)$$

Integrating

$$T = T_E - \frac{H'}{C_{p_S}} \left[\frac{\theta - \theta f}{\theta f} \right] \quad \ldots\ldots\ldots (124)$$

The condition of parabolic advance of the liquid-solid interface, equation (111), for the model requires a parabolic rate of heat removal,

that is, $$q = C_2\theta^{-1/2} \quad \ldots\ldots\ldots\ldots (125)$$

Such a heat flow condition would be largely true for temperatures not to far below T_E when resistance to heat flow is primarily thermal diffusivity of the mold as in (1) sand castings, (2) chill castings, locations near the chill, mold-metal interface resistance negligible.

For parabolic heat removal,

$$\frac{dX_i}{d\theta} = \frac{q}{\rho H'A} = \frac{C_2}{\rho H'A} \quad \frac{1}{\sqrt{\theta}} = \frac{\lambda}{2\sqrt{\theta}} \quad \ldots\ldots (126)$$

and again, after solidification, equation (122) will hold. Substituting (122) into (126), rearranging, and integrating

$$T + T_E - \frac{H'}{C_{PS}} \left[\frac{\sqrt{\theta} - \sqrt{\theta_f}}{\sqrt{\theta_f}}\right] \ldots\ldots (127)$$

Once the appropriate time temperature path has been selected, equation (118) can be evaluated iteratively from the eutectic temperature to a temperature at which the diffusion contribution is no longer significant.

2. Qualitative Results; Diffusion During Freezing.

An important parameter in the numerical analysis technique is M (defined in Equation 119). It is a characteristic of the analysis that when $\triangle X$ represents the amount of solid to form in a solidification time $\triangle\theta$; for $M \ll 2$ the gradients will tend to level out as fast as the dendrites grow; for $M \gg 2$ there will be little diffusion and segregation will approach

the maximum. The parameter M can be related to the growth model through γ' as defined first in equation (56)

$$d = \gamma' \theta_f^{1/2} \qquad \ldots\ldots\ldots\ldots (128)$$

It is demonstrated below that, within the assumptions of the above analysis, over any range that the value of the proportionality factor for an alloy is truly a constant, the solute segregation pattern will be the same for every dendrite spacing and cooling rate. The only difference will be that of scale (the ratio of the dendrite spacings). For two ingots made from an alloy with a constant value of γ', the solute content at dendrite centers will be identical, the solute contents at equal fractions of the dendrite spacing will be identical, and the amounts of non-equilibrium second phase will be identical.

Let the position of the interface be proportional to the n^{th} power of the solidification time (similar to equations 111 and 112).

$$X_i = \eta \theta^n \qquad \ldots\ldots\ldots\ldots (129)$$

Then, the following relation exists between γ' and η

$$\gamma'^2 = (2\eta)^{1/n} d^{(2n-1)/n} \qquad \ldots\ldots\ldots (130)$$

Consider then the diffusion in the J^{th} slice during the time the interface moves from $X_1 = (J - 1)\, da/$ to $X_2 = J\, d/a$, and

$$\triangle X = \frac{d}{a} \qquad \ldots\ldots\ldots\ldots (131)$$

where a = number of spaces taken across the dendrite. Then,

$$\theta = \theta_2 - \theta_1 = \frac{Jd}{a\eta}^{1/n} - \frac{(J-1)d}{a\eta}^{1/n} \quad \ldots (132)$$

$$\theta = \left[J^{1/n} - (J-1)^{1/n}\right] \left(\frac{2}{a}\right)^{1/n} \frac{d^2}{2} \quad \ldots\ldots (133)$$

Now evaluating M

$$M = \gamma \frac{2}{D} \quad \ldots\ldots\ldots (134)$$

where $\gamma = \left[2^{1/n} (J^{1/n} - (J-1)^{1/n} a^{2n-1}\right]^{-1}$ is a numerical factor dependent on the relative position of the calculation and not on the absolute distance. Thus M is dependent only on D and γ^2 but not individually on d or θ_f In particular for parabolic growth, n = 1/2:

$$M = \frac{1}{2J-1} \frac{\gamma^2}{D} = \frac{4}{(2J-1)} \frac{\lambda^2}{D} \quad \ldots\ldots (135)$$

for linear growth, n = 1:

$$M = \frac{1}{2a} \frac{\gamma^2}{D} = \frac{1}{a} \frac{d}{D} \quad \ldots\ldots (136)$$

It should be pointed out here that the calculation of the solidification curve for the limited solid diffusion case also gave the result that the amount of non-equilibrium second phase was dependent only on γ^2 and not on d or θ_f individually Using the relations

Linear growth: $\gamma^2 = 2ud \quad \ldots\ldots (137)$

Parabolic growth: $\gamma^2 = 4\lambda^2 \quad \ldots\ldots (138)$

Equations (34) and (61) can be rewritten

$$f_S = \frac{-\left(\frac{C_o}{C_L}\right)\left[1 - \frac{\left(\frac{8D}{\gamma^2}\right)k}{1-k}\right]}{1 - \left(\frac{8d}{\gamma^2}\right)k} \qquad \ldots\ldots (139)$$

$$f_S = \left(1 + \left(\frac{4D}{\gamma^2}\right)k\right)\left(1 - \left(\frac{C_o}{C_L}\right)^{(1/(1-k))}\right) \qquad \ldots (140)$$

which are seen to depend only on γ^2.

If a value of γ is known for an alloy, then it is possible to casimate the effectiveness of solid state diffusion by computing $2D/\gamma^2$.

If $\alpha' = 2D/\gamma^2 << 1$ tendency for maximum segregation

$\alpha' = 2D/\gamma^2 \simeq 1$ significant reduction of segregation

$\alpha' = 2D/\gamma^2 >> 1$ tendency for minimum segregation

Previous researchers have reported γ to be a constant over a considerable range of dendritic solidification conditions.[8,9] Closer study, however, may demonstrate that γ is not a constant but actually a function of the solidification time. Representing the relation as

$$\gamma = \gamma_o \theta_f^m \qquad \ldots\ldots\ldots\ldots (141)$$

when $m = 0$, γ_o is a constant and, as shown above, the segregation pattern will not alter with solidification time.

When $m < 0$, the value of γ^{λ} decreases as the solidification time increases and the severity of coring will be lessened for slow cooling rates when $m > 0$, the value of γ^{λ} increases as the solidification time increases and coring becomes less severe for a high cooling rate.

3. Quantitative Results; Diffusion During Freezing.

The numerical analysis technique described above was applied to an aluminum-4.5 per cent copper alloy assuming a parabolic rate of interface advance (condition III) using a limited solid diffusion envelope (assumption 7b) and using the following numerical value:

$$D_o = 0.084 \text{ cm}^2\text{sec}^{-1}$$

$$Q = 32{,}600 \text{ calories mole}^{-1}$$

$$\gamma^2 = 1.2 \times 10^{-8} \text{ cm}^2\text{sec}^{-1}$$

The concentration profiles at progressive stages of solidification and cooling to room temperature, plotted in Figure 18, demonstrate the build-up of the solute in the solid behind the advancing interface. Just above the eutectic temperature, the solute content at the center of the dendrite is predicted at 1.32 per cent copper. This value is to be compared to the 0 61 per cent copper predicted by the normal non-equilibrium conditions. Just below the eutectic temperature, the solute content at the dendrite center is predicted at 1.34 per cent copper and, at room temperature, 1.38 per cent copper.

The fraction solid is calculated from the numerical analysis results by subtracting the solute content as integrated over the primary phase from the overall alloy solute content and considering the difference to be dispersed in the second phase, i.e., at the liquid or eutectic composition; e.g., at the eutectic temperature:

$$f_S = \frac{C_E - \left(C_o - \frac{2}{d} \sum_{X=0}^{X=X_1} C_{J,k} \Delta X\right)}{C_E} \quad \ldots\ldots (142)$$

For the results plotted in Figure 18, the fraction of primary solid solution just above the eutectic temperature is 0.927; just below the eutectic temperature, 0.930; at room temperature, 0.935. For normal non-equilibrium, 0.909 is the predicted fraction solid.

The amount of solute build-up within the primary solid, is of course, sensitive to the value of λ'. The dependence is demonstrated by the plot of centerline composition versus λ'^2, of Figure 19. The transition from normal non-equilibrium behavior to equilibrium behavior occurs in the range of λ'^2 from 10^{-6} to 10^{-10} cm^2sec^{-1}. The range of the transition predicted by the numerical analysis technique is in accord with the range previously calculated by the analytic expression (45) for limited solid diffusion that is depicted in Figure 13.

The weight per cent of eutectic predicted at the eutectic temperature, after eutectic transformation, and at room temperature are plotted in Figure 20 as a function of λ'^2 for the assumptions (1) parabolic growth,

(2) straight line phase boundaries, and (3) normal non-equilibrium envelope. It is clearly demonstrated by the curves that the most significant reduction of segregation due to diffusion in the primary solid occurs during solidification and not during direct cooling of the solid casting.

The dotted line of Figure 20 is a comparable curve calculated by the analytic expression for limited solid diffusion, parabolic growth, and straight line phase boundaries (equation 42). As the value of γ' decreases, and consequently the value of α approaches 1, the analytic expression tends to overestimate the amount of homogenization. This result is due to the assumption stated by equation (27) that solid diffusion will not change significantly the gradient of solute at the interface. The change that does occur is the consequence of (1) the increased rate of solid formation and (2) the buildup of the solute behind the interface. The analytic expression is nonetheless sufficiently accurate for the common range of values of γ' .

Two envelopes were used to express the interface compositions, the normal non-equilibrium and the limited solid diffusion, see assumption 7, page 36. The points plotted in Figure 20 are calculated for a limited solid diffusion envelope whereas the solid curves are for a normal non-equilibrium envelope. The former envelope is expected to be more accurate and the latter more convenient; however, it is evident from Figure 20 that closely similar results are obtained using the two envelopes.

III. EXPERIMENTAL APPARATUS AND PROCEDURES

A. General

In the study of ordinary ingots and sand castings it is difficult, if not impossible, to separate the interdependent variables that effect solidification. It is expedient, therefore, to utilize equipment and procedures designed to independently control the various solidification conditions and isolate the important parameters.

Apparatus used for the controlled solidification studies and described below (Figures 21 - 25) was designed to permit: (1) extended solidification with a constant rate of heat removal, (2) programmed time temperature paths during solidification and subsequent cooling, (3) unidirectional cooling with heat removal by air or water, (4) mechanical stirring during cooling, and (5) mechanical vibration during cooling.

Specific requirements of the apparatus were that it would.

(1) Provide a wide variety of solidification times, ranging from one half hour to one thousand hours, (2) provide an environment for the metal that would prevent contamination even after exceedingly long periods of contact, (3) permit close control and observation of the progress of solidification, (4) incorporate a mold of such a shape as to facilitate mathematical analysis, (5) employ a relatively insulating mold material of low total heat content, and (6) permit solidification studies to be made with a minimum set-up time

1. Melting Practice.

Charge materials for aluminum-copper heats were aluminum (99.99+ purity) and electrolytic copper. The metal was prepared for casting in three stages. First, copper was alloyed with liquid aluminum which was held and stirred above 1700°F with a high frequency induction furnace. The resulting hardener alloy of nominal composition 50 per cent aluminum-50 per cent copper was cast into thin ingots in cast iron pig molds Next, one hundred sixty pound heats of aluminum-4.5 per cent copper alloy were made by combining the virgin aluminum and the 50-50 hardener alloy in a gas-fired air furnace. The resulting alloy was cast into approximately 6 pound slab ingots in cast iron molds. Finally, individual heats of twenty to forty pounds were made by remelting the master alloy, stirring for sixty seconds, degassing with chlorine for sixty seconds, and then pouring into the test ingots. Clay-graphite crucibles were used for all heats. All metal tools and pig molds were coated with either fiberfrax or zircon wash and dried before use The procedure described above was used to assure complete dissolution and uniform distribution of the copper, consistent composition from ingot to ingot, and minimal contamination from iron and silicon

2. The Mold.

A cylindrical steel mold was fabricated by welding a 1/8-inch steel plate to the bottom of a seamless steel tube of 1/8-inch wall thickness. Two mold sizes were employed, 5-inches diameter and 2-1/2 inches diameter respectively, each approximately 10 inches in height Mold-metal reaction

was prevented by coating the inside mold surface with Fiberfrax cement* and/or Fiberfrax paper. The top of the mold was covered by a transite plate The insulating ability of the mold was adjusted by wrapping layers of Fiberfrax paper around the outside surface of the steel shell.

3. Solidification Furnace, Controls, Thermal Measurements.

The furance for the controlled solidification studies was a resistance-wound recirculating air furnace capable of a maximum temperature of 1350°F, Figures 21 - 25. Two Brown proportional band control units were available; one a duration adjusting type (DAT), the second a current adjusting type (CAT). The calibration accuracy of the controllers is $\pm$0.2 per cent of full scale (1500°F for DAT, 300°F for CAT). Two Speedomax N model S recorders having interchangeable ranges and scales of one millivolt, ten millivolts, and fifty millivolts were also available for thermocouple reading and recording. A constant millivoltage was connected in opposition to the thermocouple when the scale range in use was less than the thermocouple output.

Thermocouples were fabricated from Hoskins special chromel-alumel wire with a guaranteed accuracy of $\pm$3/8 per cent. The wire was calibrated before shipment and the calibration was checked in the laboratory in the range 200°F to 1220°F If the rate of temperature change was 2 F/min or less, 18 gauge

---

* Product of Carborundum Company, Niagra Falls, New York

wire was used and the thermocouple beads coated with fiberfrax The coating limited interaction with the melt and reduced stray current pickup. If a faster response were required, uncoated 22 gauge thermocouple wire was used.

B. Procedure

In the following paragraphs, detailed procedures are described that were employed for producing test castings in the controlled solidification apparatus in the following ways: (1) extended solidification, (2) interrupted solidification, (3) isothermal solidification, (4) programmed solidification, (5) unidirectional solidification, (6) solidification with stirring, and (7) solidification with vibration.

In this report, however, detailed results are presented only for those experiments which fall under 1 and 2 above (plus some limited data from 5) Experiments in the remaining categories were largely exploratory in nature during the fiscal year covered by this report, these experiments are continuing and will be reported in detail in the next annual report of this contract

1 Extended Solidification

Ingots were solidified over extended periods ranging from eight hours to one thousand hours while maintaining (1) the rate of heat extraction constant and (2) the temperature gradient in the melt very shallow (less than 0.1°F inch). The experimental setup is sketched in Figure 21 and the procedure is summarized below:

1. Ingot molds were placed in the recirculating air furnace and preheated at 1300°F for at least twelve hours.

2. The molds were filled, and the melt temperature stabilized at the furnace temperature.

3. The melt and furnace were cooled with control responding to a differential thermocouple that measured the difference between the temperature of the melt and the temperature of the furnace chamber. As depicted by Figure 21, the differential thermocouple consisted of one chromel-alumel junction in the melt connected in parallel with a second junction in the furnace. The potential across the differential thermocouple, which represented the temperature difference between the two measuring points, was input to the controller which acted to keep the temperature difference at a set, constant value.

4. When the recorded melt temperature indicated the ingot has passed through the eutectic hold, the ingot was removed from the furnace and water quenched.

The rate of heat extraction is directly proportional to the temperature difference and is a constant as long as the difference is a constant The rate of heat extraction is reduced (and the solidification time extended) by (a) reducing the temperature difference or (b) increasing the insulation around the mold. The temperature gradient in the melt is simultaneously reduced by either of these two procedures.

At times as many as six individual thermocouples were used in a differential thermocouple package. Three in the furnace were connected in series, thus multiplying the millivoltage reading by three. Similarly, three thermocouples in the melt were connected in series. When these thermocouples were connected to form a differential thermocouple, the voltage across the package corresponded to three time the actual temperature difference. Not only does this method scale small temperature differences up to a poin. where they are read more easily and controlled more accurately, but this method also averages temperature variations in the furnace and averages error in thermocouple readings

2. Interrupted Solidification.

A variation of the above techniques was to slow cool several 2-1/2 inch diameter ingots in the furnace setting the differential thermocouple control from just one of the ingots. At each of a series of temperatures below the liquidus, one of the ingots would be removed from the furnace. The mold was then quenched to 150°F by dropping into a large tank of water Less than two minutes elapsed from the time the slow solidification was interrupted and the metal temperature brought to 150°F. Thus the portion of the alloy that was still liquid when the slow solidification was interrupted was cooled, by the quench, about 3600 times faster than the remainder of the alloy.

A secord technique employed to interrupt solidification consisted of pouring lead of the same temperature as the melt into the mold The fraction

of the alloy still liquid would be displaced, but the solid crystals would be trapped by a fiberglass screening fastened across the center of the mold.

3. Isothermal Solidification.

A mold with a minimum amount of insulation was placed in the furnace and preheated to 1300°F. The mold was filled with the furnace door open and the metal temperature was lowered to a position intermediate to the solidus and the eutectic. The solidification temperature was maintained for a specified time and then the mold removed from the furnace and quenched

At times several 2-1/2 inch diameter ingots were cooled to the solidification temperature simultaneously and each was held at that temperature for a different length of time before quenching.

4. Programmed Solidification.

A Beck Programmer was used in conjunction with the control units to program temperature-time cycles for the metal and/or furnace. Figure 22 is a sketch of one experimental set-up which was employed. The programmer outputs a time-varying millivoltage that either added or opposed the output of a control thermocouple. The algebraic sum of the two millivoltages was then connected to a control unit, which maintained it at a constant value Thus, as the output from the programmer varied the controller changed the power input to the furnace to the point where the control thermocouples compensated for the change. The programmer is capable of producing up to

three different linear cooling rates within the specified millivoltage intervals.

5. Unidirectional Solidification.

A chill was fabricated connecting four 1/4-inch diameter channels using two 1/2-inch channels in a steel block 5" x 5" x 1/2" and welding it to the bottom of a 5-inch diameter cylindrical mold. The chill was coated with Fiberfrax cement and the inside and the outside surface of the mold walls were wrapped with Fiberfrax paper. The experimental set-up is sketched in Figure 23. Typically, the ensemble was placed in the furnace and preheated to 1300°F. After the mold was filled and the metal temperature stabilized, either water or compressed air was run through the chill block at a high rate (while the furnace temperature was maintained above the liquidus). Essentially all heat flow in the ingot was "unidirectionally", downward.

6. Solidification with Stirring.

A 1/3 horsepowder motor and 1/2-inch chuck were mounted on a frame attached to the top of the furnace. The circuit bringing power to the stirrer motor contained a potentiometer to adjust the power input and voltmeter and ammeter to measure the power input. Various paddle arrangements could be inserted into the chuck and one arrangement is shown in Figure 24. The paddle and shaft were generally made of type 316 stainless steel and coated with aluminum and/or fiberfrax.

7. Solidification with Vibration.

An Eriex Hi Vi model V3A30N electro-magnetic vibration unit having a maximum power input of 40 watts was mounted on a frame below the furnace and coupled to the mold by a stainless steel rod which extended through the furnace bottom A stainless steel plate was threaded and locked onto the rod and the mold itself was securely bolted to the plate. Figure 25 is a photograph of an experimental setup. The vibrator power could be turned on at any time during solidification and the vibrator power adjusted by means of a rheostat.

IV RESULTS OF CONTROLLED SOLIDIFICATION EXPERIMENTS

A Thermal Analysis of Extended Solidification Heats

Several ingots of aluminum-4.5 per cent copper were solidified over extended periods ranging from twelve to 1000 hours, at a constant rate of heat extraction using the differential thermocouple technique. Photographs of polished and etched macrosections of ingots solidified twelve, sixty, one hundred and one thousand hours are shown in Figure 26. Thermal record of ingots solidified over twelve, thirty six, and eighty two hours are plotted in Figure 27. The plots are similar in shape to the heat content (Figure 16) and solidification curves (Figure 9) calculated earlier for this alloy. The slope decreases sharply as the first solid appears and remains relatively shallow and linear for a good part of the solidification time The slope near the end of solidification is close to the value previous to the transformation. The horizontal portion represents the eutectic hold and finally the slope increases to a value characteristic of a single phase field. Neither the amount of undercooling below the liquidus prior to the initiation of freezing nor the undercooling below the eutectic prior to the initiation of the eutectic transformation was ever measured as greater than two degrees Farenheit

1 The Solidification Curve, Comparison with Computations

Due to the fact the ingots were cooled with a constant rate of heat extraction, the abscissa of the thermal record differs from the heat content by a constant factor and the cooling curves may be compared to solidification curve (fraction solid versus temperature, Figure 9), using the method of

Stonebrook and Sicha.[14] The method assumes that the heat of fusion liberated for each per cent of transformation is the same and that the heat capacity of the solid and liquid are the same. The heat content calculations of Section II-C demonstrate that these assumptions are individually inaccurate, especially so when an intermetallic, such as $CuAl_2$ is one of the transformation products. But, the construction, when applied to an aluminum-4.5 per cent copper alloy is accurate within 15 per cent during the bulk of solidification. The converted thermal data is plotted in Figure 9 with the calculated curves for the three cases. The data is seen to agree reasonably well with the case of limited solid diffusion and a value of $\lambda^2 = 1.2 \times 10^{-8}$.

2. The Amount of Non-Equilibrium Second Phase.

It is interesting to note that there is only a very slow increase in the amount of solid diffusion when the time of solidification is increased over two orders of magnitude. The ratio of the time of the eutectic hold to the total solidification time may be, through the calculations of Section II-C, equilibrated with the weight fraction of eutectic formed. These values, summarized in Table II, change only slightly in the runs twelve to eighty two hours. There was no hold recorded for the one thousand hour heat, however, some eutectic is observed in the macrostructure.

It is obvious from the macrostructures (Figure 26) that the dendrite spacing is increasing along with the solidification time. Even though the time for solid diffusion to take place may be increased, the diffusion paths becomes extended and thus the concentration gradients, representative of the driving force for diffusion, become shallow. The somewhat simplified model

TABLE II

Solidification Time (hours)	Duration of Eutectic Hold (hours)	Weight Fraction Eutectic (calculated*)
12	0.25	.03
36	0.7	.03
60	1.3	.03
82	1.7	.03
1000	None Observed	-

and calculations of Section I (in particular, equation 141) indicate that if the dendrite spacing increases in a manner such that the ratio of the square of the dendrite spacing to the solidification time (λ_2^2) remains constant, the segregation pattern will not change. The experimental evidence clearly indicates that the extension of solidification times is not, in itself, a practical means of eliminating microsegregation in aluminum-4 5 per cent alloys.

* The method of calculating a heat content curve for the solidification interval is described in some detail in Section II-C: heat content of solidifying alloy. The fraction eutectic is derived from the calculated heat content curve that has the ratio heat released at eutectic· total heat released within solidification interval equal to the ratio from the cooling curve of time at eutectic temperature: time within solidification interval.

B. Microsegregation Measurements*

1. Microprobe Measurements; Unidirectional Ingots.

The segregation pattern within the dendrites of a series of ingots cast from aluminum-4.5 per cent copper was analyzed quantitatively with the aid of an electron microprobe. The photomicrograph of Figure 28 is a section taken perpendicular to the heat flow direction and seven inches from the chill from an ingot that was water chilled and unidirectionally solidified. The sample was prepared for analysis by first polishing metallographically and then placing microhardness indentations to mark the area of observation. The electron probe traces are apparent in the photomicrograph and the results of one trace are plotted on the same figure with the scale of the abscissa such that horizontal distances are the same. The composition along the centerline of the dendrite element is fairly uniform and for this sample a minimum value of 1.3 per cent copper was obtained.

The minimum copper content measured at the centerline of dendrite elements of samples taken from locations on this and other ingots is summarized in Table III The minimum solute content expected if the solidification followed normal non-equilibrium conditions is 0 6 per cent copper for an aluminum-4.5 per cent copper alloy. The fact that the minimum compositions observed are about 1.3 per cent copper indicates that the

---

* The ingots used for these microsegregation measurements were prepared by Dr. T. F. Bower and the electron microprobe measurements were made under his direction.

TABLE III

A. Unidirectionally Solidified Ingots

	Method of Chill	Distance from Chill	Minimum Copper
1.	Water Chill	1/16 inch	1.4
		3 inches	1.4
		7 inches	1.3
2.	Air Chill	1/16 inch	2 2
		7 inches	1.3
3.	Air then Water	1/2 inch	0.8
		3/4 inch	0 9
		7/8	1 4

B. Slow Cooled Ingots

1.	Interrupted at	1201°F	5% Solid	0 7
2.	Interrupted at	1187°F	40% Solid	1 0

assumptions of this limiting case are not completely valid and that one of the two following conditions contributes to the discrepancy (a) there is a significant build-up of solute ahead of the initial dendrite growth forms due to limited liquid diffusion or (b) some solutionizing occurs in the primary dendrites during solidification If there were a build-up of solute in the liquid, the minimum solute content measured within the solid phase would be the same throughout solidification On the other hand, solid diffusion in the dendrites would cause the minimum solute content to gradually

increase during solidification similar to the prediction of Figure 18. Two experimental techniques of interrupting solidification, described below, were used to demonstrate that the solute content within the dendrites does, indeed, increase during solidification, and that, therefore, the increase in copper concentration at the center of dendrite arms above the value kC_o results from diffusion in the solid.*

2 Microprobe Measurements, Interrupted Solidification.

First, an ingot was solidified unidirectionally by air chilling until, according to thermal data, the most advanced solid reached 3/4 inch into the inget. Then water was put through the chill to effectively quench in the existing structure The data in Table I shows that the primary solid phase had 8 - .9 per cent copper at the time of quenching The region above 3/4 inch had a normal minimum solute content for a water chilled ingot, 1.4 per cent copper.

Second, ingots were slow cooled to temperatures below the liquidus and then lead of the same temperature as the alloy was poured into the ingot to displace the liquid. In this case an inget that had its solidification interrupted at 1201°F, equivalent to 5 per cent solid, had a solute content of 0.7 per cent copper within the primary dendrites. An inget that had its solidification interrupted at 1187°F, equivalent to 40 per cent solid, had a solute content of 1 0 per cent copper

---

* Also, relatively simple calculations and computer calculation now underway as a part of this program show that under conditions of solidification considered herein there can be no significant build-up of solute in the liquid in front of, or between dendrite arms.

The experimental results substantiate the results of calculations which indicate that limited solid diffusion can occur during normal solidification. The value of the minimum solute contents measured is consistent with a value of $\gamma^2 = 1.2 \times 10^{-8}$ cm $sec^{1/2}$ for the calculation of Section D and Figure 19.

V CONCLUSIONS

This report covers the first years work on a continuing project for the fundamental study of the solidification behavior of aluminum alloys. An analytic study has been made of microsegregation in ingots cast from substantially alloyed metals The solidification process has been idealized, for the sake of analysis, by the selection of the microscopic transport conditions and of a growth model with the following results

1. The solidification curve (fraction solid as a function of temperature) for binary alloys has been described and quantitative results have been presented for several aluminum base alloys This method is easily applied to ternary (and more complex) alloy systems provided adequate phase diagram information is available

2. Analyses given account for limited diffusion in the solid phase during solidification and during cooling to room temperature These analyses allow more accurate description of the solidification conditions and more useful analysis of the solidification structure than computations based on the usual assumptions, (a) complte diffusion in the solid (equilibrium), or (b) no diffusion in the solid (normal non-equilibrium)

3. The amount of non-equilibrium phases and coring present in the final solidification structure is shown to be dependent on the ratio of the square of the size of the growth element (for example, dendrite arm spacing) to the solidification time, expressed as λ^2/t For the dendritic solidification of an aluminum-4 5 per cent copper alloy a

value of [illegible], would, in essence, result in the maximum segregation, a value of $\lambda_2 = 1 \times 10^{-10}$ would, in essence, result in an equilibrium structure. A value of λ_2 ranging between these limits would result in varying amounts of solid diffusion and curves that describe the amount of non-equilibrium eutectic formed in aluminum-copper alloys as a function of λ_2 have been presented

4. As a consequence of solid diffusion, the solute content within the primary solid will increase during the solidification process A numerical analysis technique has been described which computes the concentration profile at various solid fractions. The analysis applied to an aluminum-4.5 per cent copper alloy demonstrates:

   (a) the dependence of the microsegregation on λ_2

   (b) the copper concentration of the primary solid phase is quite uniform during the initial stages of solidification

   (c) whenever there is substantial solid diffusion the reduction of microsegregation during cooling in the solidification range will be more significant then the leveling that will occur during the eutectic hold and during cooling of the solid structure to room temperature

5. Once the solidification curve of an alloy has been computed the behavior within the solidification range of many physical properties can be described with the use of data for the alloy that has been measured within the single phase regions As an example, expressions have been derived for the heat content and rate of heat release of a binary alloy in the solidification region The expressions have been evaluated for an aluminum-4.5 per cent copper alloy

Through the analysis of ingots cast from aluminum-4.5 per cent copper alloy experimental verification was obtained for the major assumptions of the analyses.

1. Thermal analysis of ingots solidified by a differential thermocouple technique indicate that the solidification curve of aluminum-4.5 per cent alloy is more aptly described by the limited solid diffusion conditions than either the equilibrium or normal non-equilibrium conditions.

2. Electron microprobe measurements of the copper distribution within dendrites from unidirectionally solidified ingots showed a minimum value of 1.3 - 1.4 per cent copper rather than the 0.6 per cent predicted by the phase diagram. Examination of dendrites from ingots that had their cooling interrupted at various stages of solidification demonstrated that initial solid to solidify did have a composition close to 0.6 per cent and that the solute content of the solid increased during the solidification process

3 Observation of ingots cooled with solidification times ranging from twelve hours to one thousand hours demonstrated that the dendrite structure coarsens with increasing solidification time at such a rate that the resulting decrease in concentration gradient hinders solid diffusion to an extent comparable to the enhancement brought about by the increased time available for diffusion. The reduction of micro-segregation resulting from extended solidification times is too slight

to be, in itself, a practical means for eliminating the non-equilibrium micro-inhomogeneities from solidification structures

VI. REFERENCES

1. M. C Flemings and D. Peckner, "Premium Quality Castings", Materials in Design Engineering, No 209, August 1963.

2. Department of Defense, Milatary Specification, "Aluminum Alloy Castings, High Strength", MIL-A-21180B, August 4, 1960

3. S. Lipson, Frankford Arsenal, unpublished research.

4. A. P. Haarr, Research Laboratories, Aluminum Company of America, "Development of Aluminum Base Alloys", Second Annual Progress Report, Department of the Army, Ordnance Corps , Contract No DA-36-034-ORD-3559RD, October 30, 1963.

5. G. M Gulliver, Metallic Alloys, Appendix I, Charles Griffen (London, 1921).

6. E. Scheil, "Bemerkungen Zur Schiehlkristalbildung", z fur Metal, v. 34, 1942

7. W G. Pfann, Zone Melting, John Wiley (New York, 1958)

8. P. E. Brown, "Mass Transport in Dendritic Solidification", Sc D Thesis, Department of Metallurgy, M I T , 1960

9 Foundry Section, Metals Processing Division, Department of Metallurgy, Massachusetts Institute of Technology, "Investigation of Solidification of High Strength Steel Castings", Interim Summary Report, Department of the Army, Ordnance Corps , Contract No. DA-19-020-ORD-5443

10 R. A. Rosenberg, M C Flemings, and H. F Taylor, "Hot Tearing in Non-Ferrous Binary Alloys", Trans A F S , v 68, 1960

11. M C. Flemings, S. Z. Uram, H F. Taylor, "Solidification of Aluminum Castings", Trans A F S , v. 68, 1960

12 K. K Kelley, "Contribution to the Data on Theoretical Metallurgy", U.S Bureau of Mines Bulletin No 476 (Washington, 1949)

13. O Kubaschewski and J A Catterall, Thermochemical Data of Alloys Pergamon Press (New York, 1956)

14. E E Stonebrook and W E. Sicha, "Correlation of Cooling Curve Data with Casting Characteristics of Aluminum Alloys", Trans A F S , v 65, 1957

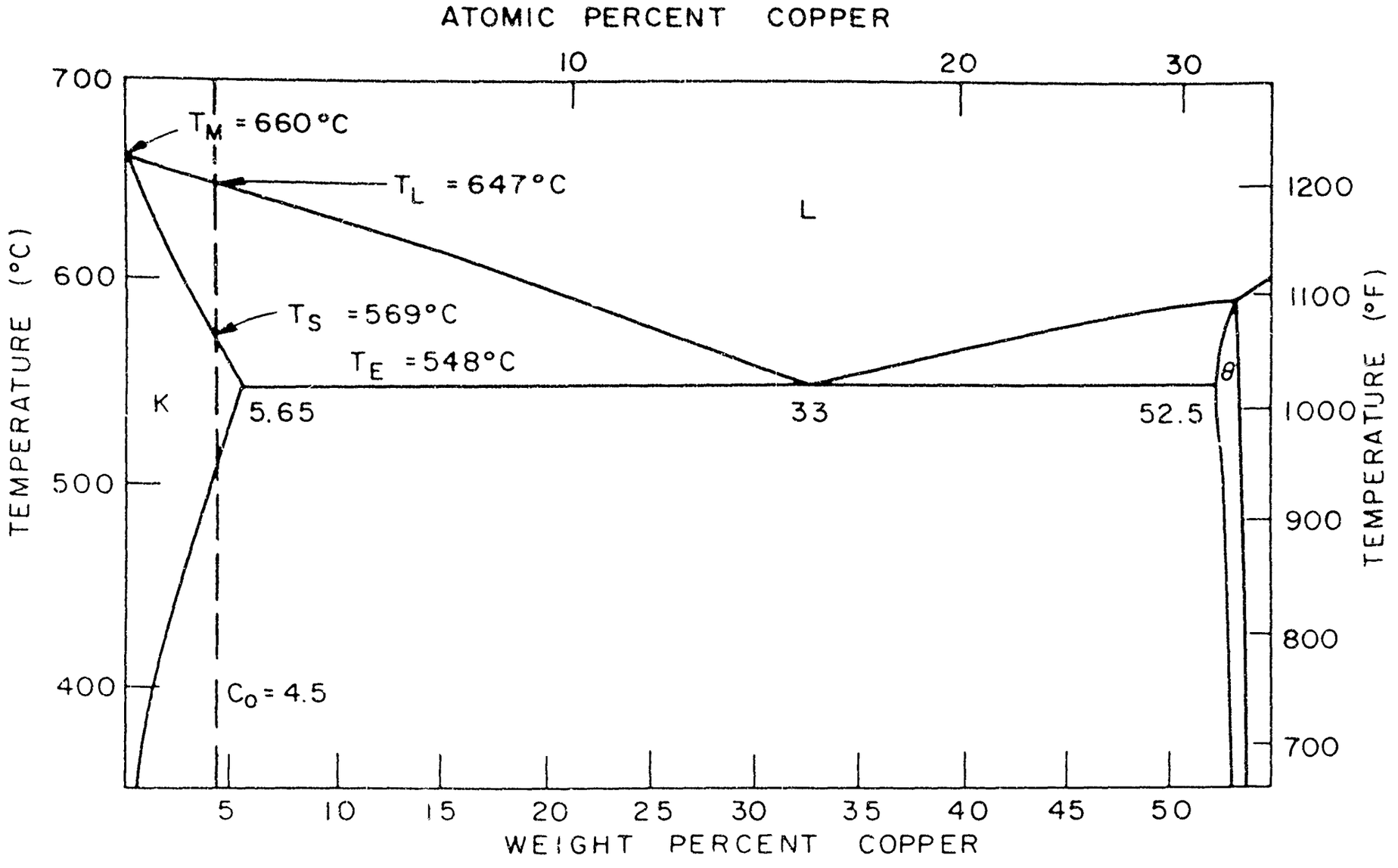

Fig. [illegible] phase diagram [illegible] alloys (A S M , Metals Handbook, 1948)

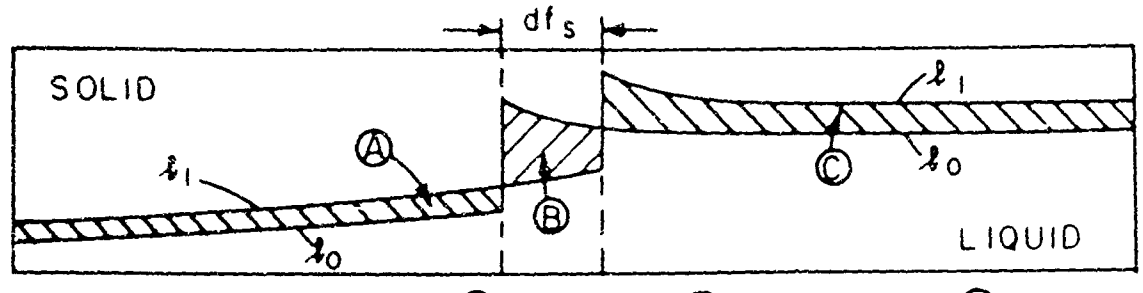

a) GENERAL - AREA Ⓑ = AREA Ⓐ + AREA Ⓒ

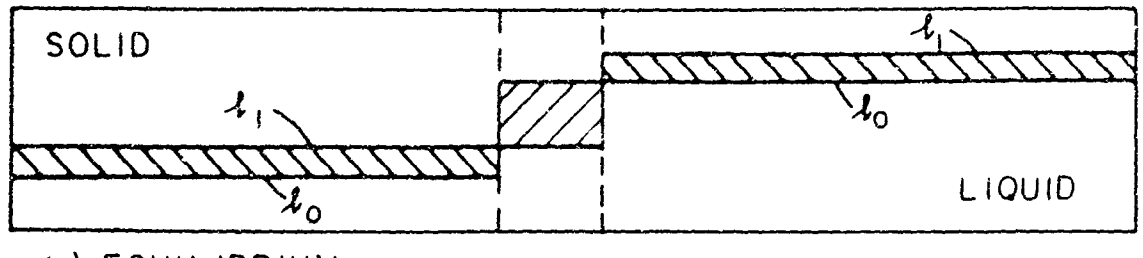

b) EQUILIBRIUM

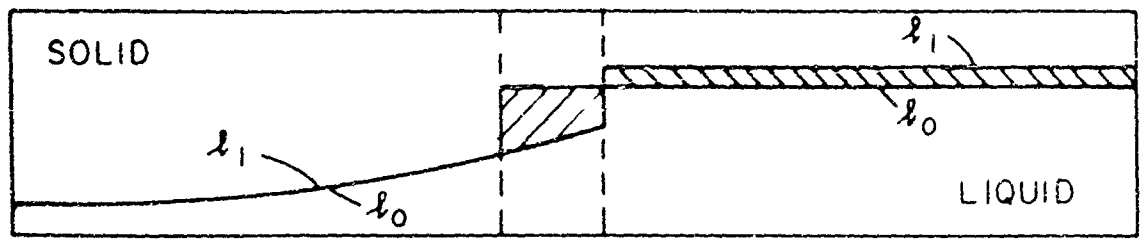

c) NORMAL NON-EQUILIBRIUM

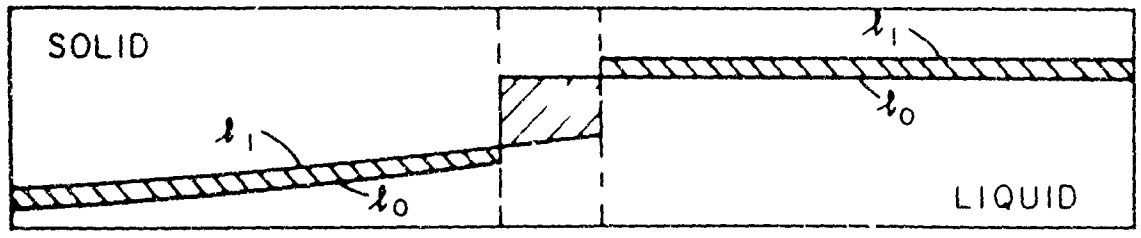

d) LIMITED SOLID DIFFUSION

Fig 2 Schematic representation of the materials balance for a small amount of solidification by the most general case and the three idealized cases described in the text

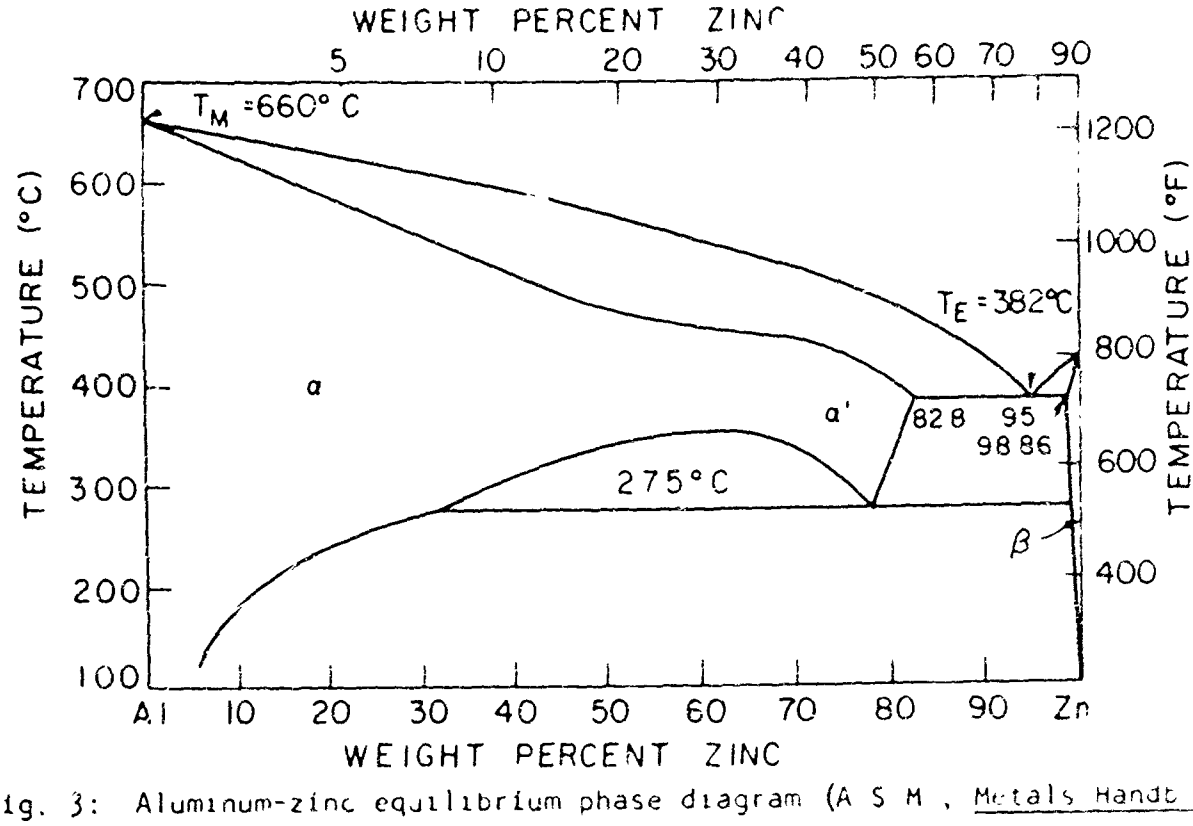

Fig. 3: Aluminum-zinc equilibrium phase diagram (A S M , Metals Handbook, 1948)

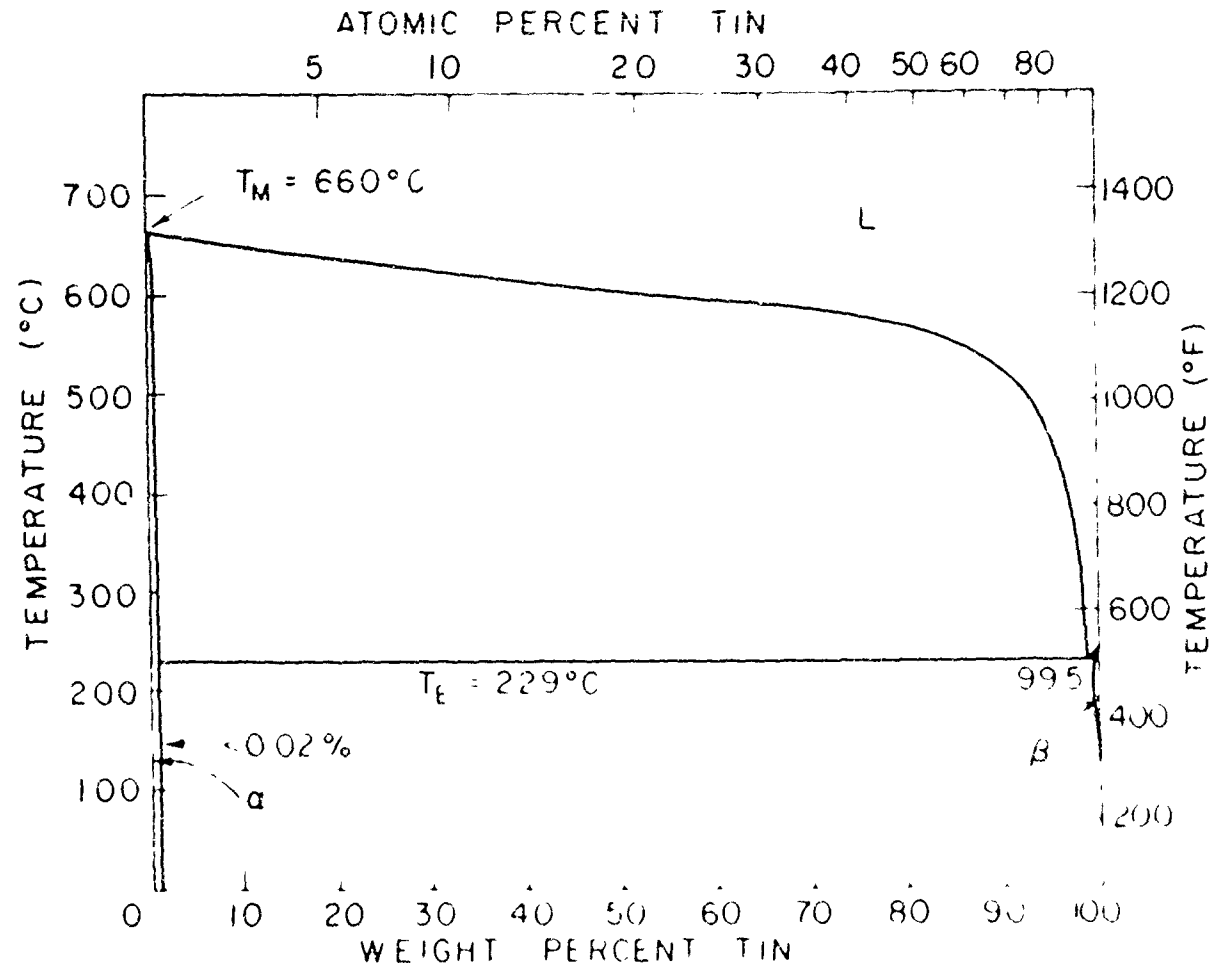

Fig. 4 Aluminum-tin [illegible]

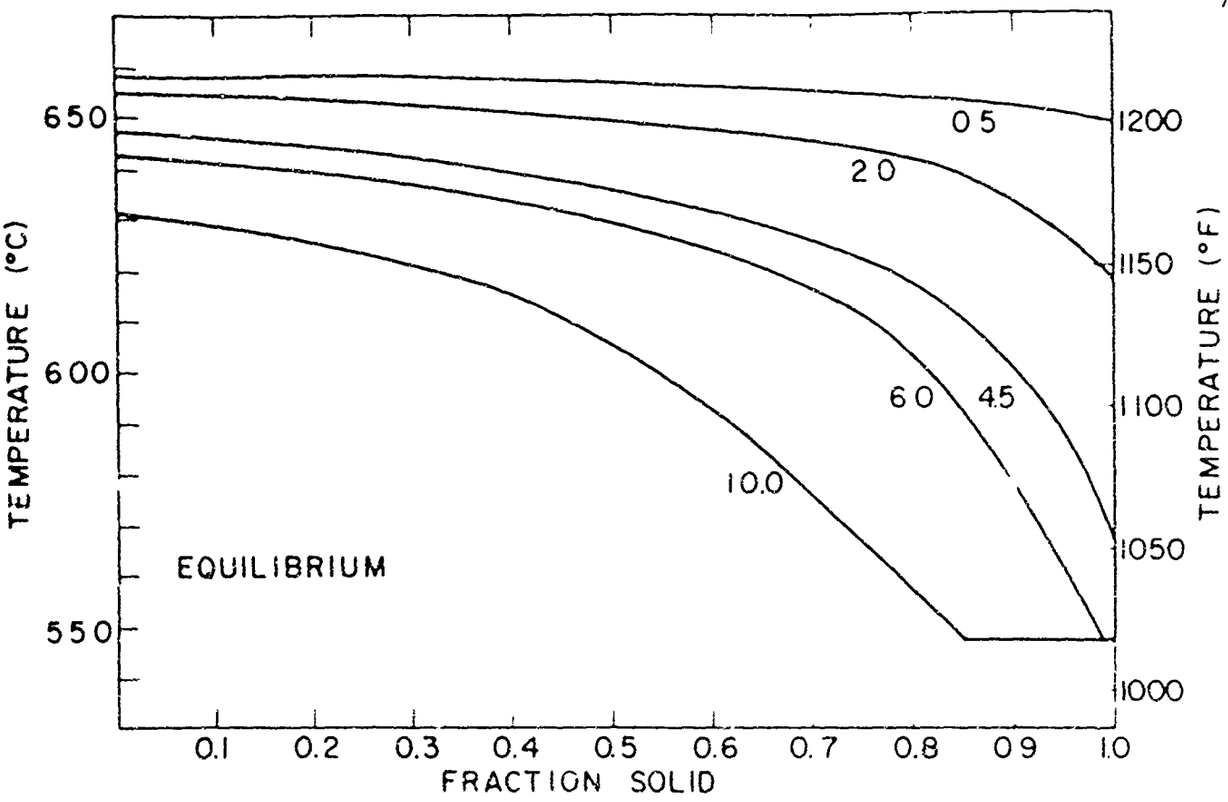

Fig. 5. Solidification curve for equilibrium case of several aluminum copper alloys.

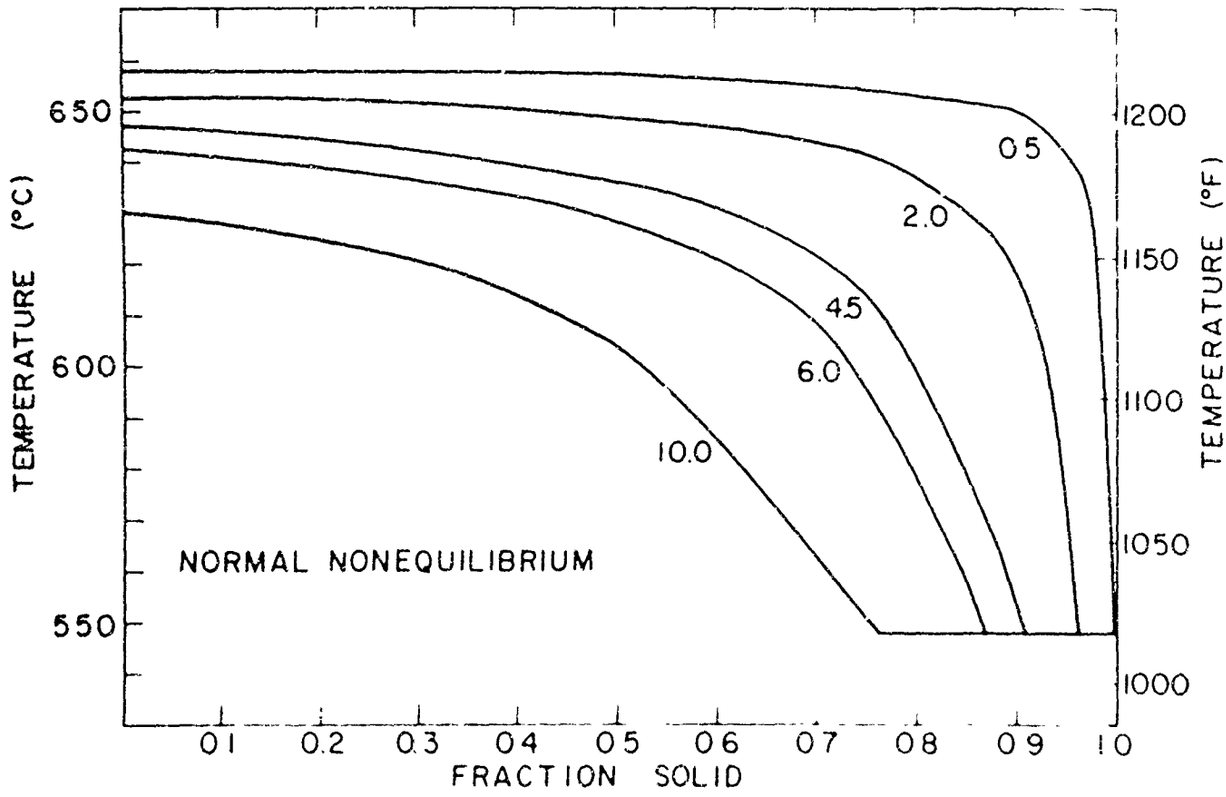

Fig. 6. Solidification curve for normal non-equilibrium case of several aluminum-copper alloys.

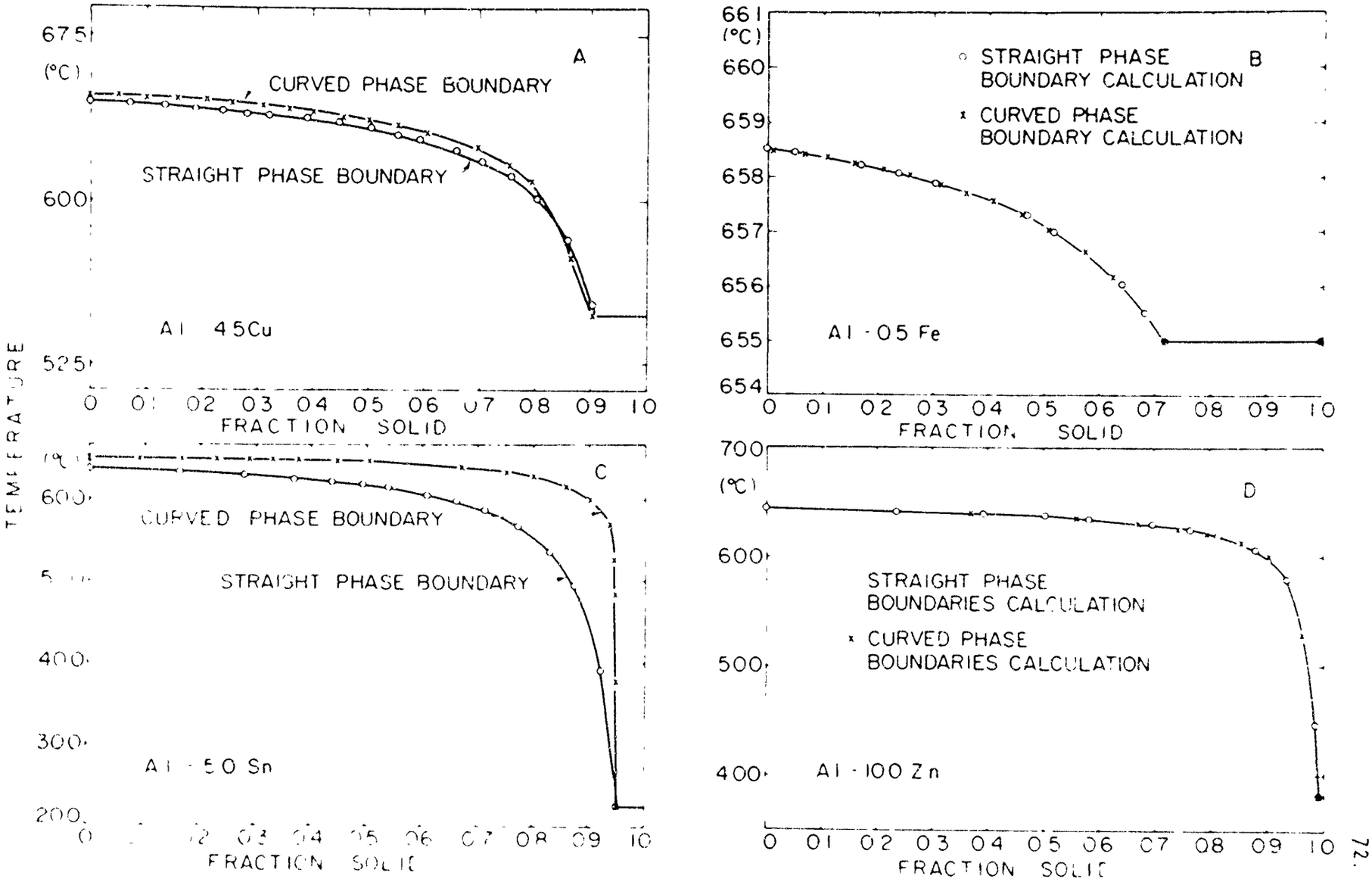

Fig. 7 Comparison of the [illegible] calculated by assuming the phase boundaries straight lines to those calculated taking into account the curvature of the phase boundaries

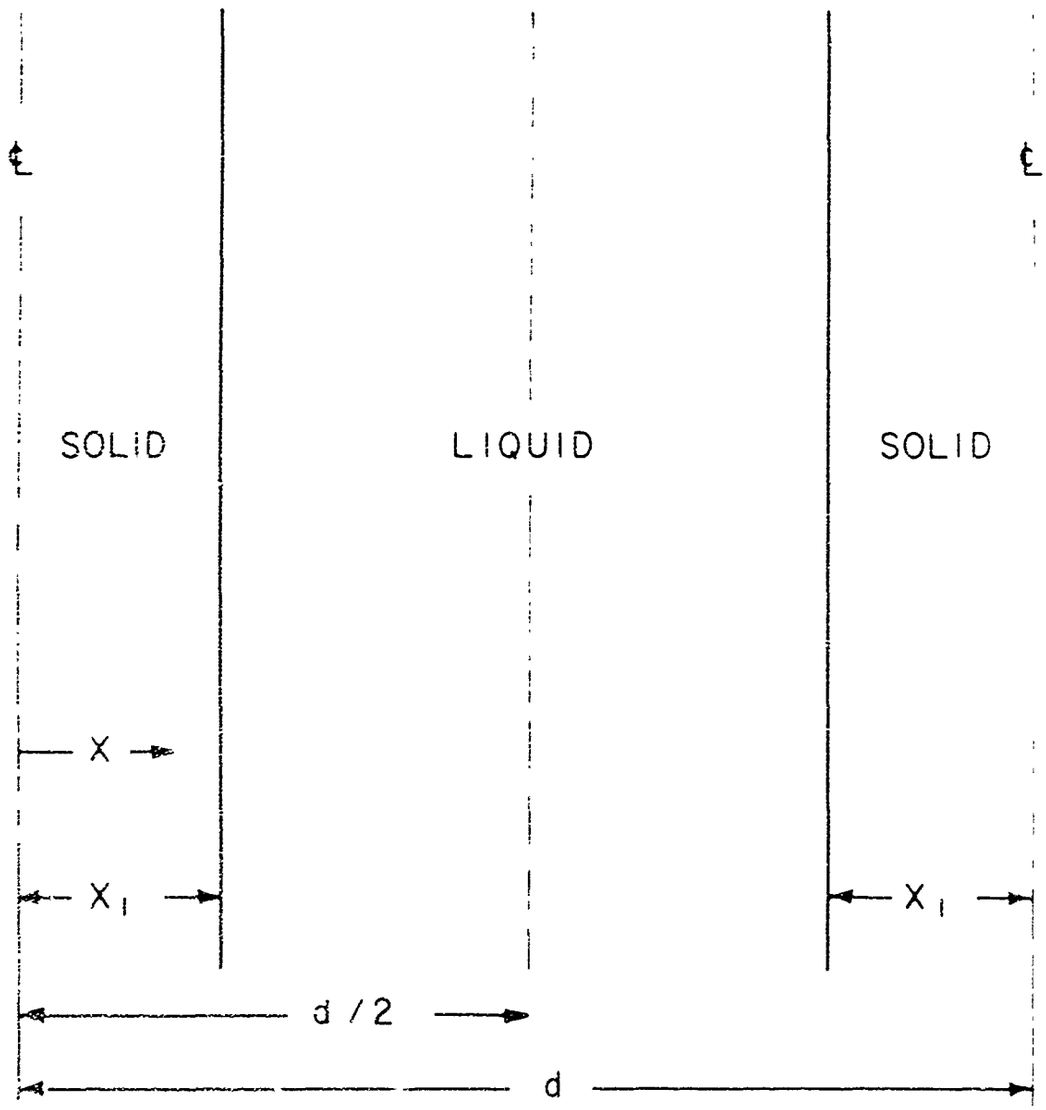

Fig 8 Model of growth element selected for computations involving diffusion in the solid state

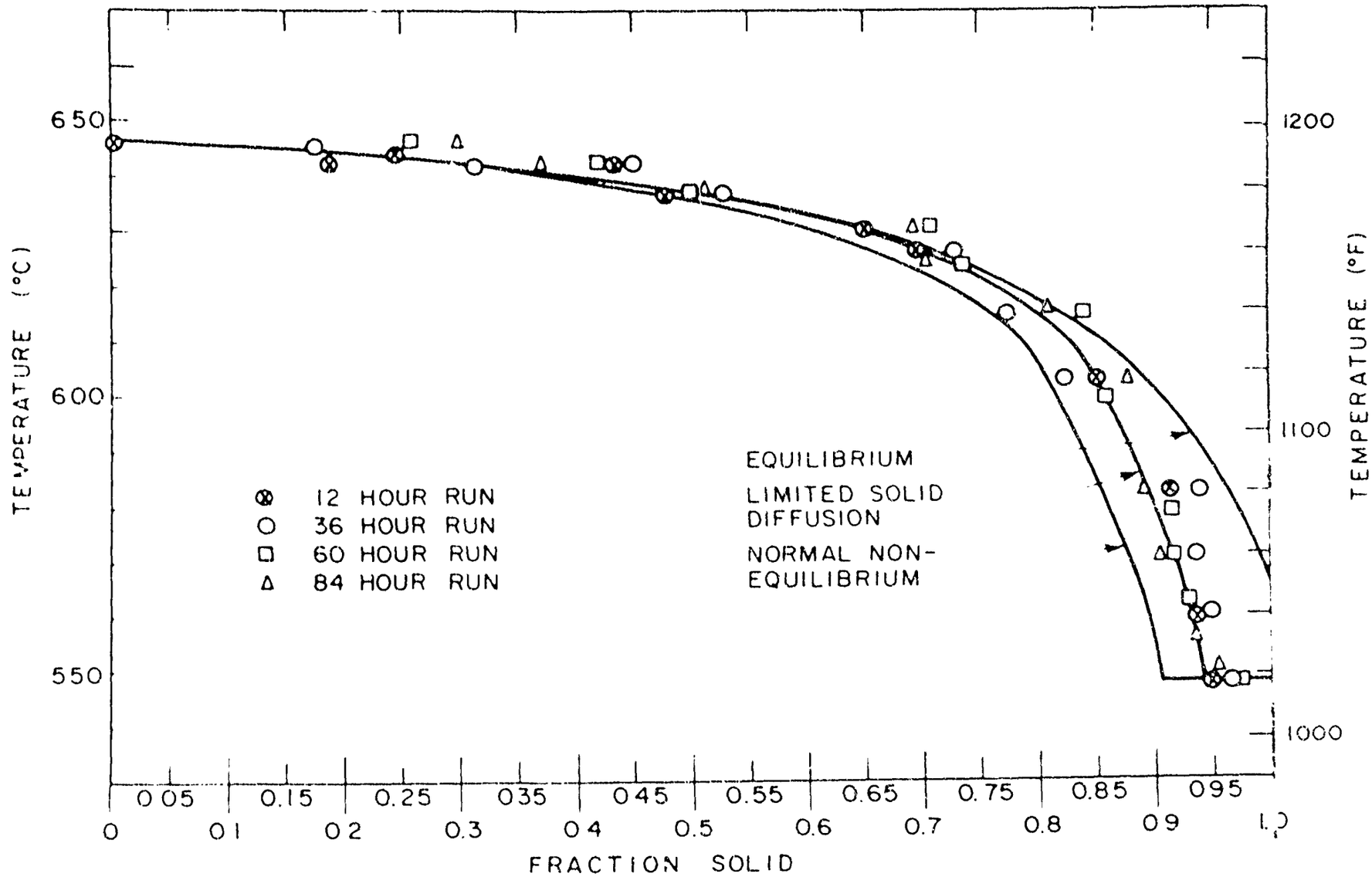

Figure 9 Comparison of the solidification curve of an aluminum-4.5 per cent copper alloy for the three cases, equilibrium, normal non-equilibrium, and limited solid diffusion and some experimental data. The derivation of the experimental data from time-temperature records is described in the text

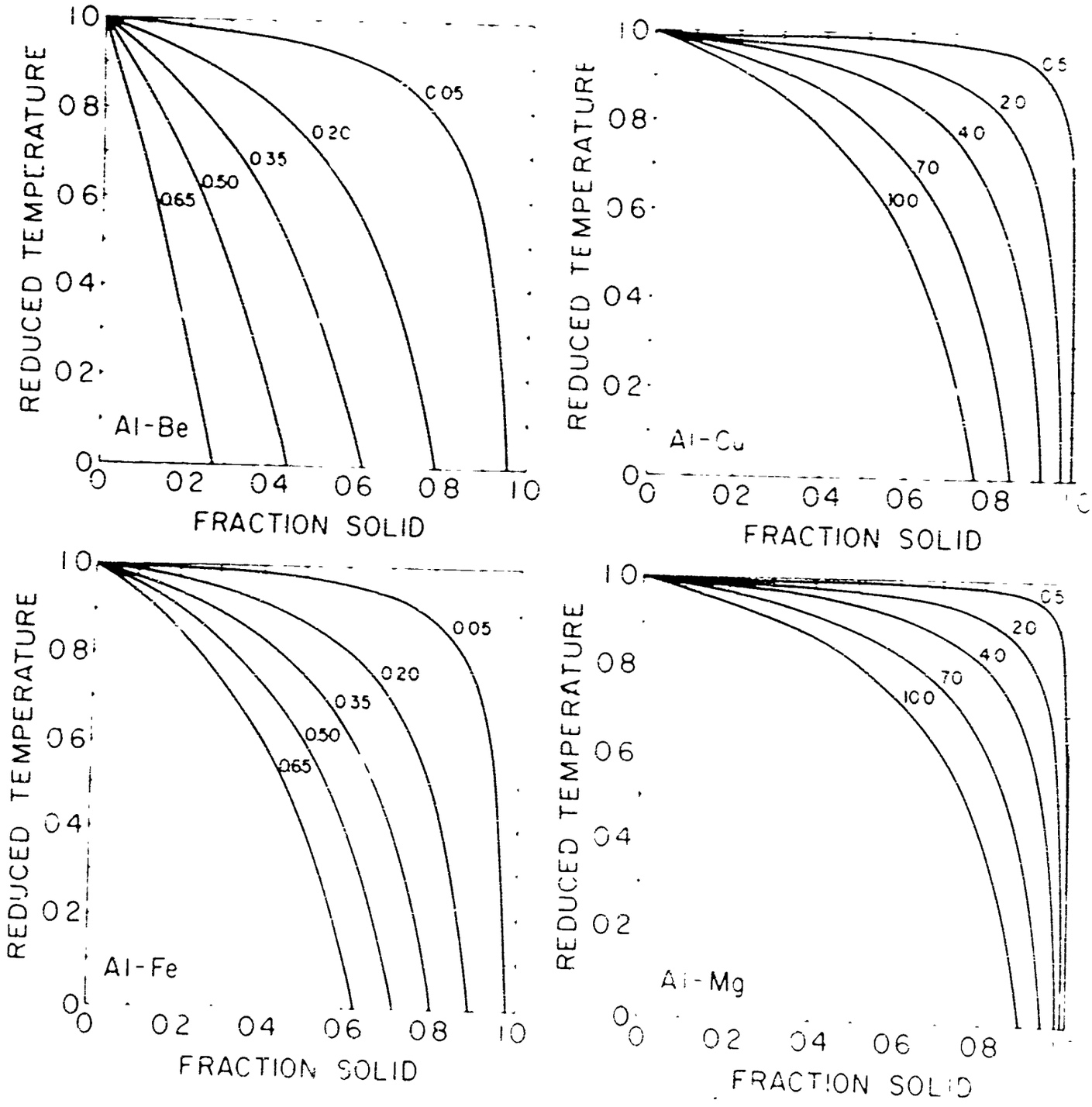

Fig. 1[illegible] [illegible] alloys from [illegible] a relative temperature [illegible]

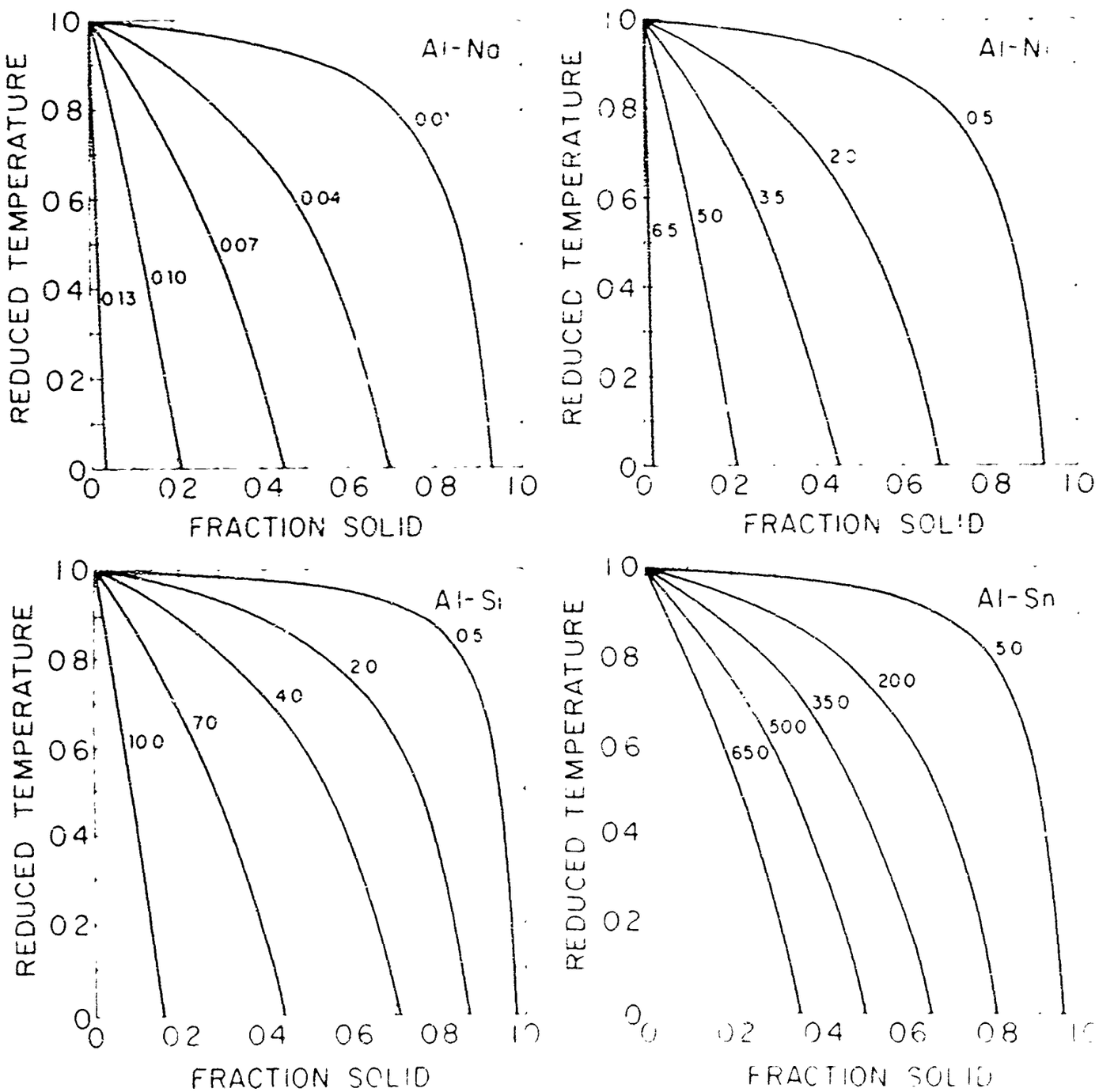

Figure 10 (cont'd): Solidification curves for the normal non-equilibrium case

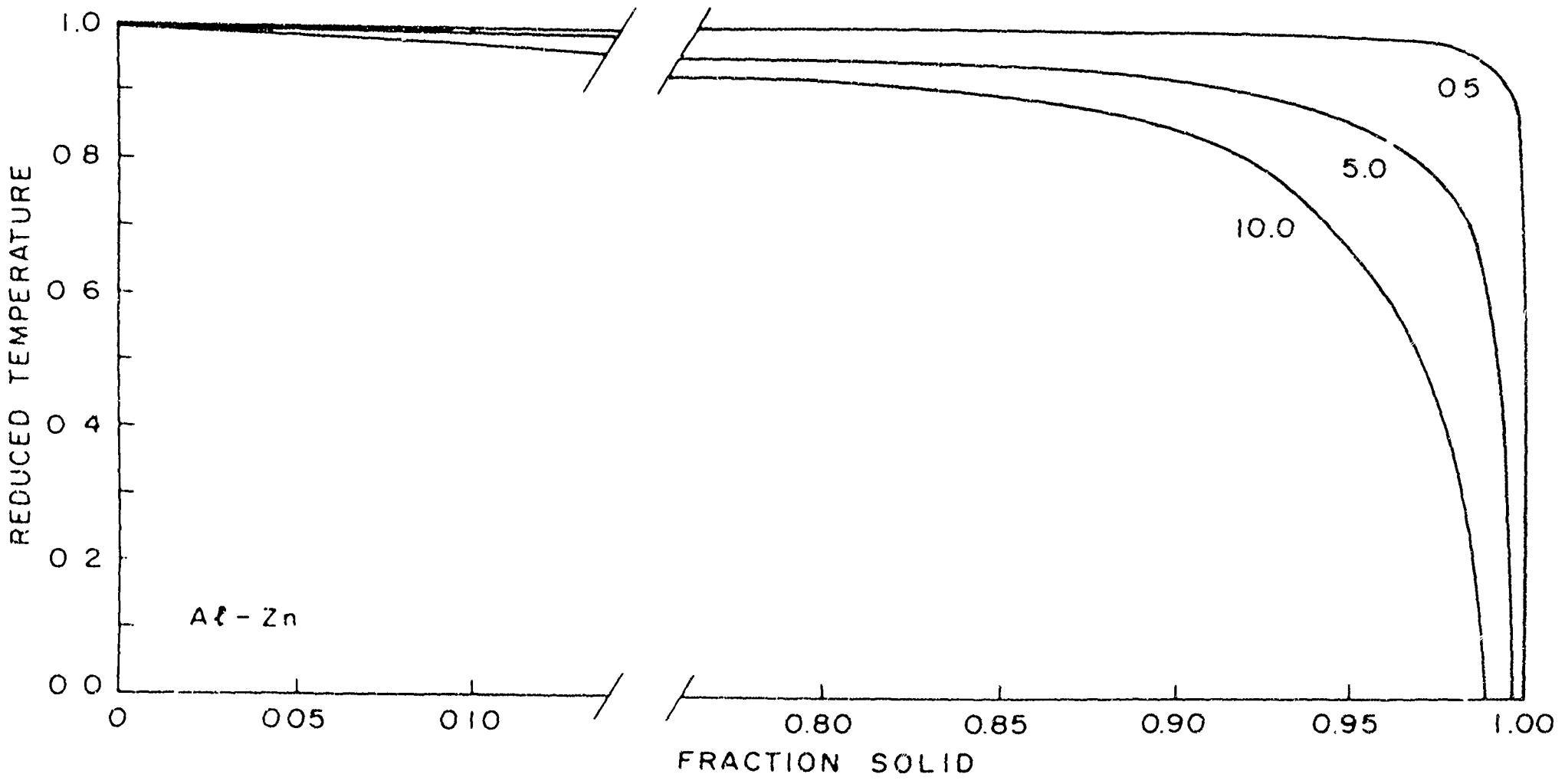

Figure 10 (cont'd). Solidification curves for the normal non-equilibrium case.

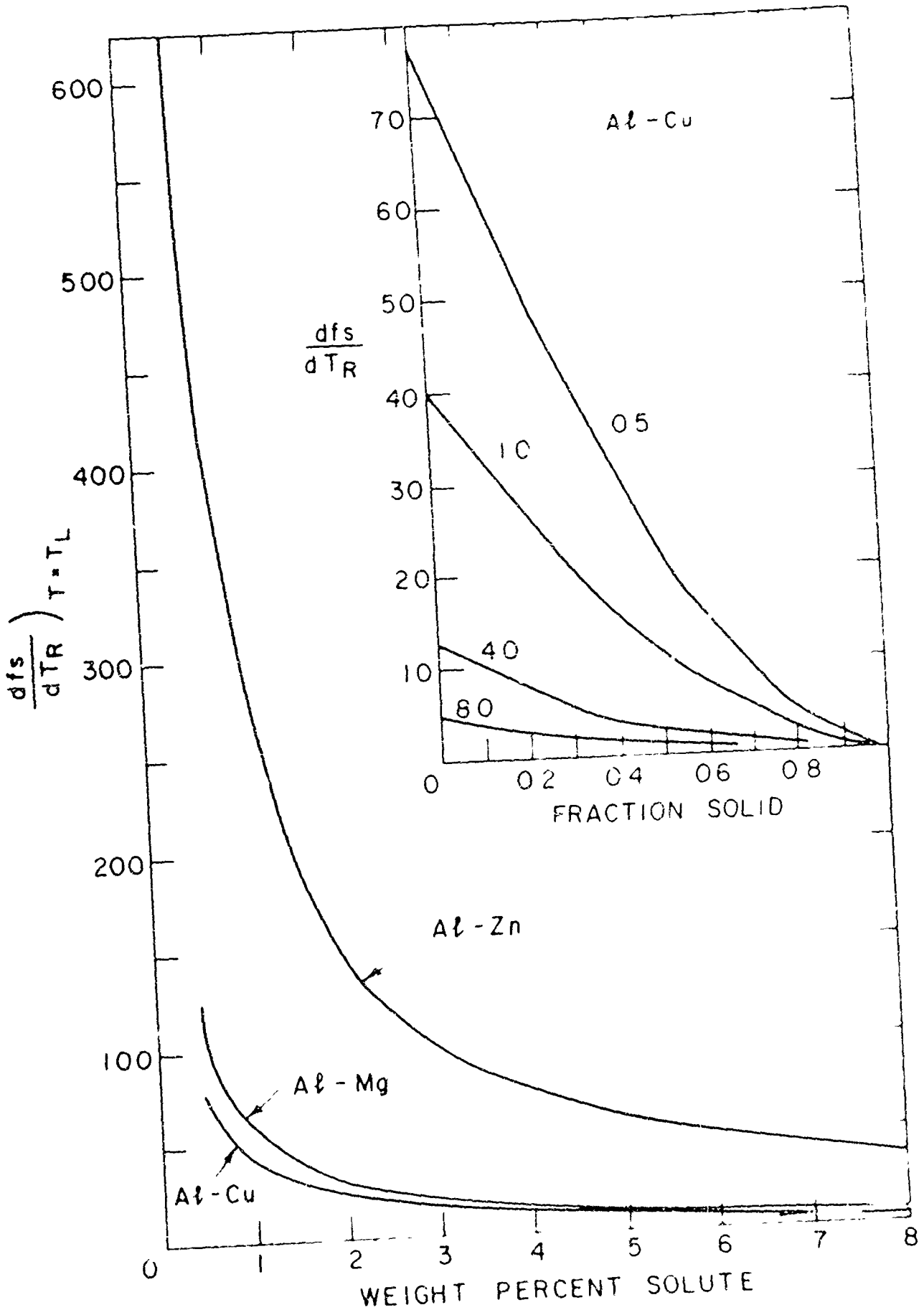

Fig. 11 The [illegible] the system Al [illegible] from the Al

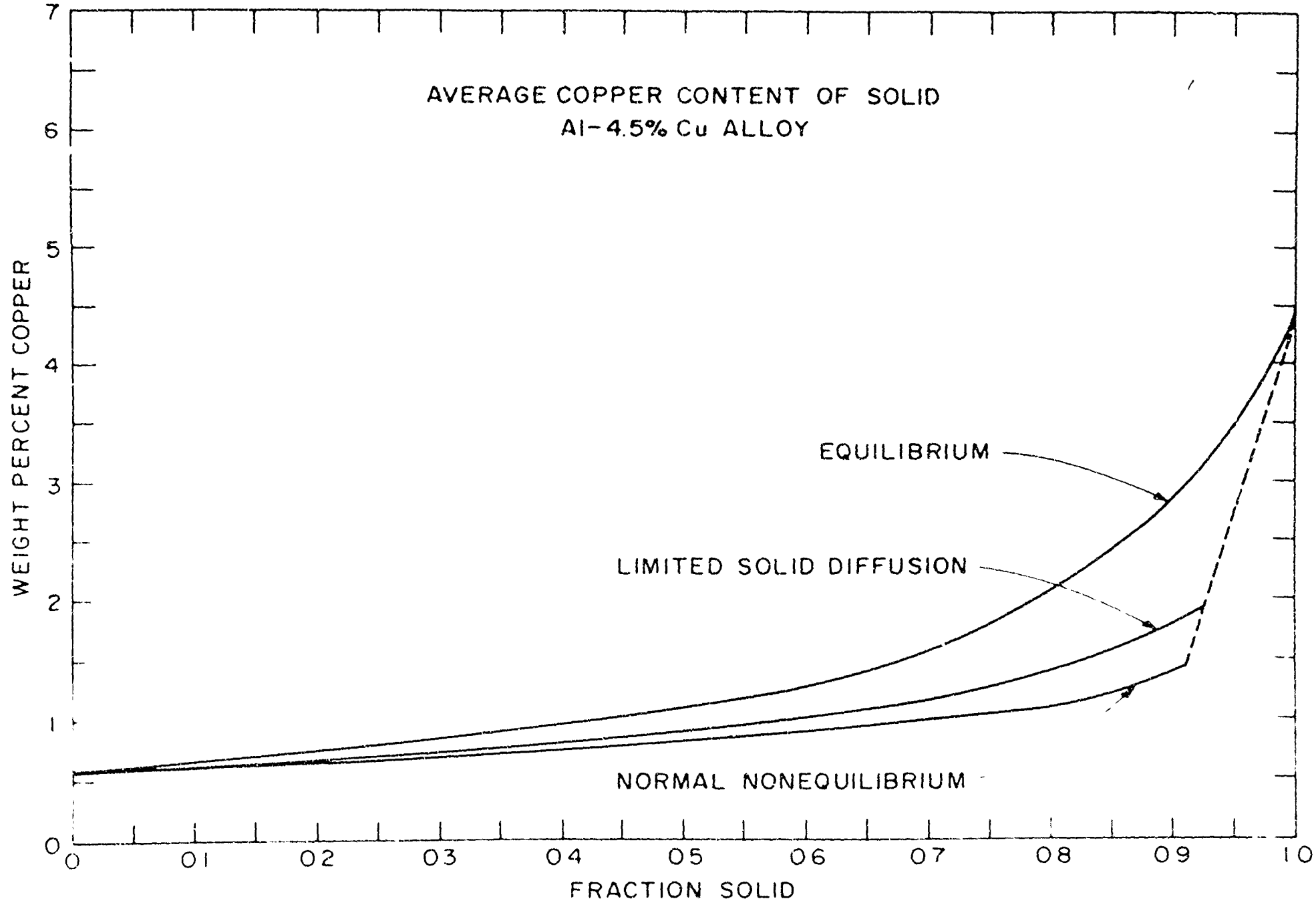

79

Figure 1. Average copper content of the solid during solidification, comparison of three cases

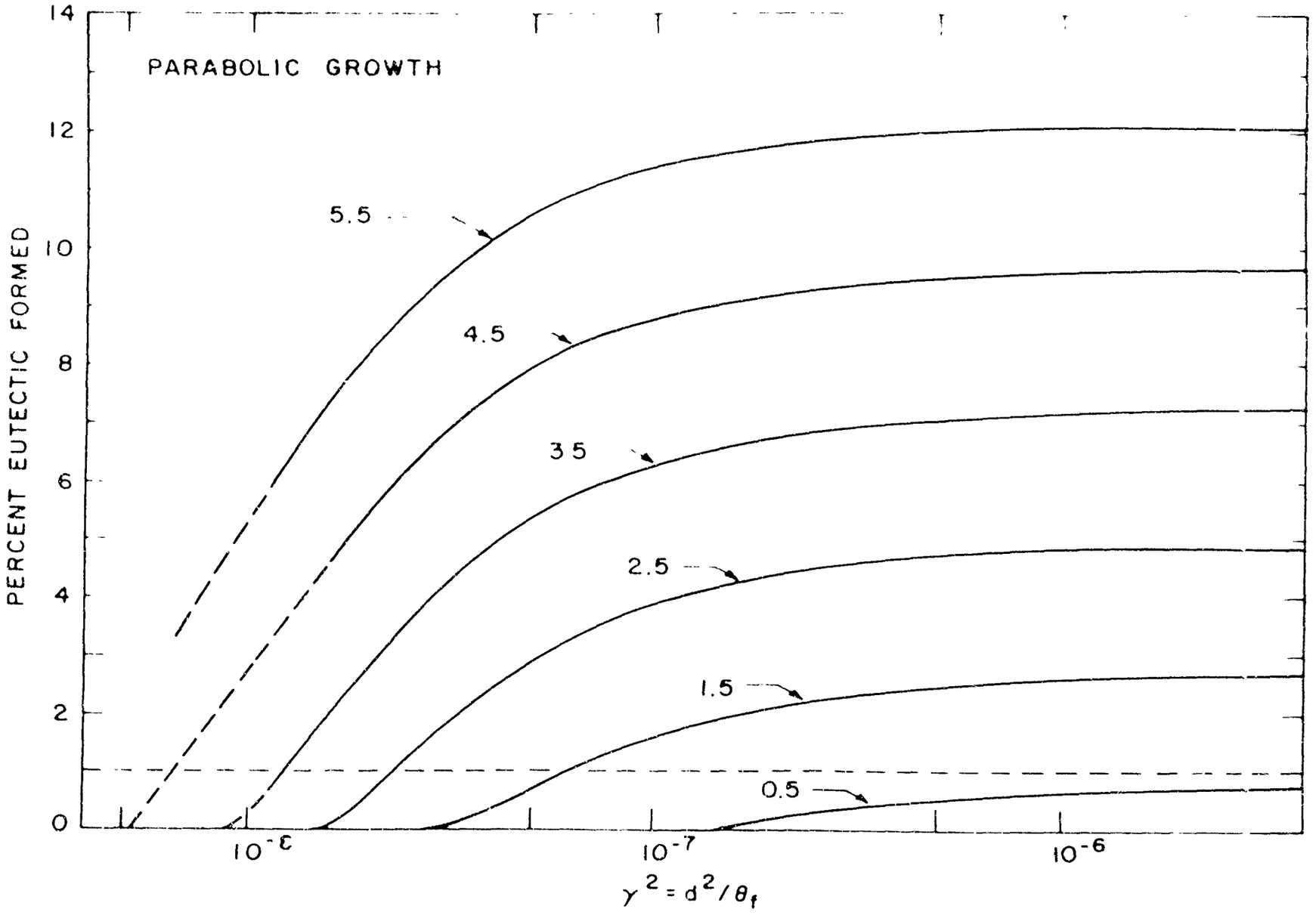

Fig 13 Weight per cent of the non-equilibrium eutectic formed as a function of γ^2 for six aluminum-copper alloys with less copper than the solubility limit Parabolic growth is assumed

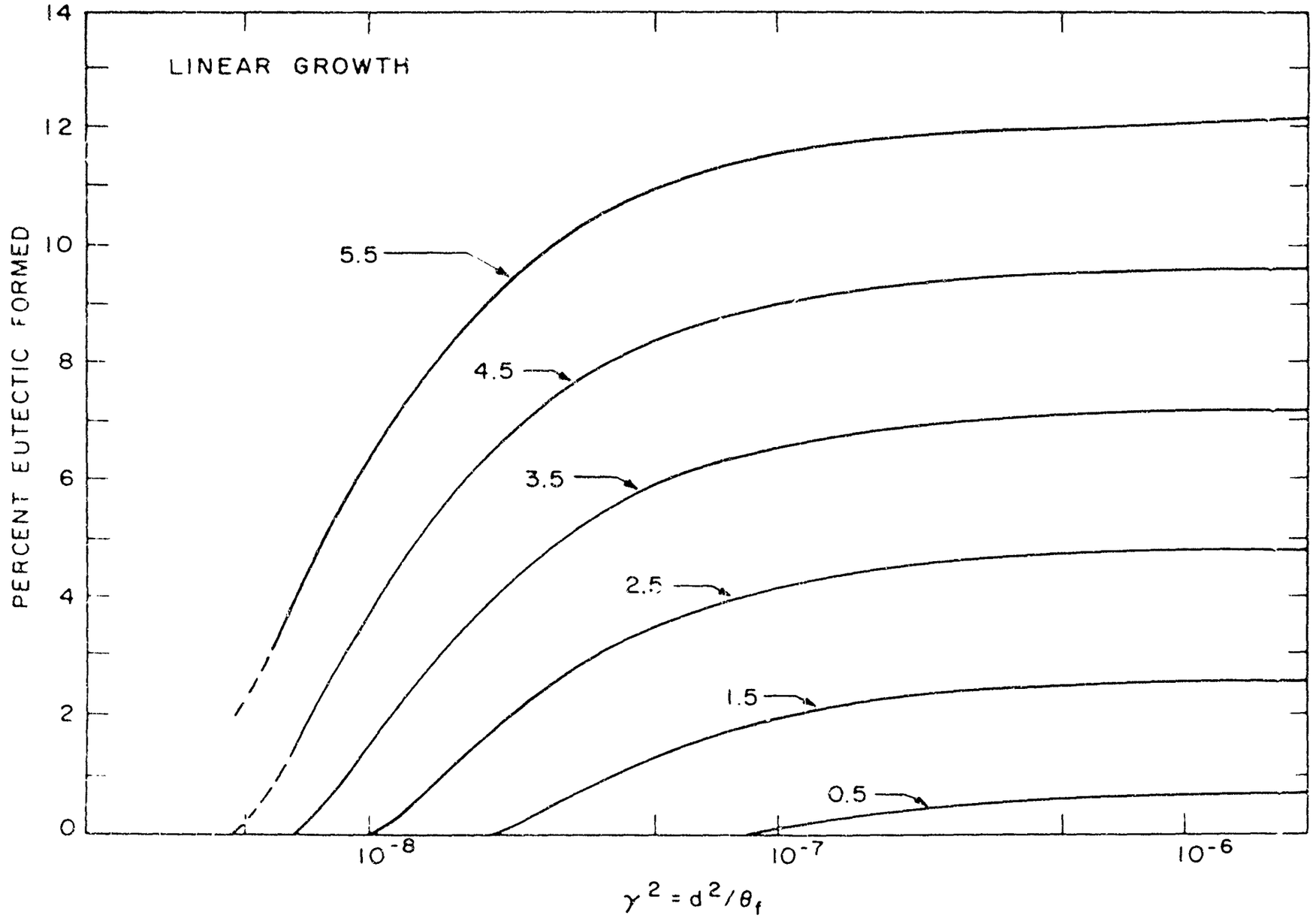

Fig. [illegible] ... per cent non-equilibrium eutectic formed as a function of γ^2 for several aluminum-copper alloys with less copper than the solubility limit. Linear growth is assumed.

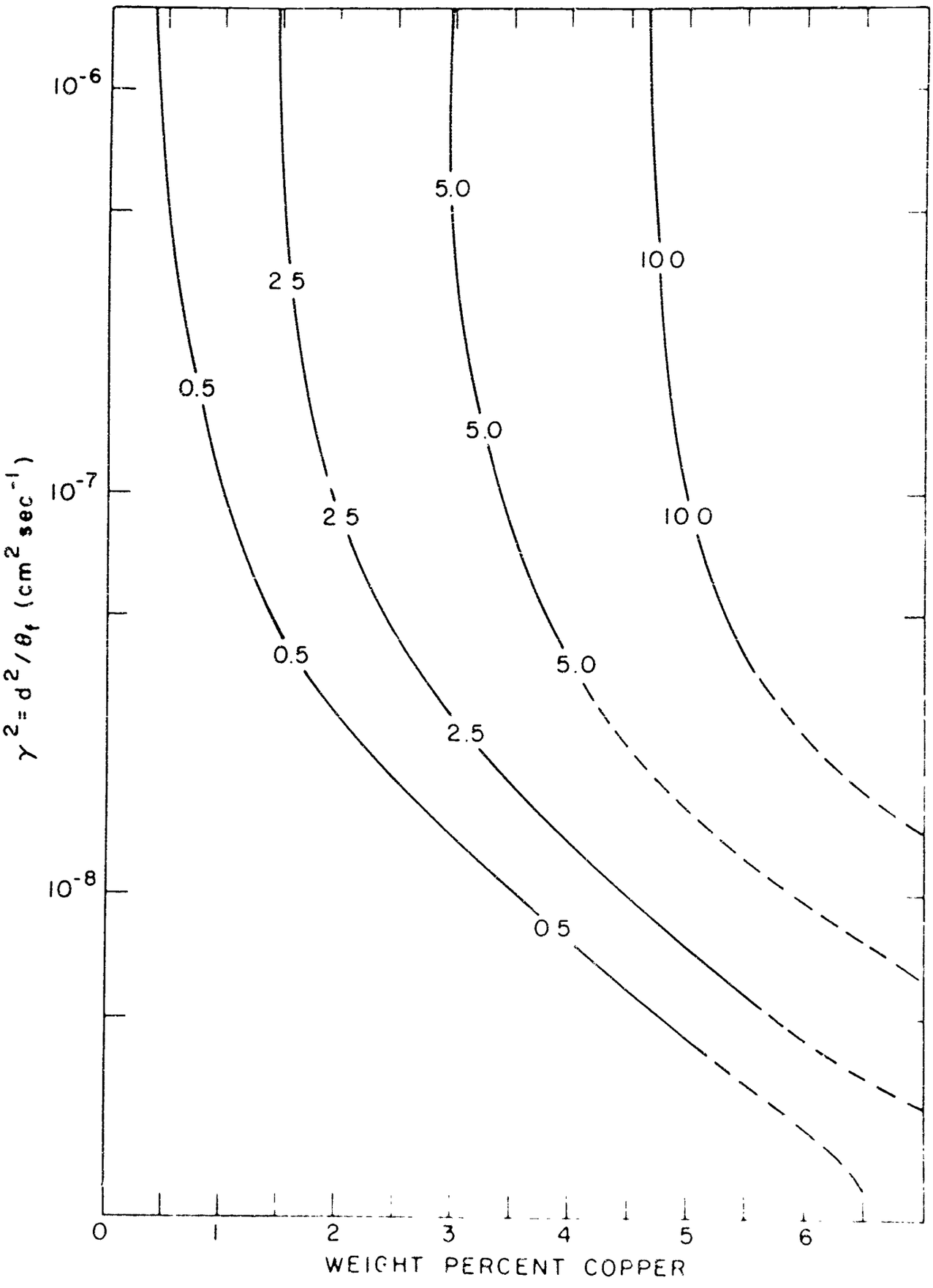

Figure 15. Value of γ^2 required for the formation of a given amount of non-equilibrium eutectic phase in cast aluminum-copper alloys

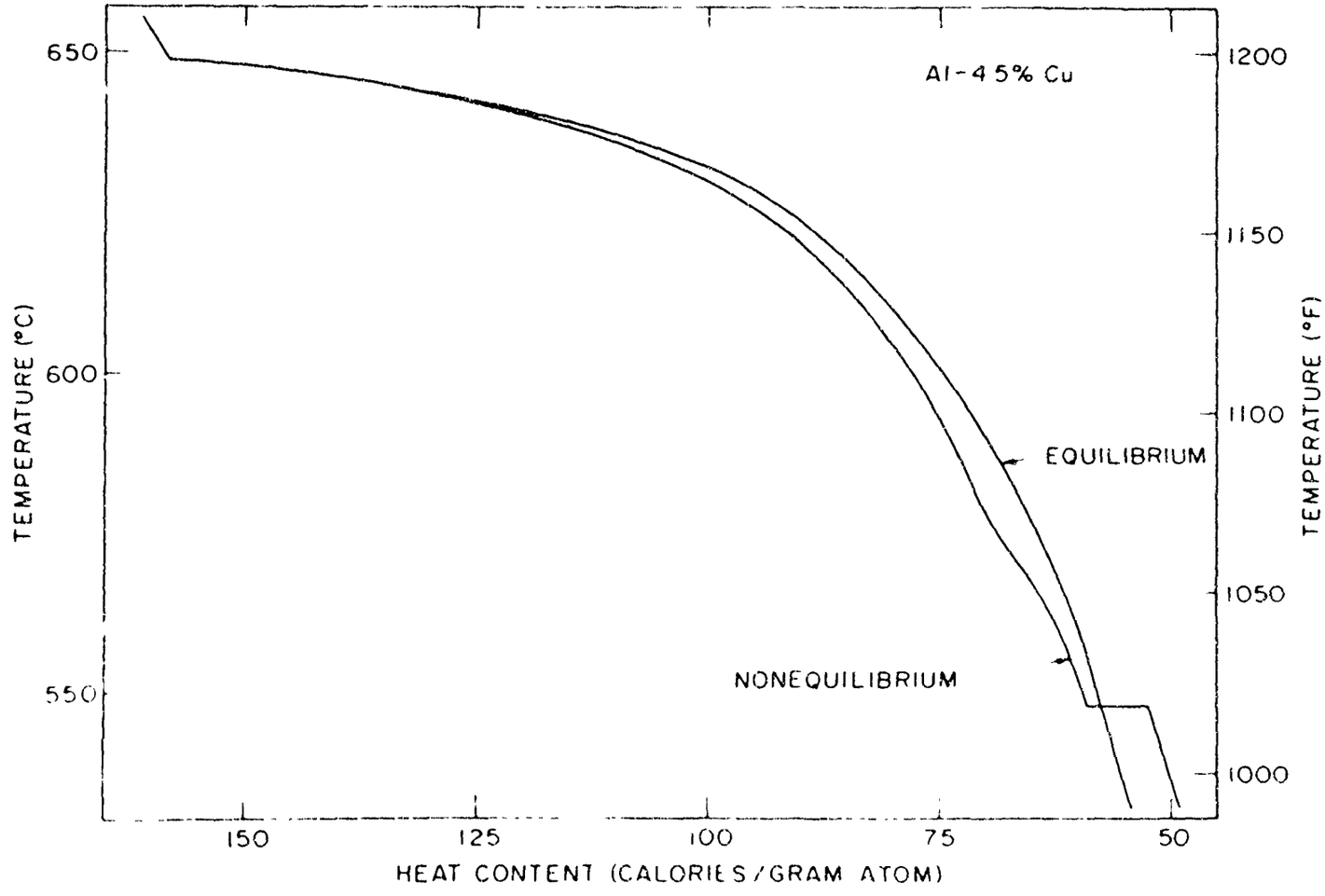

Figure 16 Heat content as a function of temperature for an aluminum-4.5 per cent copper alloy solidifying according to equilibrium and normal non-equilibrium conditions.

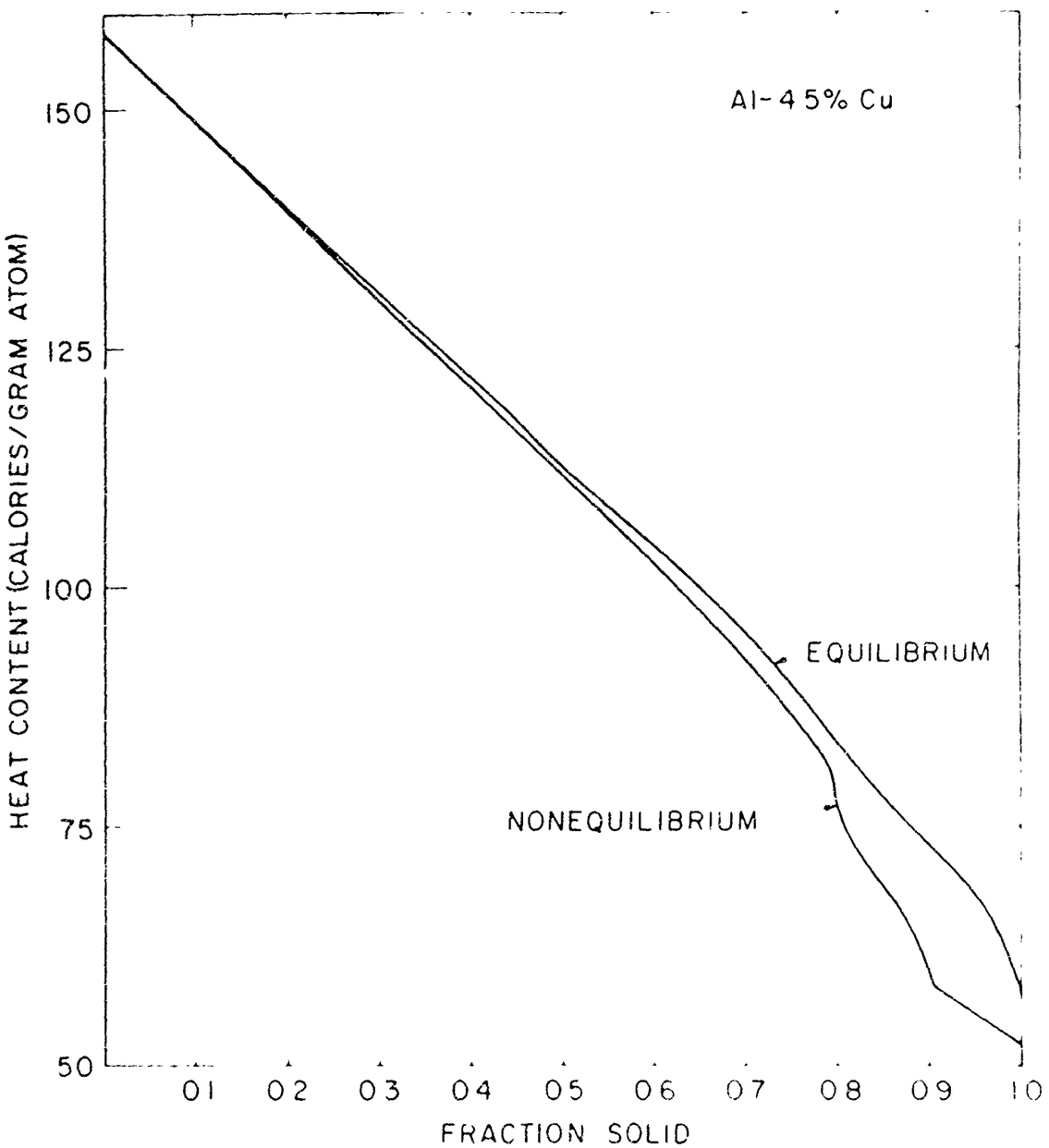

Figure 17 Heat content as a function of fraction solid for an aluminum-4.5 percent copper alloy solidifying according to equilibrium and normal non-equilibrium conditions

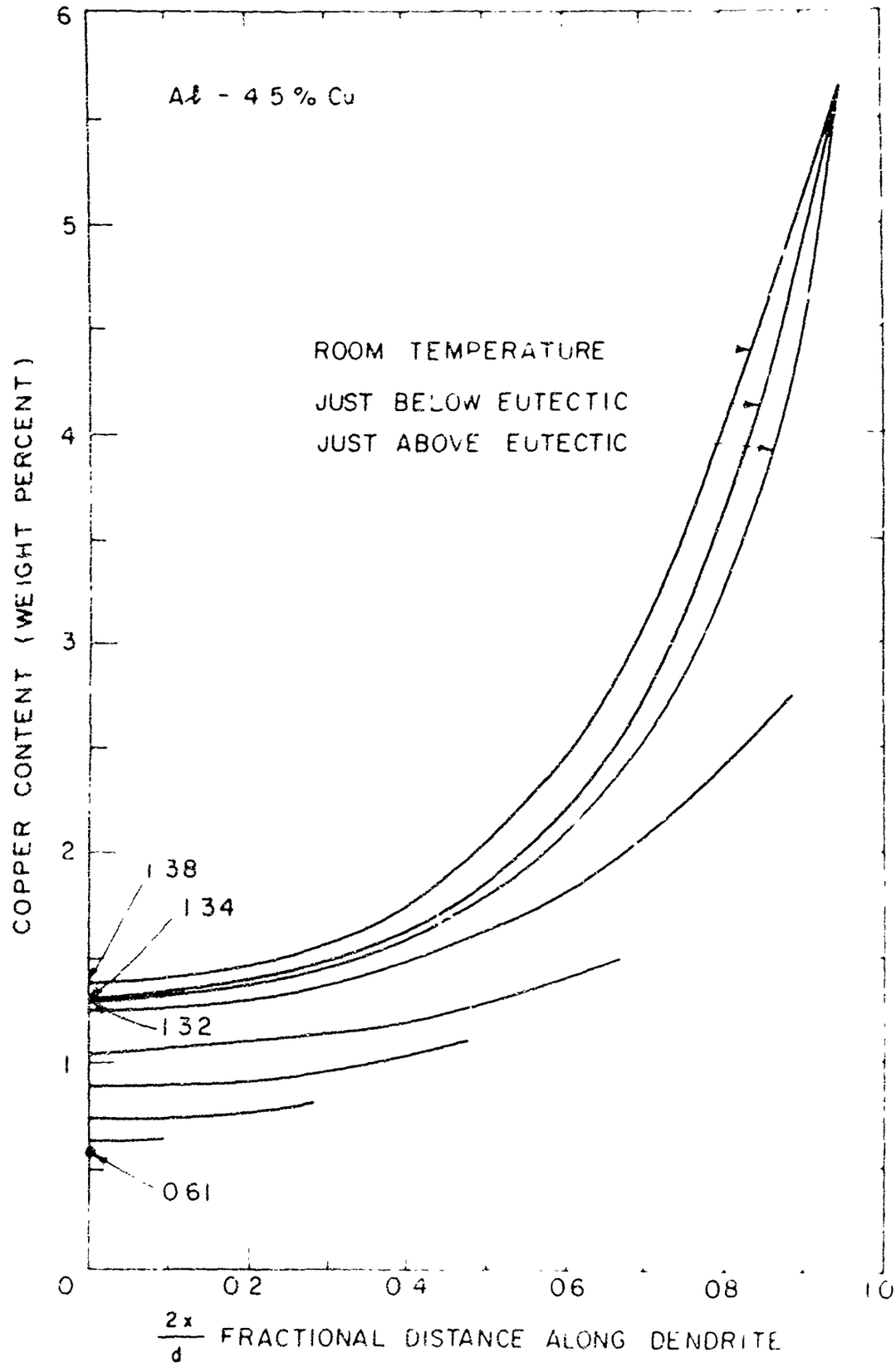

Figure 18. The concentration profile in the solid phase of an aluminum-4.5 per cent copper alloy at several stages of solidification and after cooling to room temperature. Calculation is based on a value of $\lambda^2 = 1.2 \times 10^{-8}$ cm^2 sec^{-1}.

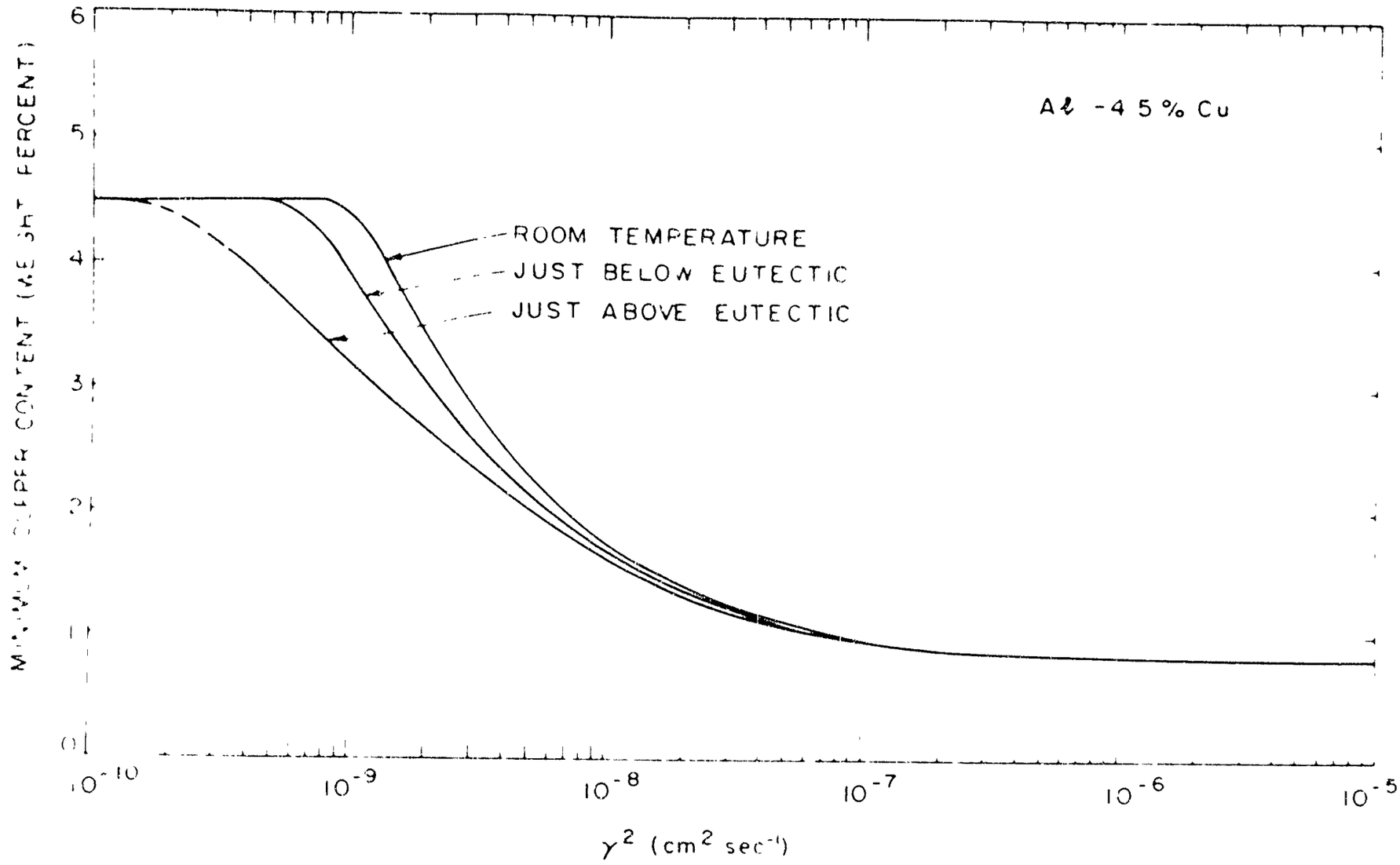

Figure 19 The minimum solute content of the solid phase calculated as a function of ^{2} for an aluminum-4.5 per cent copper alloy cooled to just above the eutectic, to just below the eutectic, and to room temperature.

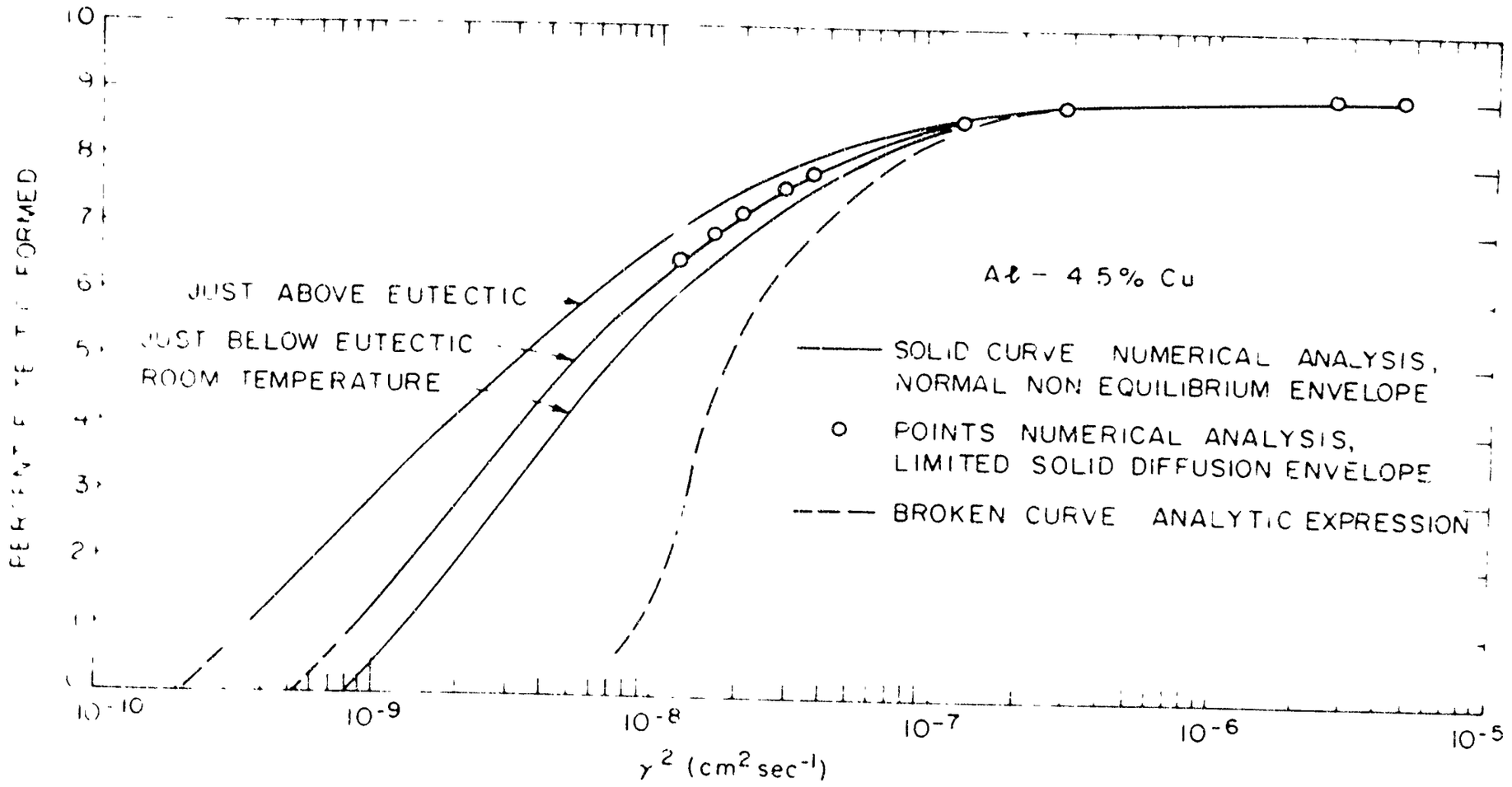

Figure 20 The per cent eutectic formed in an aluminum-4.5 per cent copper alloy calculated as a function of γ^2 using (a) the numerical analysis technique and the normal non-equilibrium envelope, (b) the numerical analysis technique and limited solid diffusion envelopes, and (c) the analytic expression for limited solid diffusion, equations (45) and (55).

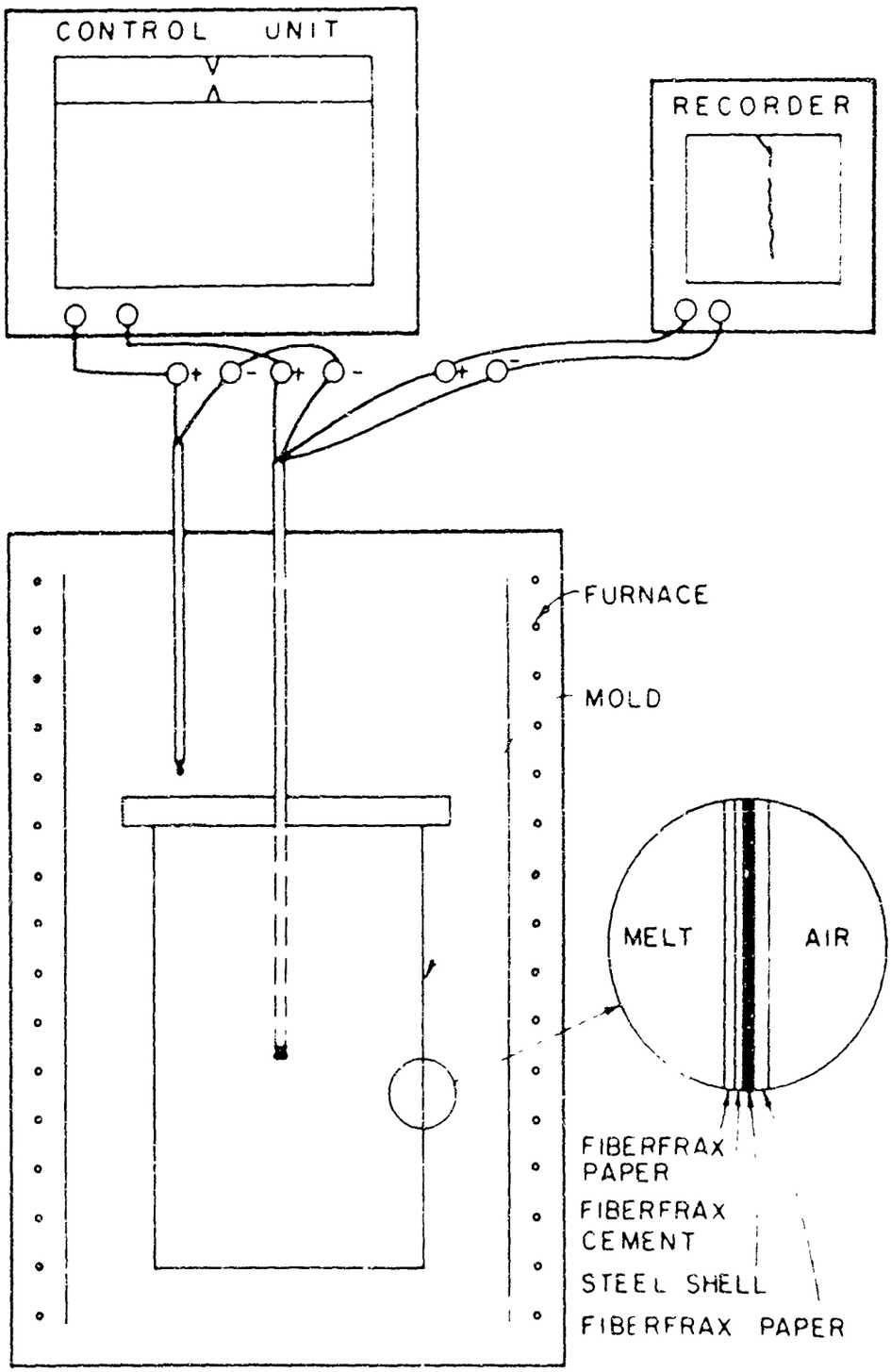

Figure 21 Schematic diagram of the experimental set-up for extended solidification using differential thermocouple control

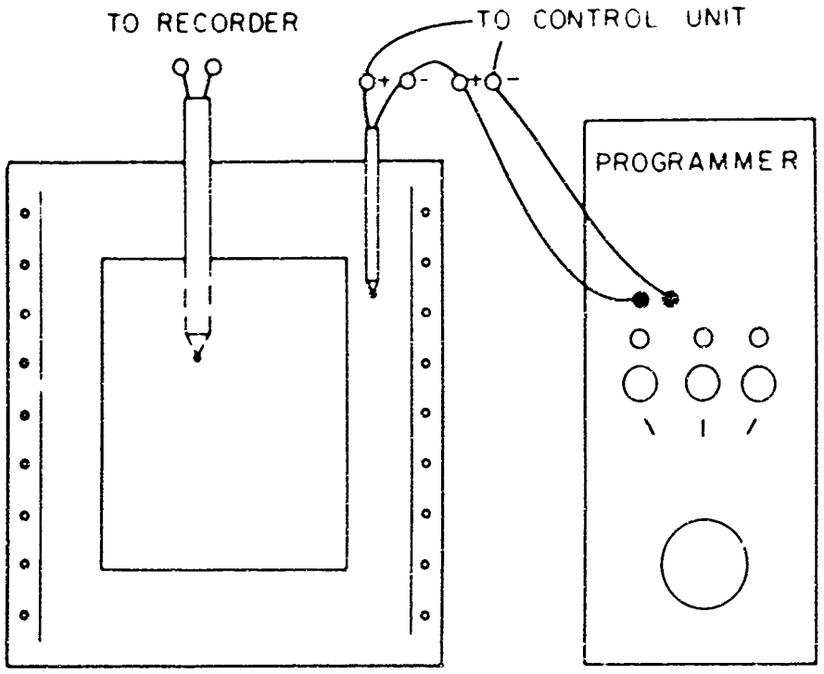

Figure 22: Schematic diagram of a possible experimental set up for solidification by a programmed cooling cycle.

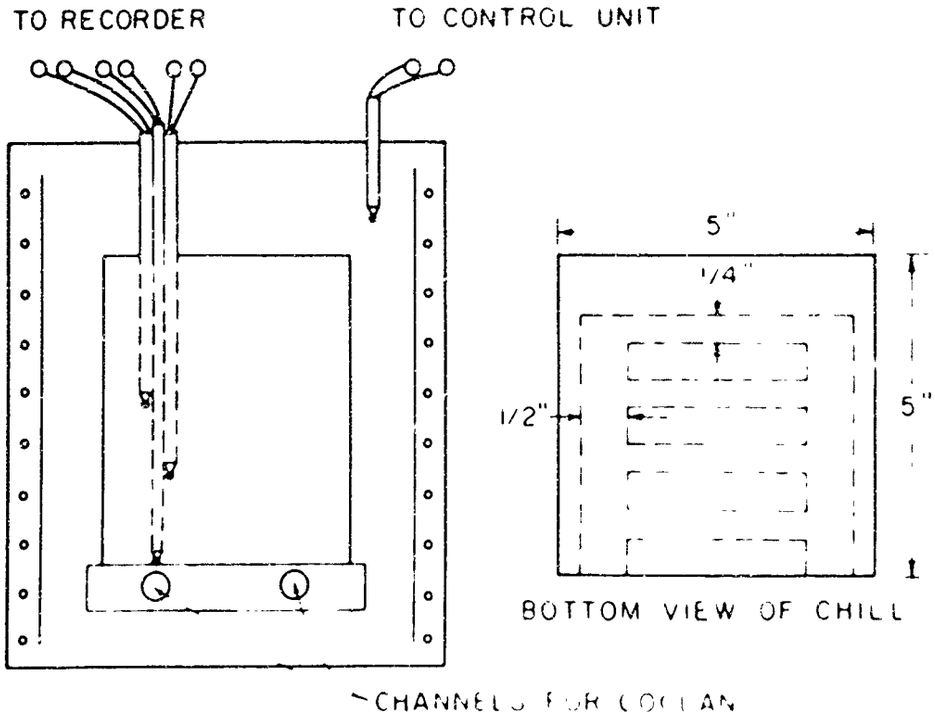

Figure 23. Schematic diagram of an experimental set up for unidirectional solidification of an ingot.

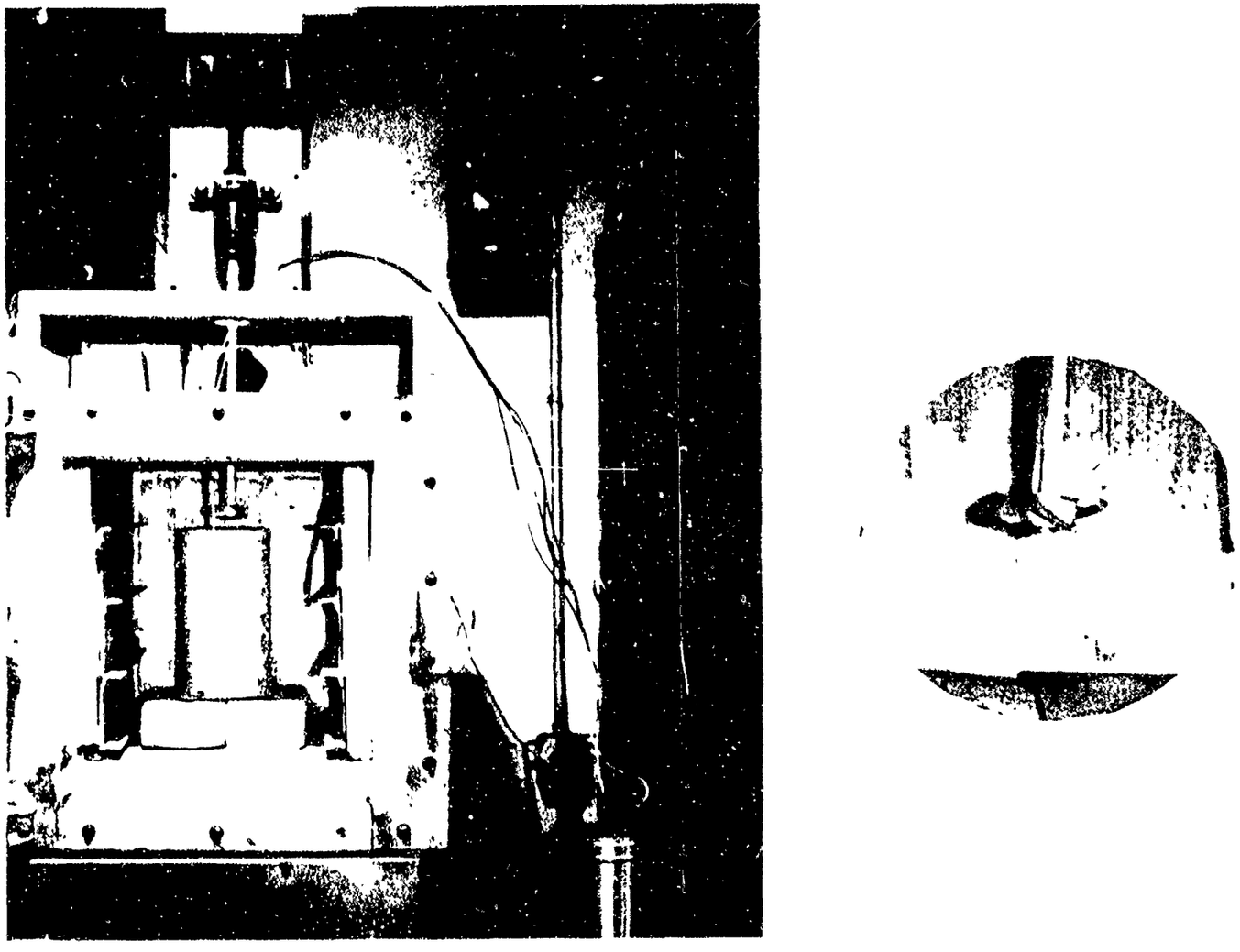

Figure 24 Photograph of apparatus for mechanical stirring of ingots Close up shows paddle blades of stirrer

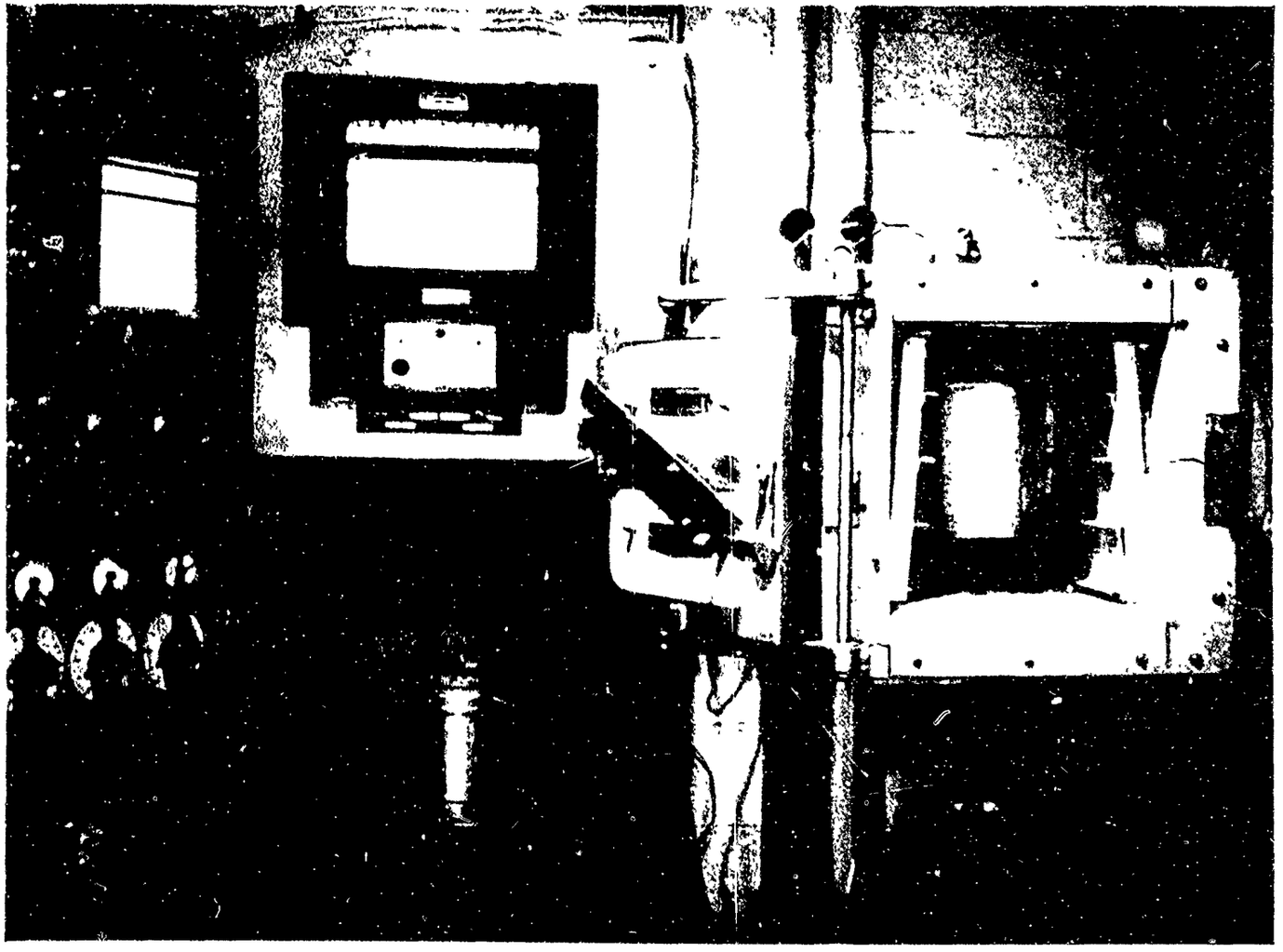

Figure 25: Photograph of apparatus used for vibration of ingots.

(a) twelve hours

(b) sixty hours

Figure 26 Photographs of the macrostructure of polished sections of ingots solidified over (a) twelve hours, (b) sixty hours, (c) one hundred hours and (d) one thousand hours (concentrated Keller's etch, 2/3 of original size)

(c) one hundred hours

(d) one thousand hours

Figure 26 (cont'd): Macrostructures of extended solidification ingots

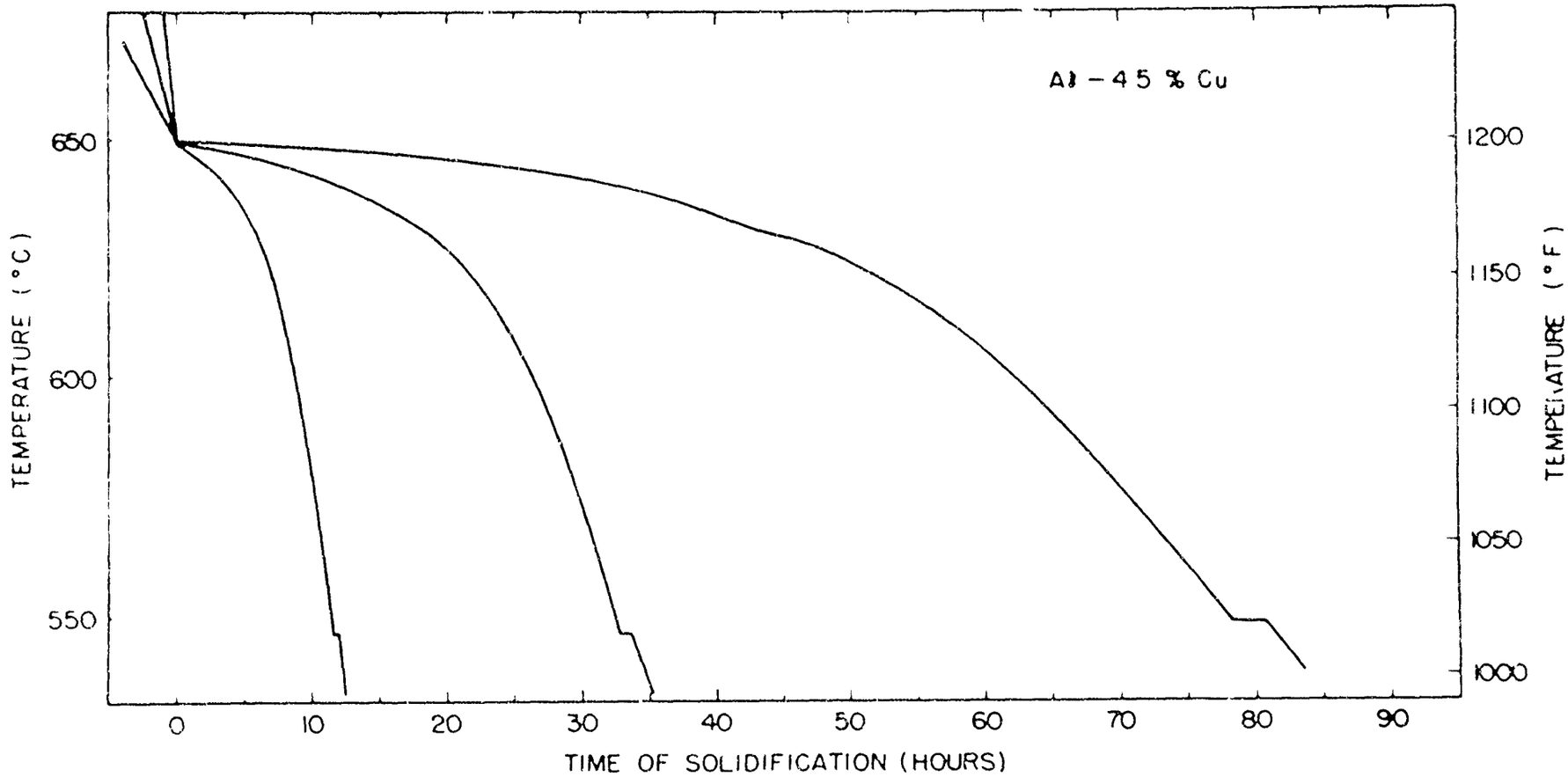

Figure 27 Thermal records of extended solidification ingots having overall solidification times of twelve, thirty four, and eighty two hours.

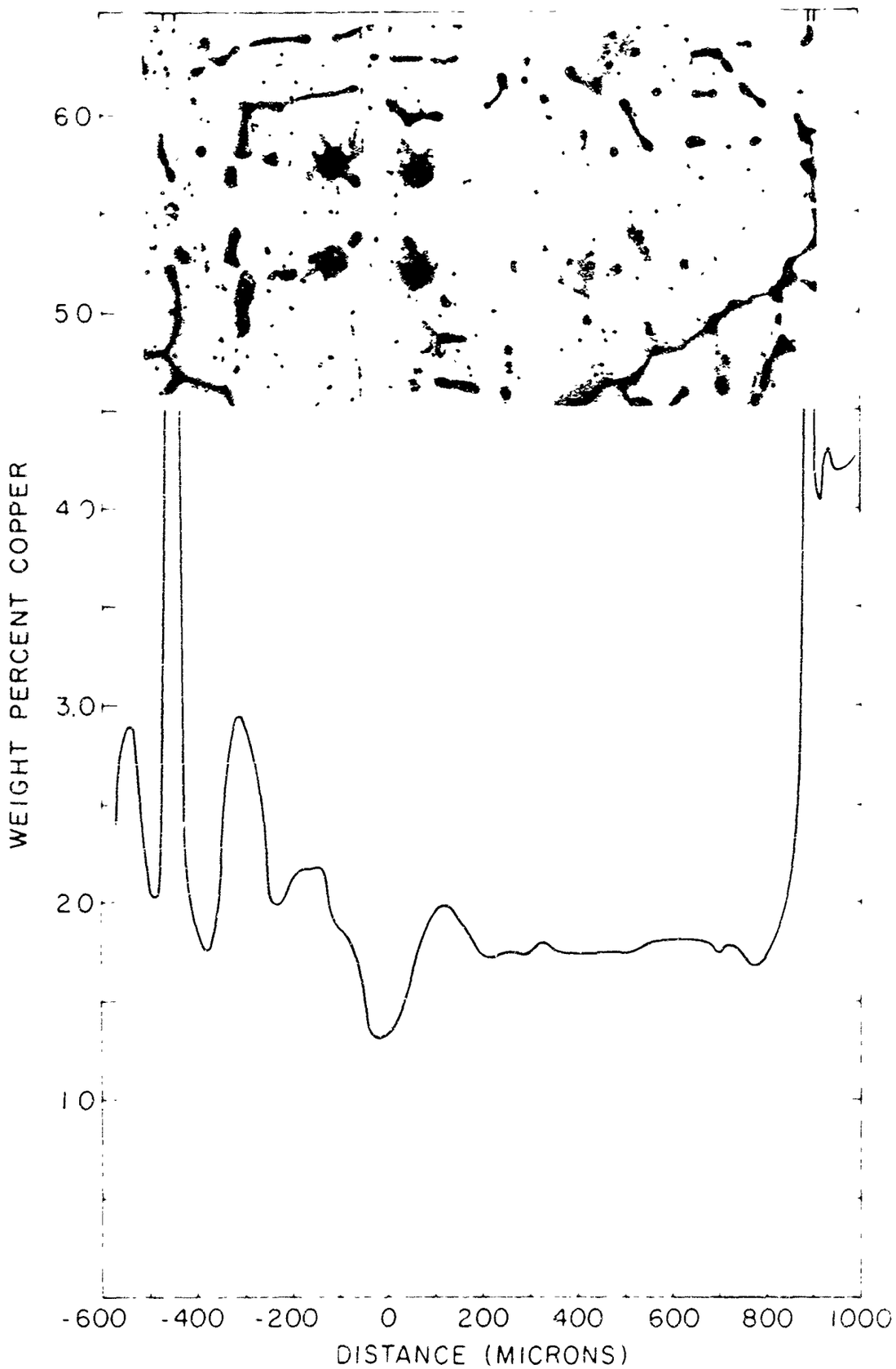

Figure 28 Composite figure showing microprobe trace and photographs of microstructures of ar aluminum-4 5 copper unidirectional ingot Both graph and photograph have same scale in the horizontal direction

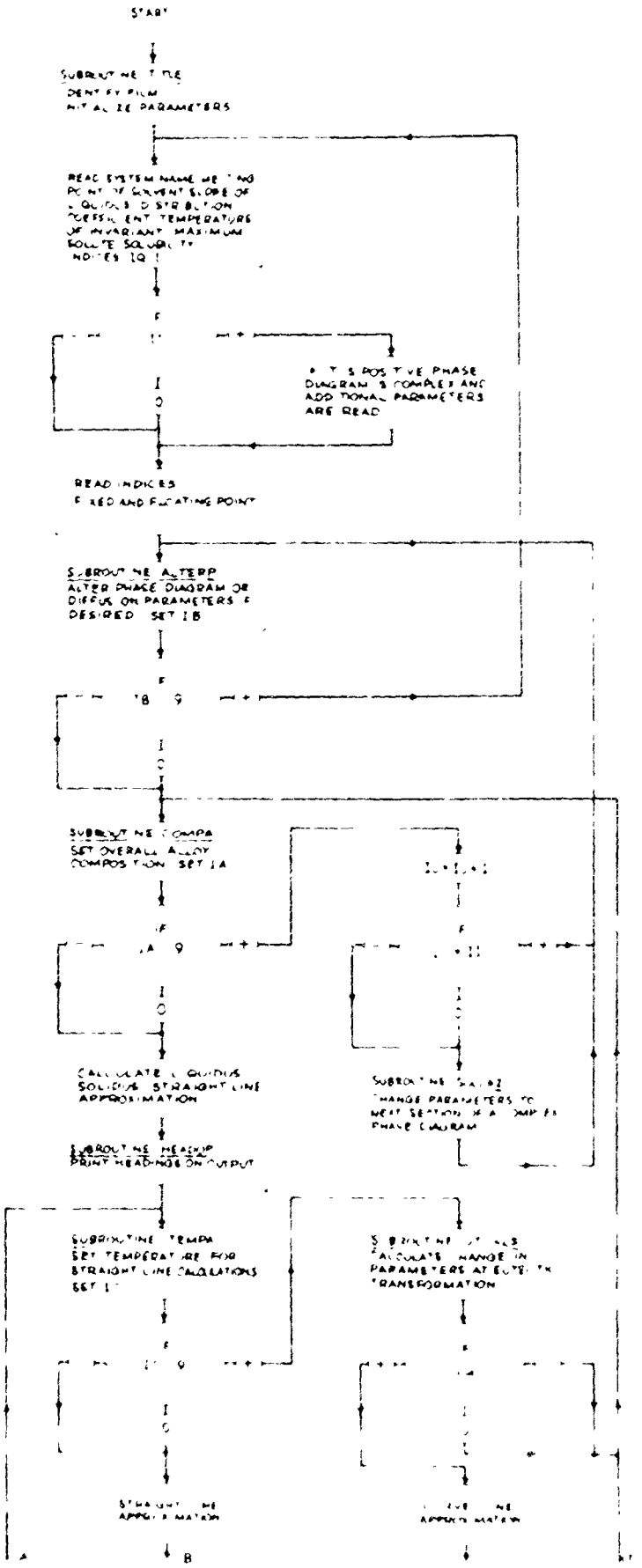

Figure 23 Flow diagram of the active subprogram (MAIN) of FORTRAN program MACRO for computation of macrosegregation solidification parameters.

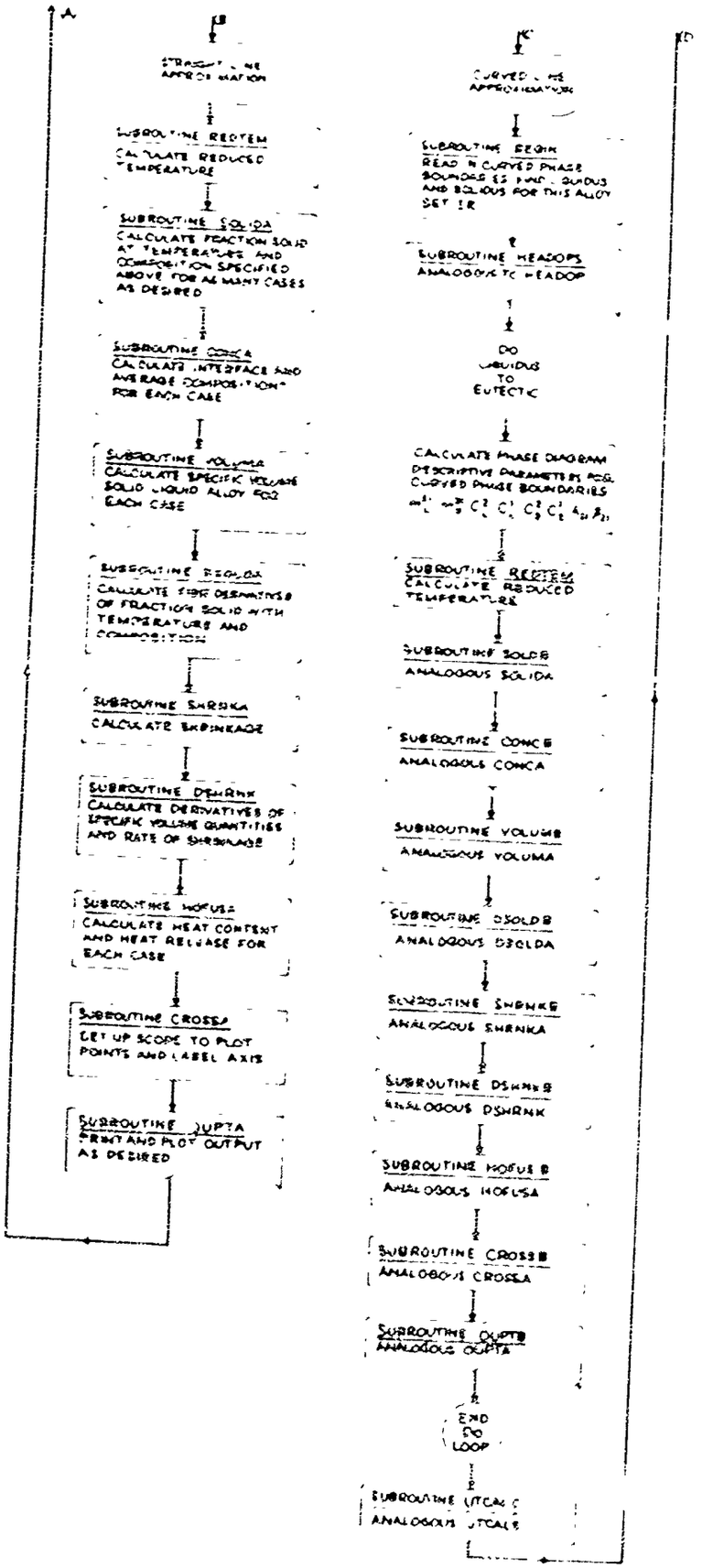

Figure 29 (cont'd). Flow diagram for MALKO.

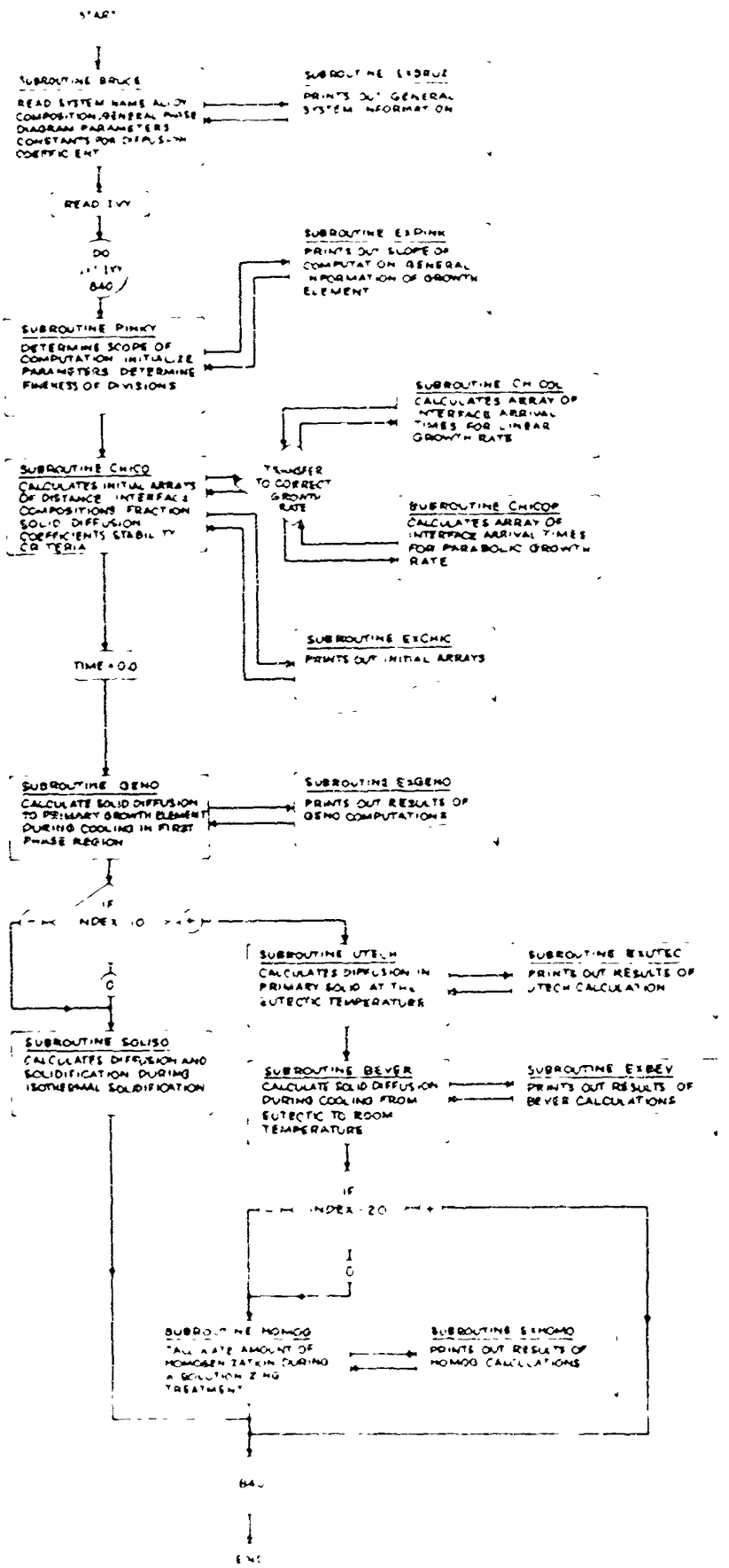

Figure 30 Flow diagram of executive sub-program (MAIN) of FORTRAN program MICRO for calculation of microsegregation pattern of an ingot

APPENDIX A List of Symbols

A_J = constant descriptive of a binary phase diagram in the J^{th} interval

B_J = constant, descriptive of a binary phase diagram in the J^{th} interval

C_o = overall weight fraction of solute in a binary alloy

C_{pS}, C_{pL} = heat capacity of solid and liquid states, respectively

C^*_S, C^*_L, C^*_E = weight fraction solute at interface of solid, liquid, and eutectic phases, respectively

$\bar{C}_S$, $\bar{C}_L$ = average weight fraction solute in solid and liquid phases, respectively

C_{S_J}, C_{L_J} = equilibrium solid and liquid weight fraction at reference temperature T_J of the J^{th} interval of the phase diagram

d = growth element spacing

D_o = frequency constant for diffusion

D_S = volume diffusion coefficient of solute in solid

f_S, f_L, f_E = weight fraction solid, liquid, and eutectic, respectively

H' = heat released for each fraction solidified

H_F = heat of fusion

H_S, H_L = heat content of the solid and liquid phase, respectively

H^M_S, H^M_L = heat of mixing of the solid and liquid phases, respectively

H_T = heat content of a binary alloy

J_I = flux at the interface in the solid phase

k = partition ratio

M = finite difference method constant, $\Delta X^2/D\Delta\theta$

m_S, m_L = slopes of liquidus and solidus

m_{S_J}, m_{L_J} = slopes of liquidus and solidus in the J^{th} interval

ζ = heat of activation of diffusion

q = rate of heat transfer

R = gas constant

T = temperature

T_B = base temperature for heat content measurements

T_i = temperature of an invariant reaction, e g , eutectic transformation temperature

T_K = temperature in degrees kelven

T_L = liquidus temperature

T_J = reference temperature of J^{th} interval of phase diagram

T_m = melting point of pure solvent

u = growth rate constant, linear growth

X = distance along growth element

X_i = position of solid-liquid interface

$\alpha = 2D_S/\lambda^2$

$\alpha_L = 2D/U_R d$

γ^2 = empirical ratio of square of dendrite spacing to solidification time, d^2/θ_f

$\zeta = 1 - (1 - A_J)$

λ = growth rate constant, parabolic growth

ρ = density of alloy

θ = time since beginning of solidification

θ_f = total solidification time

APPENDIX B: Organization of Computer Programs

Evaluation of the solidification parameters introduced in Section II has been achieved with two FORTRAN programs. The first, MACRO, computes the parameters that are descriptive of an entire phase or the entire alloy and are, at least hypothetically, ammenable to macroscopic measurement (pyrometry, calorimetry, dilatometry, etc.). These are the parameters discussed in Sections II-A, II-B, II-C. The second program, MICRO, computes the concentration profile in the growth element on the basis of microscopic diffusion conditions as described in Section II-D. The organization of each is described by a flow diagram of the executive routine of each; MACRO, Figure 29, MICRO, Figure 30.

MACRO consists of an executive sub-program (MAIN) that calls a sequence of computational and input/output subroutines. The calling sequence of (MAIN) is presented in Figure 29. Many variations have been compiled for each computational and output subroutine and the particular series of subroutines selected to buildup a deck for a computer run is a choice dependent on the nature of the alloy system (e.g., real or imaginary), the assumed solidification conditions, and the parameters to be evaluated and/or compared. The general purpose of each subroutine is indicated in Figure 29. A program of this design was deemed most suitable for a research project in which the assumptions, parameters, and systems taken under consideration are continually changing and expanding.

MICRO consits of an executive sub-program (MAIN) and several computational and input-output subroutines. The calling sequence of (MAIN) is delineated by the flow diagram, Figure 30, as are the functions of each subroutine. The scope of job to be run on the computer is read in as part of the data and thus with the exception of subroutine CHICO only one subroutine of each name is needed Because output is a relatively slow computer step, the output routines have been designed to be easily altered by octal correction cards whenever computer time must be conserved

APPENDIX C: Thermal Data for Heat Content Analysis of Al - 4.5 Per Cent Cu

1. Thermal Properties of the Pure Elements

K K. Kelley[12] fits the temperature variation of heat content of an element to an expression of the following general form

$$H(T) = aT + bT^2 + C$$

The evaluation of this expression for liquid and solid aluminum and copper are

$$H_S^{Al} = \left\{(4.94)T + (1.48 \times 10^{-3})T^2 + (-1,604)\right\} / (26.98) \quad (cal/gr)$$

$$H_S^{Cu} = \left\{(5.41)T + (0.75 \times 10^{-3})T^2 + (-1,680)\right\} / (63.54)$$

$$H_L^{Al} = \left\{(7.00)T + (330)\right\} / (26.98)$$

$$H_L^{Cu} = \left\{(7.50)T + (-20)\right\} / (63.54)$$

and the heat capacity expression is the fit to the derivative of the above expressions, that is

$$C_p = a + 2b\,T$$

and $C_p{}^{Al}{}_S = \left\{(4.94) + (2.96 \times 10^{-3})T\right\} / (26.98) \quad (cal/gr°C)$

$C_p{}^{Cu}{}_S = \left\{(5.41) + (1.50 \times 10^{-3})T\right\} / (63.54)$

$C_p{}^{Al}{}_L = (7.00)/(26.98)$

$C_p{}^{Cu}{}_L = (7.50)/(63.54)$

2. Heat of Mixing Data

(a) Assume H_S^M to be negligible. The average copper content of the primary solid is less than two per cent (less than one atomic per cent).

(b) From O. Kubashewski and J. A. Catterall[13] the heat of mixing of the liquid up to 33 weight per cent fits the relation

$$H_L^{M\prime} = -(9000)N_{Cu} \quad (cal/gram)$$

where N_{Cu} = atom fraction copper

$$N_{Cu} = \frac{C_L\ (26.98)}{C_L\ (26.98) + (1 - C^*_L)(63.54)}$$

Define Ψ such that

$$\Psi - 1 = N_{Cu}(63.54) + (1 - N_{Cu})(26.98) = \frac{\text{grams liquid}}{\text{gram atom liquid}}$$

Then

$$H_L^M = -(9000)\ N_{Cu}\ \Psi \quad (cal/gr\ liquid)$$

To evaluate dH_L^M/dC_L

$$\frac{dH_L^M}{dC_L} = -(9000)\ \frac{dN_{Cu}}{dC_L} + N_{Cu}\ \frac{d\Psi}{dN_{Cu}}\ \frac{dN_{Cu}}{dC_L}$$

which becomes

$$\frac{dH_L^M}{dC^*_L} = \frac{63.54}{9{,}000}\ \frac{H_L^{M\,2}}{C^{*}_L{}^2}$$

(c) For the intermetallic phase $CuAl_2(\theta)$

$$H_{\theta}^{M\prime} = -3,250 \text{ (cal/gr atom)}$$

and

$$H_{\theta}^{M} = -3,250 \text{ (cal/gr)}$$